# BIOMIMICKING AND BIOACTIVE COMPARTMENTS: FROM NANOSCALE TO MICROSCALE VESICLES

**Inauguraldissertation**

zur

Erlangung der Würde eines Doktors der Philosophie

vorgelegt der

Philosophisch-Naturwissenschaftlichen Fakultät

der Universität Basel

von

Luisa Zartner

2021

Genehmigt von der Philosophisch-Naturwissenschaftlichen Fakultät
auf Antrag von

Prof. Dr. Cornelia G. Palivan
Erstbetreuerin

Prof. Dr. Wolfgang P. Meier
Zweitbetreuer

Prof. Dr. Dimitrios Fotiadis
externer Experte

Basel, den 22.06.2021

Prof. Dr. Marcel Mayor
Dekan

"All kinds of interesting questions which the science knowledge only adds to the excitement, the mystery and the awe of a flower. It only adds. I don't understand how it subtracts."

R. Feynman, Ode to a Flower

# TABLE OF CONTENTS

# ACKNOWLEDGEMENT

# ABSTRACT

Cellular model systems are essential platforms used across multiple research fields for exploring the fundaments of biology and biochemistry. By multicompartmentalization, systems can be created where nanocompartments (serving as artficial organelles) are encapsulated in microscale compartments (serving as the cellular structure).

The first topic of this thesis focusses on polymersomes that are supplemented with membrane proteins and enzymes. The biomolecules endow such bioactive vesicles with specific cellular functions and enable diverse applications in nano- or pharmatechnology. In this work, we particularly introduce a new strategy for modifying the membrane proteins via chemical-oriented approach. Until now, significant progress in functionalization of polymersomes has been obtained by embedding modified proteins into the membrane for stimuli-responsive permeability. Inside the polymersomes, enzymes are encapsulated and catalyze distinct reactions with molecules diffusing through the membrane. Due to the resulting triggerable activity, such bioinspired vesicles are able to detect diverse environmental signals and show a remarkable potential for diverse applications such as biosensing and triggerable drug release. We introduce a small, periodate-sensitive designed linker blocking the passage through a protein channel (OmpF) reconstituted into the membrane of polymersomes. By combining tools of organic and bioconjugation crosslinkers, we synthetized this organic linker. OmpF was successfully modified with the linker and led to a stimuli-responsive permeability of the vesicles. In presence of periodate, the linker was cleaved and allowed substrates to diffuse inside the compartments where encapsulated laccase catalyzed the reaction to the respective radicals with a characteristic absorbance that was detected. Additionally, the labelling of OmpF with the stimuli-responsive linker is performed under mild conditions (no organic solvents, room temperature, pH 7) and therefore it has the potential to be adapted for diverse proteins that are more sensitive than OmpF.

With regard to the microscale compartments, synthetic Giant Unilamellar Vesicles (GUVs) and Giant Plasma Membrane Vesicles (GPMVs) are one of the most prominent cell-like compartments. GUVs are formed by self-assembled lipids or polymers while GPMVs, are directly derived from cells. The second project presented here, focusses on GPMVs as a platform of cell-like compartments. GPMVs include most of the cellular components and thus, provide the highest similarity to real cells. GPMVs will facilitate the investigation and the understanding of different behaviors and characteristics of cellular processes. Our aim is to

promote the further development of GPMVs with regard to the study of nanoparticles (NPs) under physiological conditions. We studied molecular factors that determine the successful transfer of cellularly taken-up NPs transferred into formed GPMVs. In particular, we investigated the impact of size, concentration and surface charge of NPs in correlation with three different cell lines: HepG2, HeLa, and Caco-2. We observed that polystyrene (PS) carboxylated NPs with a size of 40 nm and 100 nm were successfully and efficiently transferred to GPMVs derived from all cell lines. Then, we investigated the distribution of NPs inside formed GPMVs and established the average number of NPs/GPMVs and the percentage of all GPMVs with NPs in their cavity.

# FUNCTIONAL BIOINSPIRED COMPARTMENTS

*The first chapter provides an introduction of the fundaments of bioinspired compartment attracting high scientific interest. Considering the inspiration by real cell membranes, the membrane structure of synthetic compartments composed of amphiphilic lipids and polymers is explained (both nano- and microscale compartments). Polymersomes, as prominent and frequently applied 3D nanostructures formed by self-assembly, are introduced more in detail; the focus is on polymersomes including different biomolecules for controllable multifunctionality (membrane proteins and enzymes). Such nanocompartments show high potential for various applications where the most famous of which are introduced in this chapter. In the second part, the reader is given an overview of cell-like compartments with the focus on microscale compartments synthetically produced (GUVs) or directly derived from cells (GPMVs). Regarding cell-like platforms, GPMVs are presented as promising candidates and are described in detail, since GPMVs are studied for further development in the later chapter of this work.*

# Membrane structure of synthetic nano- and microscale compartments

For many different scientical domains, the design and development of synthetic compartments in the nano- and microscale are of big advantage as they have versatile bioinspired functionalities due to resemblance to real cells and their organelles. One challenge is the mimic of the cellular membrane built up *in vitro* with laboratory equipment. Lots of different parameters and impact factors have to be taken into account and put into practice, such as the intrinsic mechanical properties, membrane composition (lipid, polymer) and orientation.[1-7]

## Inspiration by biomembranes

The synthetic membrane presents the fundamental structure of bioactive nanocompartments and cell-like compartments. The in-depth and comprehensive investigation of native cellular membrane architectures, advanced significantly the development of synthetic artificial membrane assemblies. The cell is surrounded by the membrane protecting selectively the cellular interior from the external environment. The biomembrane, also called plasma membrane, is mainly built up of dynamic phospholipid bilayers. Phospholipids are polar, amphiphilic molecules including a hydrophilic zwitterionic phosphate head group and two (un)saturated hydrocarbon chains as hydrophobic tails.[8] In an aqueous milieu as it is in animal and human bodies, phospholipids are assembled in 2D double layers (bilayer), where the hydrophilic head groups are oriented to the water interfaces due to cohesive, attractive forces. The high stability and also high flexibility of the membrane is the results of a very important and complex balance of the components.

Straight lined saturated fatty acids incorporated as the hydrophobic tails leads to a denser, stable structure. Unsaturated chains (unsaturated fatty acid) show a kink in the area of the C=C double bond and result in more lose packing of the phospholipids in the membrane supporting the flexibility. Regarding the fluidity of phospholipids in general, rigid compounds or steroids like cholesterol, have to be incorporated to allow a stable solidified structure. Their amount has to be balanced. Too many rigid components lead to a lack in flexibility and the resulting stiff membrane breaks. On the other hand, a lack of steroids in the membrane causes damage as the membrane lost stability.[9]

The main purpose of the cell membrane is the separation of the intra- and extracellular environments. In particular, the membrane is a passive partition wall for cells. The diffusion

processes though the membrane into the cell (uptake) or to the exterior (excretion) are controlled by the phospholipid bilayer. However, the active cell transport is achieved by diverse additional embedded membrane proteins allowing selective permeability towards molecules and ions. In the cell membrane are lots of different membrane proteins fulfilling particular tasks essential for pH regulation, the metabolism, the cell signaling/communication and adhesion.[1, 10, 11] The OmpF membrane protein (Outer membrane protein F), for example, occurs in bacterial membranes as a simple non-specific protein channel. It is shaped as beta barrel with a diameter of around 30 Å enabling the diffusion of molecules with a size of approximately 600 Da in both directions (in and out of the cell). The rather non-charged inner structure of OmpF further supports the transport of charged and uncharged compounds. Another advantage of OmpF is its stability towards several conditions like temperature, or solvents. In contrast to most membrane proteins, OmpF is easy to isolate from bacteria while maintaining the structure and functionality. The robust OmpF can further be engineered, biologically and chemically, which turns OmpF and mutants to frequently used tools for permeabilizing the polymeric membrane of synthetic bioactive vesicles.[12-15]

Besides that, most membrane proteins are difficult to isolate and reconstitute. The highly complex structure and dynamics of the cell membrane itself, where phospholipids and membrane proteins diffuse freely within, presents a very big challenge for mimicking the biomembrane with laboratory equipment. As first approach for membrane mimics, the components for a synthetic membrane are narrowed down in order to provide a controlled self-assembly with fundamental functions.


## Synthetic membranes based on lipids and polymers

### Lipid-based synthetic membranes

Synthetic membranes imitating the plasma membrane with a close composition, are assembled by lipids, or rather natural occurring phospholipids. This approach seems to be consequential due to the fact that phospholipids are plentifully present in biomembranes. In addition to that, the lipids are well-characterized and facile to purchase in a huge variety. They include basically 4 components: i) glycerol or sphingosine serving as basic structure, ii) a phosphate for the hydrophilic head group, iii) an alcohol, usually containing a primary/tertiary amine in addition (the alcohol binds to the phosphate, the amine determines the charge of the head group), and iv) 2 fatty acids as hydrophobic tails.[16] The fatty acids are available in many variations (saturated, unsaturated, number of carbons). The resulting 3D self-assemblies depend on the molecular conformation of the fatty acids. There are different structures, like micelles and

vesicles, that are naturally formed by phospholipids in aqueous solutions (Figure 1). The molecular structure and stability of lipidic self-assemblies is controlled by several parameters of the phospholipids, such as ionic strength, size of the heap group and saturation of the fatty acids. Additionally, external conditions such as pH, ion concentrations and temperature have an impact on the assembly.[16-18]
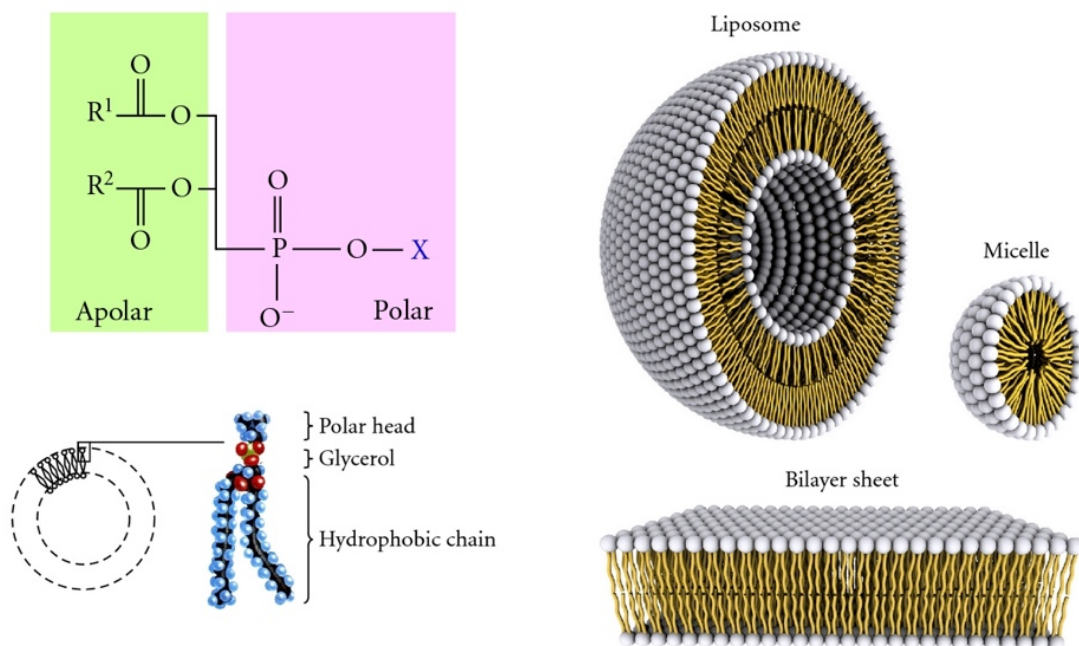


*Figure 1. Phospholipids and their self-assemblies* – *a) Scheme of the structure and charge distribution of a typical phosphoglyceride. On the left is the polar phosphoric group esterified to the hydroxyl group of an alcohol. On the right is the apolar aliphatic chains esterified to the central moiety, which is a glycerol. b) Assembly of a lipidic bilayer. The longer apolar chains are stacked in the internal department of the bilayer. c) Architecture of liposomes and micelles. The representative steric organization of a liposome (left) and a micelle (right). Liposomes have a lipidic bilayer (bottom) whereas micelles are constructed only by one lipid layer that has its apolar section turned inwards while its polar heads interact with the environment. Adapted from Bitounis with permission.[18]*

Lipidic vesicles, also called liposomes contain a lipid bilayer forming the membrane. The molecular structure of the bilayer is often formed by a mixture of bilayer-preferring lipids, like phosphatidylserine (PS), making up merely 20-50%. The majority is non-bilayer preferring lipids, such as the unsaturated phosphatidylethanolamine (PE), that have to be included additionally in order to stabilize and preserve the bilayer.[16]

The basic structure of natural plasma membrane could be mimicked with labatory equipment as the membrane mainly consists of 6 components: PS, PE, phosphatidylinositol (PI), phosphatidylcholine (PC), sphingomyeline (SM) and steroids (i.e. cholesterol). The difficult task of closer mimicking the plasma membrane is the reconstitution of the diverse membrane proteins.[1, 19] Membrane proteins are mostly very fragile building blocks. The isolation and purification of such sensitive and proteins while retaining their functionality, represent the first challenge. Second, the membrane proteins as amphiphilic biomolecules have to be suspended in aqueous solutions containing detergents, that disturb the self-assembly of the membrane. Due to this, the synthetic lipid membranes have a lack of natural permeability and stability. However, phospholipids allow close mimics of the cell membrane. Until today, lipid-based synthetic membranes have given new insights into many different important parameters considering i) lipid and protein distribution[20], ii) activity and function[21, 22], iii) the geometric flexions in the membrane (affected by protein binding) and iv) the protein-induced membrane deformation established in trafficking.[23]

**Polymer-based synthetic membranes**

Besides amphiphilic lipids, amphiphilic block copolymers are classic components for building cell-like membrane structures. In contrast to lipids, synthetic polymers form a more stable and robust membrane that allows different chemical modifications for designable properties (Figure 2).[24-26] Until today, there is a huge selection of polymers synthesized in laboratories, giving access to diverse self-assembled structures.

Usually, the polymers are grouped in homo- and copolymers and polyelectrolytes. Homopolymers consists of repetitive monomers connected by covalent bonds.[27] The monomers are units of relatively low molecular weight. (Block) copolymers are composed of at least two different blocks of covalently attached homopolymers. In order to obtain homo- and copolymers with well-defined properties and low poly dispersity, synthetic strategies such as living ionic polymerization, controlled/quasi- 'living' radical polymerization (CRP), and (ring-opening polymerization (ROP) have been developed.[28-32]

Polyelectrolytes present an individual group of polymers that assemble to polyelectrolyte multilayer (PEM) films. These films are formed by positively and negatively charged polyelectrolytes that are alternatively adsorbed onto a template. However, polyelectrolytes are beyond the scope of this thesis.[33-35]

The amphiphilic character of synthetic copolymers (containing both lipophilic and hydrophilic groups) is fundamental for forming a polymeric membrane. The final polymer chain is

composed of several hydrophilic and hydrophobic homopolymeric blocks in different ratios. The resulting self-assembled membrane architectures (spherical, cylindrical, gyroidal, lamellar) depend on the ratio, as well as on other properties of the copolymer such as length, polydispersity and mass.[36-38] This thesis focusses especially on water-enclosing spherical polymeric nanostructures, so called polymersomes.
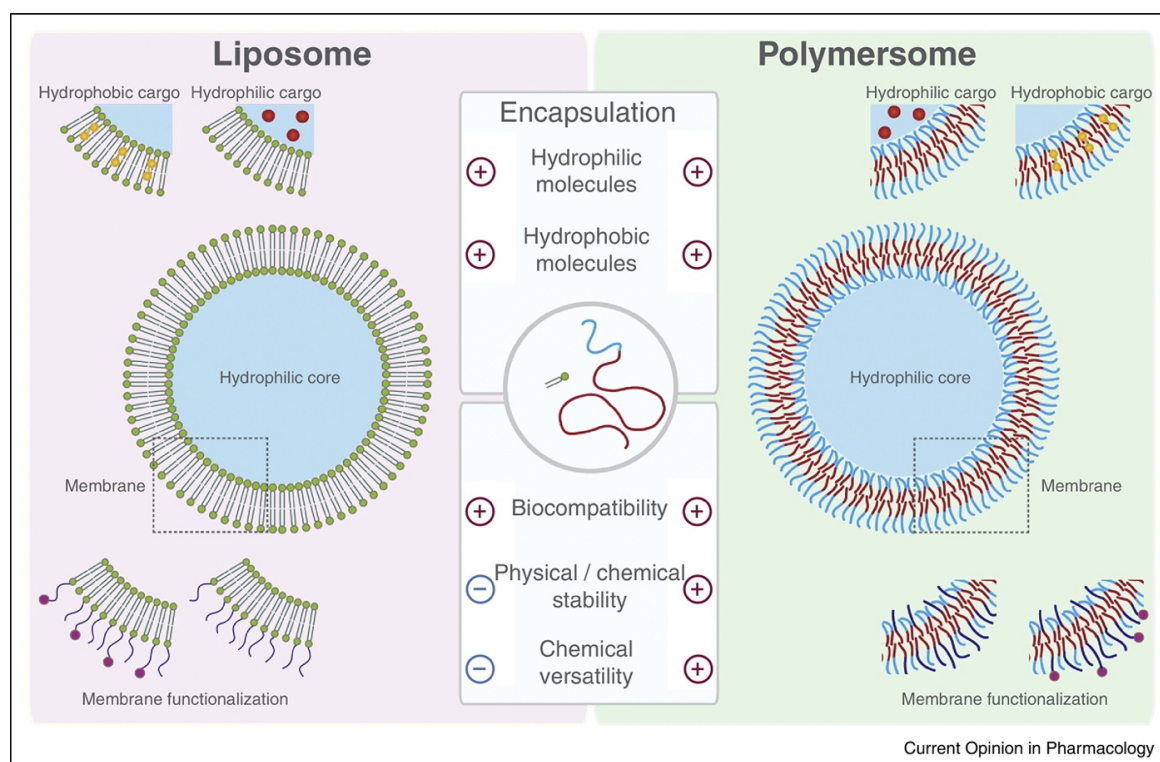


*Figure 2. Schematic representation of liposomes and polymersomes* – *Polymersomes (right) are synthetic analogues of liposomes (left) and are constituted of amphiphilic block copolymer membrane. Whilst most properties are similar for both carriers, polymersomes exhibit a high versatility and an enhanced stability. Adapted from Messager with permission.[24]*

The chemical composition of the copolymers has an essential impact on the resulting synthetic membrane and its functionality. The most common amphiphilic block copolymers used for self-assembled membranes include hydrophilic blocks such as poly(acrylic acid) (PAA), poly(ethylene oxide) (PEO), poly(ethylene glycol) (PEG), or poly(2-methyl-2-oxazoline) (PMOXA), mixed with a hydrophobic block, such as polystyrene (poly(1-phenylene-1,2-diyl), polybutadiene (PB; buta-1,3-diene), or poly(dimethylsiloxane) (PDMS).[39-41]

## Structures of 3D nanocompartments self-assembled by lipids and polymers

Synthetic nanocompartments are built up by the "bottom up" approach where lipids and polymers self-assemble to distinct structures.[36-38, 42] The most common self-assembled 3D structures at the nanoscale are nanoparticles, micelles and vesicles.[16, 43-46] All the spherical architectures are available in colloidal suspensions containing aqueous or organic solvents. The resulting structure depends on thermodynamic parameters during the formation. There are also 2D architectures based on identical components (planar membranes), but this strategy is beyond the scope of this thesis and is discussed detailed elsewhere.[47-49]

Micelles are colloidal aggregates made by macromolecules, rather smaller amphiphilic lipids and polymers. The orientation of the molecules depends on the medium they are suspended in. In contrast to inorganic nanoparticles (i.e. gold, carbonates, or iron oxide), lipid and polymer based nanoparticles have a more deformable, but less stable structure. If the lipid/polymer concentration is higher than the critical micellar concentration (CMC), micelles self-assemble. The amount of forming micelles depends on the chain length of the macromolecules, on the different interactions between the solution and on the chemical structure of the amphiphilic macromolecules (van-der-Waals, hydrogen bridge bonds).[25, 50]

A neat distinction between micelles and nanoparticles is not always possible and there are different definitions for both systems. Commonly, the term "micelles" is used for dynamic systems while "nanoparticles" are used for kinetically trapped systems. Here, the typical challenge is that the existing exchange dynamics can often not be investigated and that it is just not known whether the system is dynamic or frozen.[51, 52]

The most considerable difference between the 3D structures of nanocompartments is found by comparing nanoparticles and micelles with vesicles. Micelles/nanoparticles have a solid core. Due to steric hindrance of lipidic and polymeric chains inside the core, infiltrated bioactive components are inactive until their release. The vesicle architecture, by contrast, shows a lipidic or polymeric membrane forming a defined inner cavity (Figure 3). Vesicular structures of sizes up to 1 μm self-assembled from amphiphilic phospholipids or polymers, are termed liposomes or polymersomes.[23] The resulting hollow sphere allows the entrapment of diverse active biomolecules staying intact. The rather robust membrane of vesicles, especially a polymeric membrane, protects encapsulated cargos from external environment and prevents degradation of sensitive biological elements. On the other hand, vesicles with a lipidic membrane relate more to real cells and their organelles which supports the biocompatibility.

Depending on the favored applications, each different structure of 3D nanocompartments can be of advantage. In the following part, three very famous and dominant applications of bioactive

polymersomes are introduced; drug delivery systems, sensing nanocompartments and artificial organelles.
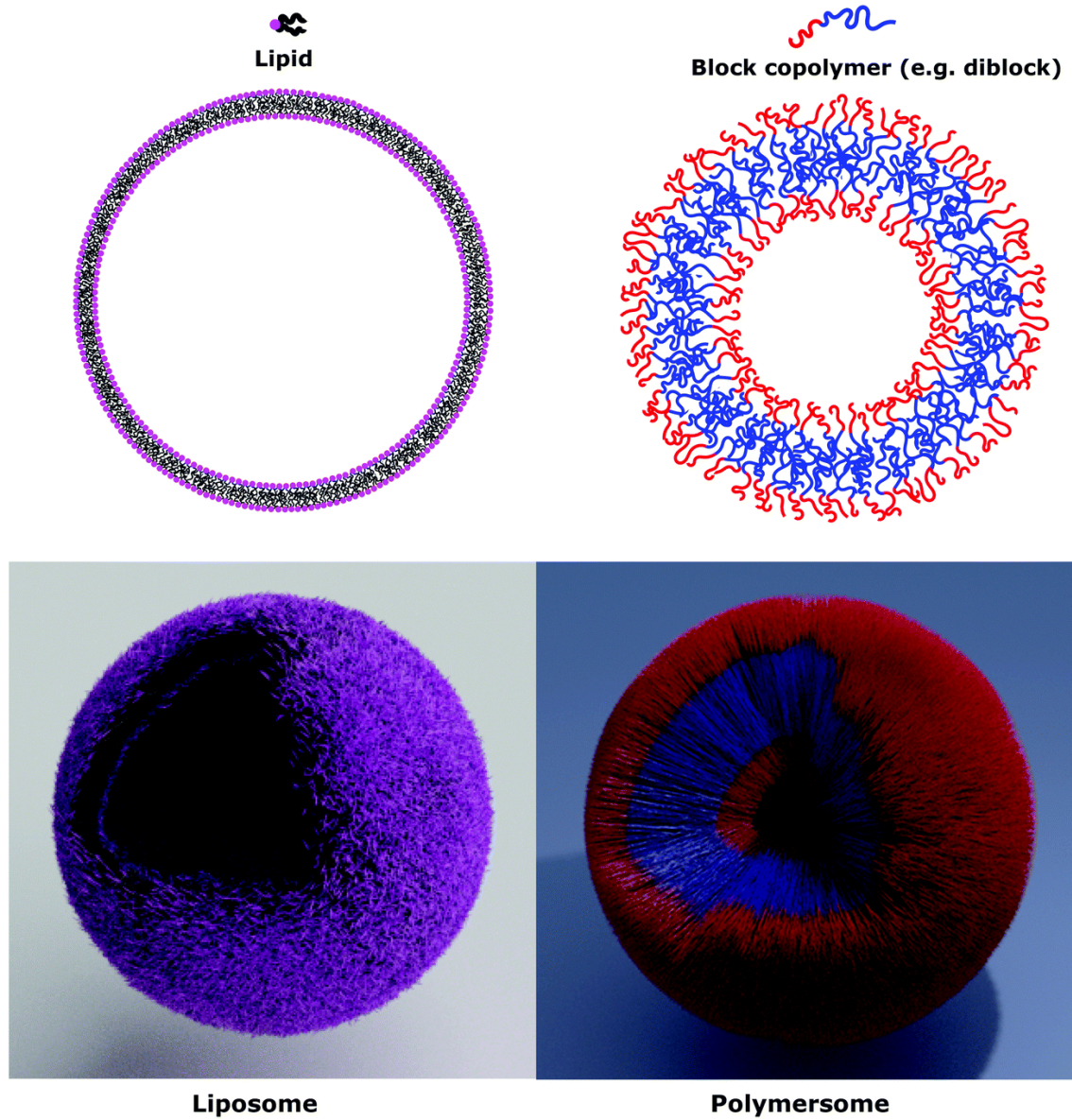


**Figure 3. Liposomes and polymersomes** – *Architecture of lipidic and polyermic vesicles presented as cross section and 3D image. Adapted from Rideau with permission.*[25]

# Self-assembled bioactive polymersomes

Living cells and their metabolism represent a complex system were various biochemical reactions take place simultaneously without reducing efficiency, and specificity. Bioactive nanocompartments are synthetic structures at the nanoscale mimicking these highly organized cellular processes and pathways. These compartments are a very promising tool in different research fields such as medicine, catalysis, and biotechnology. For developing biohybrid systems, nano-sized vesicles, especially polymersomes, are preferred over micro-sized polymeric vesicles, like giant unilammelar vesicles (GUVs). Compared to GUVs, polymersomes show a higher stability due to the enhanced surface tension caused by the smaller size. Furthermore, there is an increasing progress in the reconstitution of membrane proteins in polymersomes while such procedures have to be often optimized for GUVs.

Bioactive polymersomes show great results in therapeutics and are applied in various kinds of sensing systems for diagnostics and environmental science. These hybrid structures help to advance our understanding of engineering smart nanomaterials and allow additional insights into biological basic processes.
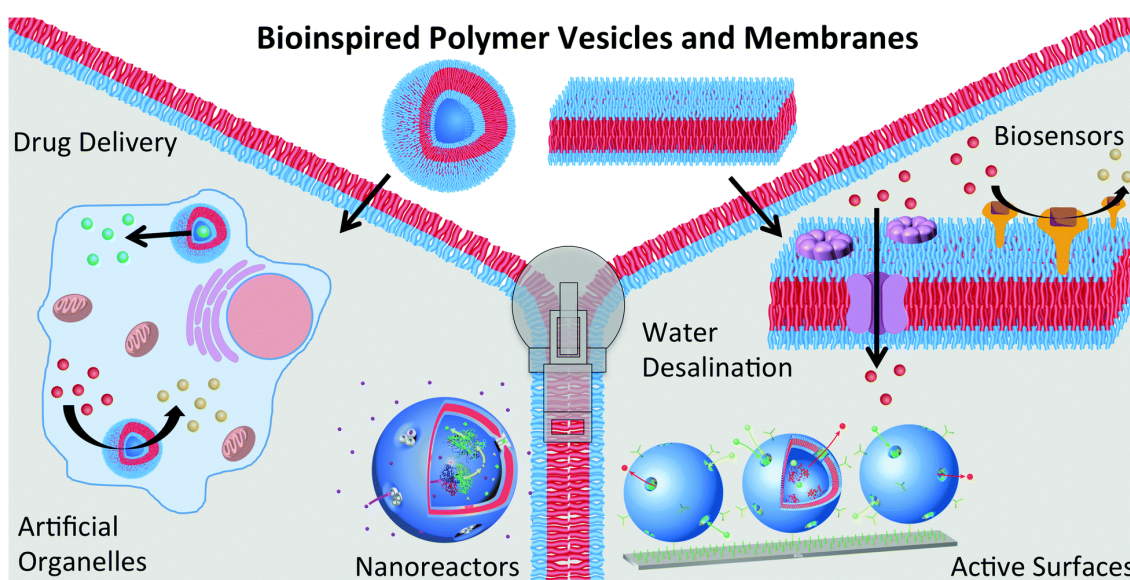


***Figure 4. Schematic representation of bioinspired polymersomes** – Conceptual overview of bioinspired polymersomes and polymer membranes highlighting some possible applications of such assemblies. Adapted from Palivan with permission.*[53]

The polymersomes are built up by the "bottom up" approach where polymers self-assemble to distinct structures. Depending on the polymer, different formation techniques have to be applied for forming nanoscale vesicular structures. The conventional techniques are the thin-film rehydration method[54-56] and solvent exchange method.[57]

With such "bottom up" techniques it is possible to combine the preparation of synthetic compartments with bioactive molecules and units. Lots of different membrane proteins have already been reconstituted in the synthetic membrane of polymersomes. Additionally, active biocompounds like enzymes, have been incorporated for developing polymersomes with engineered controllable functionalities (bioactive nanocompartments) valued for many diverse applications (Figure 4).

## Architectures of bioactive polymersomes

Polymersomes are nanoscale vesicles self-assembled by amphiphilic block copolymers representing the analogues to liposomes. In aqueous media the hydrophilic block of a diblock exposes to the surface, while the hydrophobic block form the inner part of the membrane. However, depending on the copolymer, the membranes will have a different morphologies. In the resulting membrane, the polymers are commonly aligned as as bilayers in case of diblocks (AB). Symmetric triblock copolymers (ABA) have to possible conformations: the hydrophobic block can either form a loop so as the hydrophilic chains are on the same side of the membrane (U-shape) or they can stretch forming a monolayer with the two hydrophilic blocks at the opposite sides of the membrane (I-shape). ABC triblock copolymers assemble into asymmetric membranes where the internal and external surface chemistry differ from each other in the resulting polymersomes.[58, 59] The orientation of the hydrophilic block polymers depends additionally on more parameters such as steric hindrance and polymerblock lengths. Bigger and more bulky blocks form the outer surface of the polymersomes.[60, 61]

The thickness of polymeric membranes ranges from 5-30 nm, depending on the polymer chain length.[59] The size of the polymersomes is often affected by the polymersome formation method which has to be selected accordingly for different polymers. In order to obtain high monodispersity and a decreased size distribution, the polymersomes are usually extruded with filters having defined pore sizes. In order to form vesicles by self-assembly, determining parameters have to be taken into account carefully: i) the packing parameter ($p = v/a_0 l_c = 0.5 - 1$), ii) the hydrophilic to whole mass balance in a range of 25 - 45% ($f$-value), and iii) the polydispersity index (PDI) of approximately 1 of the amphiphilic block-copolymer ($v$ = volume of hydrophobic part, $a_0$ = contact area of head group, $l_c$ = length of hydrophobic part).[36-38, 62-65]

With regard to the robust and thicker membrane of polymersomes, different strategies have been investigated in order to increase and control the permeability while the polymeric structures stay intact for extended periods of time.[59] Depending on their chemical nature, homo- and copolymers are able to form polymersomes with intrinsic stimuli-responsive properties, especially pH-responsiveness. For example, polymersomes self-assembled by copolymers with tertiary, protonable amine groups show reversible swelling properties (breathing membrane) at distinct pH-values. Such pH-sensitive copolymers can include a PDEAEMA (poly(2-(diethylamino)ethyl methacrylate)), PDMAEMA (poly(2-(dimethylamino)ethyl methacrylate), or PAD (poly(N-amidiono)docecyl acrylamide)) as protonable block.[66-68] Further polymers forming pH-responsive polymersomes are PAA[69, 70] and PSS (poly(styrene sulfonate)).[71] Additionally thermoresponsive polymersomes based on PNIPAM (poly(N-isoproylacrylamide)) have been successfully developed where the thermosensitive PNIPAM forms hydrogels *in situ* when the temperature is raised above the lower critical solution temperature.[72]

Another strategy for developing permeable poylmersomes describes stable, non-responsive vesicles, where the spontaneous formation of a porous membrane is effected by organic solvents or particular stimuli-responsive biomolecules. In contrast to organic solvents, biomolecules achieve a triggerable and thus, a more controllable permeability and present the focus of this chapter. A promising approach to allow a more controlled and selective permeabilization of the vesicles for protons, ions or small molecules is achieved by reconstituted membrane proteins and biopores. Up to now, lots of different membrane proteins have been successfully inserted; among them i) channels and pores (Outer membrane protein F; OmpF[12, 14, 73-75] , Aquaoporin; Aqp0[76], FhuA (ferric-siderophore transporter)[77], maltose pore protein; LamB[78], ii) transporters of ions and electrons (a-Hemolysin; aHL, ionomycin for divalent cations), and iii) channel forming peptides, like melittin and gramicidin (gA).[79, 80] Additonally, mutants of OmpF, especially, present an elegant strategy to develop stimuli-responsive permeability. Even though the engineering and expression of OmpF mutants require complex procedures, the resulting advantages overcome this issue. For example, a pH dependent diffusion efficiency through OmpF 6His mutant was observed where the histidine substitutions strongly influences the local electrostatic field, the channel diameter and the constriction zone. The total charge states of histideines resulted in a pH-dependent release when reconstituted in nanocompartments.[81] Second, OmpF mutants have been used to allow a selective modification of the proteins resulting in a stimuli-responsive opening/closing of the pores in polymersomes presenting the focus of the following chapter.[12, 15] Due to this, such

biohybrid nanosystems are a very promising tool for different technologies in the fields of bioengineering and biomedicine.[82]

For a successful reconstitution of membrane proteins, it is essential to choose the appropriate polymer that supports the correct orientation of the protein while preserving the natural functionality. A functional reconstitution requires polymers forming a flexible enough membrane. The polymers have to conform to the lager hydrophobic parts of the protein by coiling.[53, 59, 82] Especially larger proteins (3.3-7.1 nm) induce imbalance in hydrophobic interactions with the block copolymers (9-13 nm) and hamper the functionality of the protein. A sufficient flexibilty of the copolymer allows the reconstitution of membrane proteins although the resulting synthetic membrane is thicker than the protein itsself. Moreover, the polydispersity of the copolymer might also be an essential requirement as smaller polymer chains arrange around protein while longer chains form the stable membrane of the polymersomes to allow a successful insertion.[83] Moreover, a membrane self-assembled by ABC block copolymers allows a specific orientation of the membrane protein due to the different hydrophilic parts.[84] Triblock copolymers composed of PMOXA-*b*-PDMS-*b*-PMOXA are also great candidates for the insertion of proteins in synthetic membranes as they combine all fundamental requirements and present the focus of this part. The PDMS block offers suitable flexibility and fluidity to entangle the protein while providing the stability of the membrane.[83] With regard to the membrane proteins inserted in polymersomes, mild conditions including temperature, pH, aqueous medium, are essential for a successful reconstitution as membrane proteins are often very fragile and easily denaturate outside the cellular membrane. Therefore, For the orientation-specific reconstitution of different membrane proteins into polymersomes, diverse worked-out strategies are necessary. One strategy is the particularized membrane destabilization of the vesicles by detergents before adding the protein or the incorporation during the self-assembly process (post-hoc insertion). The operation process has to be often optimized for each membrane protein, but the general key step of all methods is the removal of the detergents the proteins are usually resuspended.[83]


**Polymersomes with modified membrane proteins and channels**

Remarkable progress in functionalized polymersomes has been obtain by reconstituting genetical and/or chemical modified protein gates, where the diffusion of molecules can be triggered by a certain stimulus.

An example for chemically engineered proteins embedded in polymersomes, describes the targeted modification of the lysin residues found inside the channel of FhuA in order to build a

reduction-triggered release system.[77] The chemical labels bind to the key amino acids and block the molecule passage through the pore until dithiothreitol (DTT) addition, that induces the cleavage of the labels. An example for genetic modification of membrane proteins, presents a mutant type of OmpF, where cysteine have been induced by point mutation.[12] In order to achieve stimuli responsive permeability of the vesicles, different molecular caps are linked to the thiol group of the cysteine.

Besides controllable permeability, the polymersome membrane can be functionalized with membrane proteins for performing distinct biochemical reactions. One approach utilizes the simultaneous incorporation of a light driven proton pump bacteriorhodopsin (BR) together with the molecular motor protein $F_0F_1$-ATP synthase. Via cascade reaction triggered by external illumination, the photon energy is transformed into chemical energy. BR builds up a proton gradient across the polymer membrane which subsequently supports the catalyzed conversion of ADP into ATP, the universal energy source in cells.[85-87]

All these examples confirm that the concept of functionalizing polymersomes by the reconstitution of proteins into the membrane was translated into action. Besides membrane proteins, lots of different catalytical active biomolecules, like enzymes, were used for equipping polymersomes for comprehensive biorelated processes, introduced in the following chapter.


**Polymersomes equipped with catalytic biomolecules**

Polymersomes offer a great potential to load hydrophilic cargoes in the aqueous core and hydrophobic parts in the synthetic membrane, respectively.[88] Via thin-film rehydration method hydrophilic compounds, such as enzymes, are added to the aqueous phase (rehydration buffer) and then are passively transferred into the polymersomes.

In contrast to enzymes free in solution, enzymes encapsulated inside polymersomes are protected from denaturation by environmental conditions and exhibit prolonged activity. Examples of enzymes are protease[89], horseradish peroxidase[12, 90], uricase and superoxide dismutase[91] that have been encapsulated in polymersomes for developing catalytic nanocompartments (CNCs). Furthermore, the enzyme NADH:Ubiquinone oxidoreductase complex I has been functionally reconstituted in the membrane for creating an active surface that mediates the electron transfer from NADH to ubiquinon.[92]Besides enzymes, other active biomolecules have been encapsulated in polymersomes like Rose Bengal Bovine serum conjugate serving as photosensitizer[93], or haemoglobin as oxygen carrier.[94] The concept behind of the

Even further, it was possible to combine different CNCs working in cascade reactions or to entrap simultaneously more than one enzyme inside the cavity of one CNC.[90, 95] Mostly, such bioactive polymersomes were also functionalized with (modified) membrane proteins to enable the (controlled) diffusion of external substrates and products formed by enzymatic reactions inside the compartments.[90]

## Characterization of bioactive polymersomes

The different characteristics of bioactive polymersomes, like size, vesicular nanostructure, homogeneity and surface charge have to be confirmed and analyzed. Overall, there are two key techniques, light scattering and microscopy.

Nanotracking particle analysis (NTA), static and dynamic light scattering (SLS and DLS) are often used in combination to determine the size distribution, concentration and architecture of polymer self-assemblies (hollow sphere or solid particle). By measuring electronic mobility of polymersomes between two electrodes, the resulting zeta potential reveals information about the surface charge.[96, 97]

Confocal laser scanning microscopy (CLSM) is a frequently used optical imaging technique to visualize nanostructures that are labelled with fluorophores. CLSM allows the visualization of fluorescently labelled polymersomes located inside mirco-sized structures (like cells).[98] In case of reconstituted membrane proteins in polymersomes, fluorescence correlation spectroscopy (FCS) analyzes how many biomolecules are incorporated if they have been fluorescently labelled. FCS measures the diffusion time of fluorescence objects at already low nanomolar concentrations through a small confocal volume where the size and concentrations can be determined.[99-103]

## Prominent potential applications

Due to designable multifunctionalities, bioactive nanocompartments, especially polymersomes are applied intensively in a lot of different medical (nanomedicine) and scientific research domains (nanomaterials). By taking a closer look, the detailed application methods of micelles/nanoparticle-based bioactive compartments differ from vesicle-based systems. In order to release the cargo with selective responses and functions, solid structures like micelles/nanoparticles have to decompose. Encapsulated biocompounds in vesicles are active and are able to move freely inside the cavity. In addition to this, the synthetic membrane of the vesicles can be designed to show selective permeability towards particular signals and

molecules, which allows a strong functionality without losing the initial structure of the compartment.

**Drug delivery systems**

Polymersomes are an efficient therapeutical delivery system. They are able to incorporate two or more agents, enhance water-solubility of drugs, improve the drugs' half-life in blood circulation and achieve a controlled drug release and targeted delivery (Figure 5).[46, 67, 104, 105] All these properties minimize the side effects and toxicity of the drugs and lowers the frequency of taking the medication.

In the past few decades, a large number of therapeutics based on bioactive nanocompartment has been clinically approved and a few pioneering systems became commercially available. In near feature the number of such drug delivery systems will increase strongly. Among these systems, the polymeric and liposomal (lipidic vesicles) platforms present the main elements with ca. 80%.[106] The unique properties of liposomes are remarkable and their popularity in therapeutics has been still growing fast. These vesicles are able to encapsulate successfully both hydrophilic and hydrophobic compounds, they can be functionalized by designed ligands for achieving targeted binding on particular cells, and much more talents are investigated. A very interesting strategy describes the equipment of liposomes with biocompatible polymers, like polyethylene glycol (PEG), to prolong their half-life in vivo. This technique was also adapted for nanoparticle-based therapeutics, especially for delivering sensitive anticancer chemotherapeutic drugs with adverse side effects.[106]
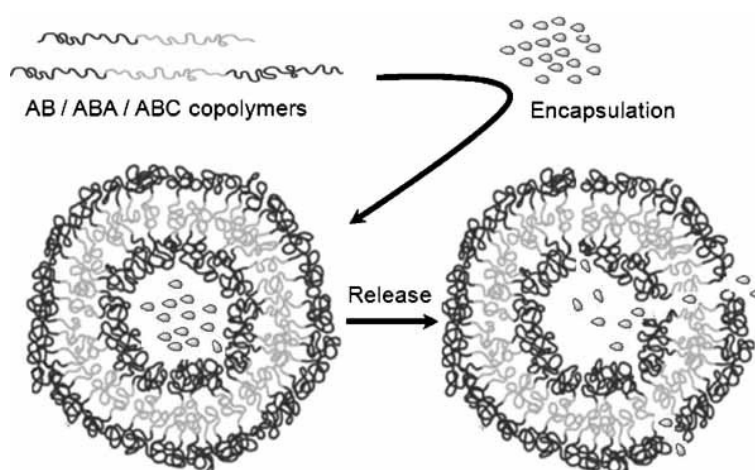


*Figure 5. Schematic representation of polymersomes applied as drug delivery systems – By encapsulation of the drug into the polymersomes it is protected from external compounds. Upon*

*a certain stimulus the drug is relaused from the vesicles. Adapted from Onaca with permission.[107]*

Consequently, the next advancement in drug delivery systems are vesicles based on polymers only. These polymersomes show the same skills as liposomes and more.[108] Research over the last two decades has yielded significant progress in the development of polymersomes for drug delivery. The vesicle membrane contain stimuli-responsive polymers resulting in a physical/chemical change or disruption in the structure to release the cargo (drug).[109] Examples for the stimulus are light[110, 111], biomolecules[112, 113], temperature[114, 115], pH[116-118], reductive environment[119, 120] and magnetic fields.[121, 122] Additionally, the enhanced stability of polymersomes, half-life and surface properties support greatly the modification with ligands (antibodies, receptors for parasite binding) and justify polymersomes as a very promising tool in therapeutics.[123, 124]

**Sensing polymersomes**

In this part, two different categories of polymersomes with detecting skills are distinguished. The first category comprises nanovesicles that create a measurable signal as a response to a certain stimulus. However, during this process the structures disassemble, like in case of drug delivery systems. Those compartments are mostly applied as direct detection or imaging contrast agents to identify irregular fragments in the body.[124-128]

The second category describes polymersomes that stay intact, and can function as applicable sensors. As polymersomes form a more robust membrane than liposomes, they are eligible for the second category, which presents the emphasis of this thesis and is further discussed in detail regarding bioactivity in chapter 4.[129, 130]

In diagnostics, synthetic vesicles are used for a selective and local detection of specific pathological disease-related conditions, especially for tumor cells causing change in pH, redox potential or glucose concentration. As the sensors are expected to maintain their structure and function, polymersomes attract most of the attention. The additional modification of the polymersomes with biomolecules results in nanocompartments exhibiting cellular and molecular functions. Such bioactive polymersomes or biohybrid systems, contain synthetic polymers and biological components (proteins, enzymes) and are valuable candidates as nanosensors (Figure 6). Their structural integrity and stimuli responsiveness are prevented over a longer period of time. The sensing mechanism is based either on the insertion/attachment of stimuli-responsive biomolecules (proteins) and/or on the encapsulation of active

(bio)molecules (dyes, enzymes). Inside the vesicles, a signal like colorimetric change or fluorescence is produced for detection.[75, 131-134]
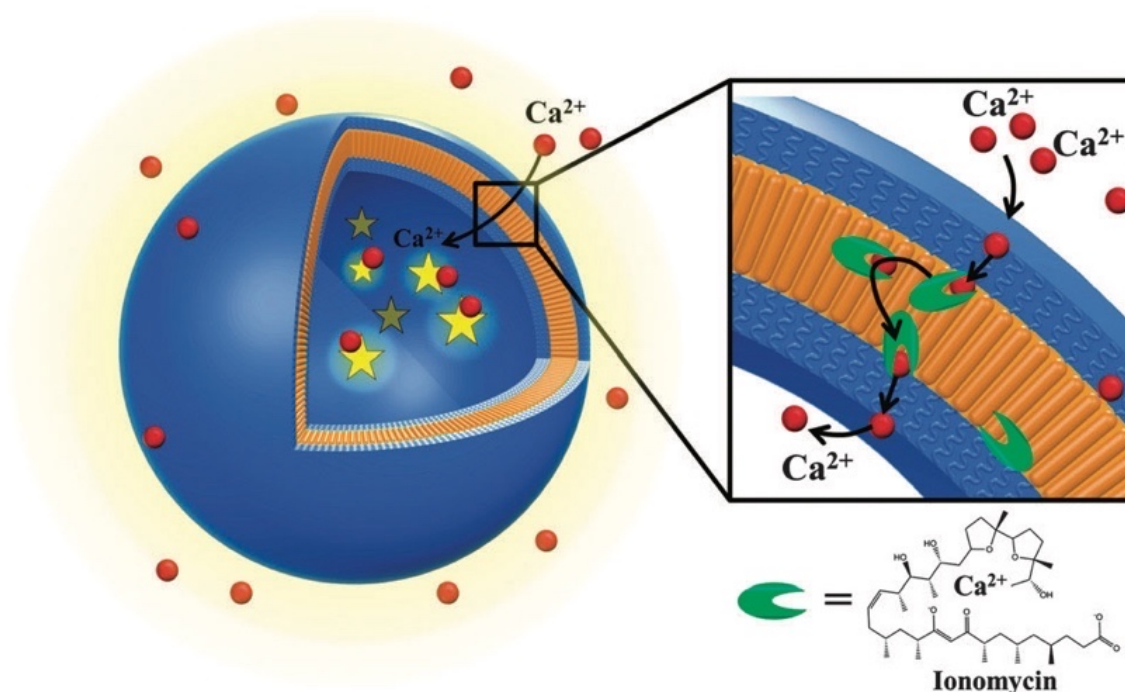


***Figure 6. Schematic representation of a potential ion sensor based on polymersomes*** *– Design of $Ca^{2+}$-selective permeable membranes by insertion of ionomycin into polymersomes. Adapted from Lomora with permission.[80]*

Polymersomes with biopores reconstituted in the membrane are promising candidates for sensing pathological conditions. For example, the membrane proteins aquaglyceroporin GlpF has been successfully inserted in the polymer membrane and allow selective permeabilization for small sugar alcohols.[135] The predominant membrane protein is OmpF and OmpF mutants.[12, 15, 75] Due to its stability, triggerable functionalities of OmpF can be engineered which is described in the third chapter in detail.

Besides membrane proteins, chemically tuned polymers forming the membrane are able to support the selective permeability of the vesicles due to their chemical nature causing attracting/distracting forces with external compounds.[66]

**Artificial organelles**

Catalytic polymersomes have remarkable abilities as sensors and concurrently as simplified artificial organelles. Such nanocompartments respond to a stimulus in a bioinspired manner related to the behavior of natural organelles in cells.[45, 95, 136]

Polymersomes equipped with active biomolecules (catalytic nanocompartments) are useful vehicles serving as artificial organelles. The idea of artificial organelles describes such catalytic nanocompartments (CNCs) that have been taken up by cells and performed particular reactions inside them. The aim is to replace damaged or missing cellular pathways with implanted artificial organelles and to facilitate techniques based on metabolic reactions steps used in the fields of tissue engineering and synthetic biology.[71, 137]

One famous example are catalytic nanocompartments working as artificial peroxisomes in cells. Natural occurring peroxisomes contribute to a defense mechanism against reactive oxygen species (ROS). In order to achieve such a detoxifying process, two antioxidant enzymes were encapsulated into polymersomes transforming superoxide radicals and $H_2O_2$ into oxygen and water via a 2-step, cascade reaction. OmpF serving as the gate for substrates and products was reconstituted into the polymeric membrane to allow a constant exchange with the external environment. In case of a high ROS occurrence (oxidative stress) associated to different diseases like arthritis, the artificial peroxisome as cellular implant is expected support the overextended organism and to recover the metabolic balance.[136]


**Compartmentalization within cell-like compartments**

In real cells, metabolic reactions are performed in organelles (subcompartmentalization) in order to provide the perfect conditions (pH, concentration of ions) appropriate for each specific need. This complex architecture performing different biochemical reactions simultaneously is the inspiration of developing cell-mimicking platforms. Cell-mimicking platforms became indispensable as tools in various scientific domains such as the design of microrecators and the investigation of cellular processes. Therefore, the aim is to develop cell-mimicking compartments combining different cell functions and including complex compartmentalization like in living cells.

This functional principle of subcompartmentalization in real cells can be adopted for microcompartments, like synthetic GUVs (Figure 7) to design cell-mimics.[39, 138, 139] The prospective challenge is to create so-called artificial cells with multicompartmentalization where diverse subcompartments with different activities and membrane permeabilization are able to perform metabolic pathways. Here, different kinds of nanosized CNCs (liposomes or polymersomes) serve as subcompartments in the GUVs and catalyze one reaction or a cascade reaction in case of multicompartmentalization (two or more different CNCs inside the cavity).[140] Due to the high stability, GUVs formed by polymers attact a lot of attention in this research field. The co-laoding of such GUVs with different nanoobjects is achieved

simultaneously by using film rehydration method. For example, an external signal can be transduced between structurally diverse nanocompartments (particles, vesicles) serving as artificial organelles in GUVs. By supplying this system with an additional cytoskeleton component (actin), the multicompartment is able to form an internal cytoskeletal network (actin polymerization) via ion channel recruitment from the environment.[141] The preparation of multicompartments by film rehydration method, however, shows some challenges like the low encapsulated content and limitations in membrane compositions. To achieve a fine control of these parameters, the preparation of multicompartments by double emulsion microfluidics attacts a lot of attention.[139] The resulting GUVs are able to serve as a ideal cell-sized template with a very narrow distribution of GUV size and internal content.[142]
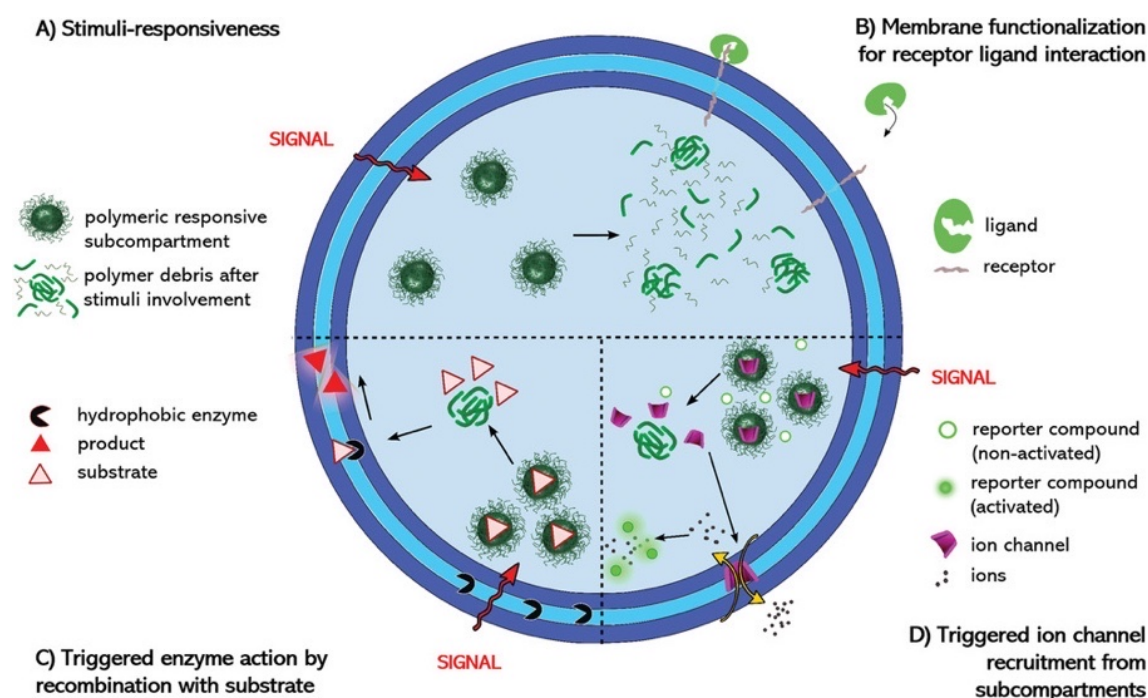


***Figure 7. Subcompartmentalization within GUVs*** *– Schematic representation of multicompartment system composed of reduction sensitive subcompartments for triggered enzymatic activity and ion channel recruitment, encapsulated within polymeric giant unilamellar vesicles. The reducing agent DTT was used as the signal (red arrow) that passively traverses the polymeric GUV membrane without addition of biopores or channels. Adapted from Thamboo et al. with permission.*[140]

Additionally, multicompartmentalization can be performed by transferring bioreactive polymersomes in GPMVs to create bioinspired molecular factories and customizable cell mimics. The advantage of GPMVs over all GUVs is the very cell-similiar composition that

cannot be achieved via bottom-up approaches. The GPMVs are directly formed by cells. Recent studies further showed that polymersomes inside GPMVs are able to perform distinct catalytic reactions and demonstrate that also GPMVs can be supplemented with nanocompartments serving as artificial organelles.[14] In fourth chapter, the procedure of transferring nanoscale objects from cells into GPMVs is discussed in detail with the focus on optimized conditions for an efficient GPMV modification.

# GUVs as cell-like compartments based on lipid and polymer membranes

Lipid- or polymer-based compartments at the microscale, are termed giant unilamellar vesicles (GUVs). GUVs are a very promising platform for the reconstitution of a wide variety of membrane or peripheral proteins resulting in complex biomimics. Due to this, GUVs have been widely used for developing artificial cells models in order to understand cellular functions and to investigate bilayer interactions within the membrane. In the 19th century, cell-free enzymatic reactions have been discovered for the first time, showing that biochemical reactions don't necessarily require the whole living organism.[143] In the following century, the concept of building up synthetic vesicles at the microscale via "bottom up" approach attracted a lot of attention.[144] These compartments include lipid- and polymer-based GUVs[138, 145-148] lipid coated porous silica nanoparticles[149], layer-by-layer capsules[150], membrane free microdroplets, and microscaled proteinosomes.[151]

GUVs are regularly used in synthetic biology. They are able incorporate a huge number of different biomolecules or inorganic compounds that undergo, initiate or catalyze distinct reactions in a very effective manner (Figure 8). The most prominent reactions are those catalyzed by stable enzymes found in the cavity of biomimicking compartments. These cell mimics have a great potential for synthetizing proteins[152], synthetic polymers[153], and RNAs.[154] Concurrently, GUVs are a valuable tool for determining the molecular parameters supporting a single, systematically isolated reaction existing within the whole complex metabolism. In cells, many interactions between different biomolecules or assemblies take place at the same time and it is impossible to define each single pathway.[155] However, GUVs are simultaneously cell-like and simple enough to gain new aspects of essential biological processes without giving biased measurement data.

Another advantage of GUVs over living cells is the facilitated handling. Cells have to be cultivated under certain conditions including temperature, $CO_2$ atmosphere and nutrition. The stability and working efficiency of the biomimicking compartments, lacking of an own metabolism, are commonly independent of the external environment.
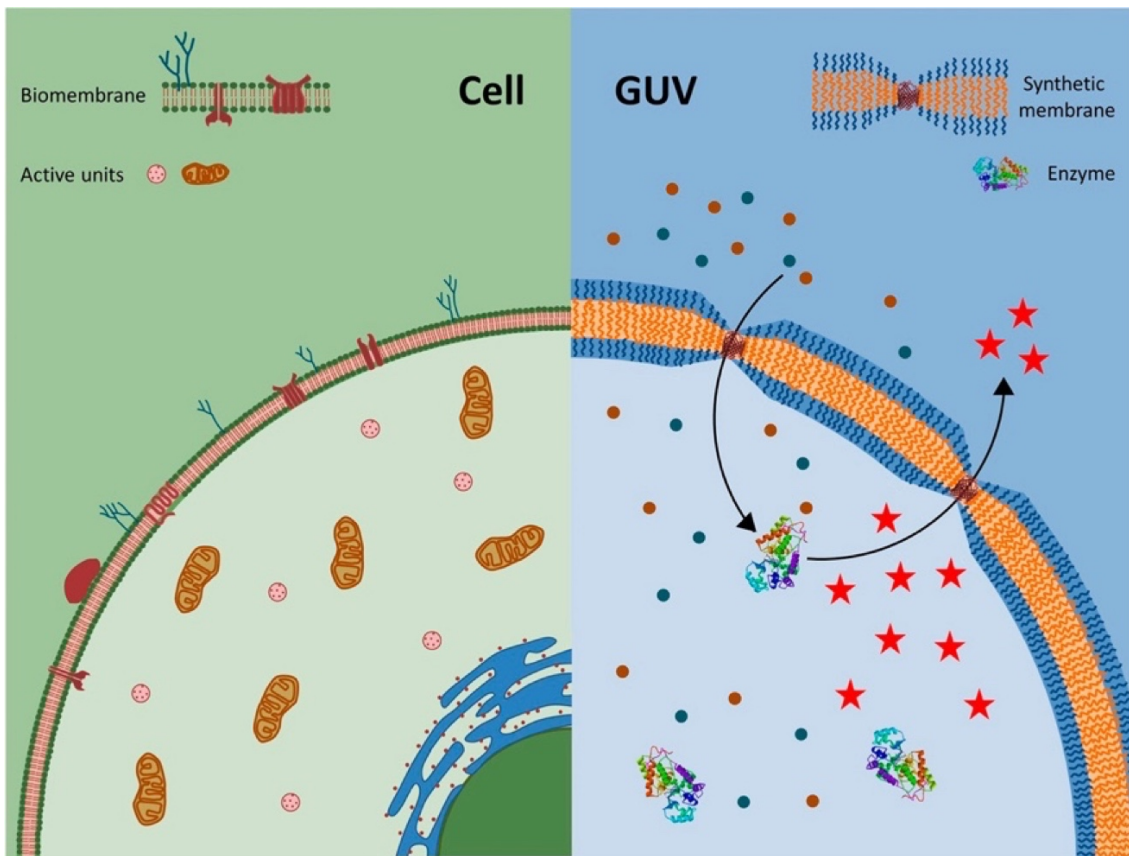
*Figure 8. Comparison of real cell and synthetic GUV* – *Design of (left) a natural cell and (right) a synthetic giant unilamellar vesicle (GUV) with encapsulated enzymes engineered for selective permeability to substrates and products based on reconstitution of outer membrane protein F (OmpF) to visualize a model enzymatic reaction inside the cavity. Adapted from Garni with permission.[13]*

## Why cell-like compartments?

A central objective in biology is the template-dependent generation of the inseparably associated units of life. The cells of all organisms consist of four essential macromolecular components: Lipids, glycans, nucleic acids and proteins (Figure 9).[14, 156] Within living cells, the fundamental builidng blocks form highly complex, but well-organized structures that work with remarkable efficiency and precision on the molecular and atomic level.[157] I order to cur diseases effectively, we have to acknowledge and understand the fundamental building blocks of life first; how they are constructed and interact during the cell metabolism with all its diverse reaction steps.
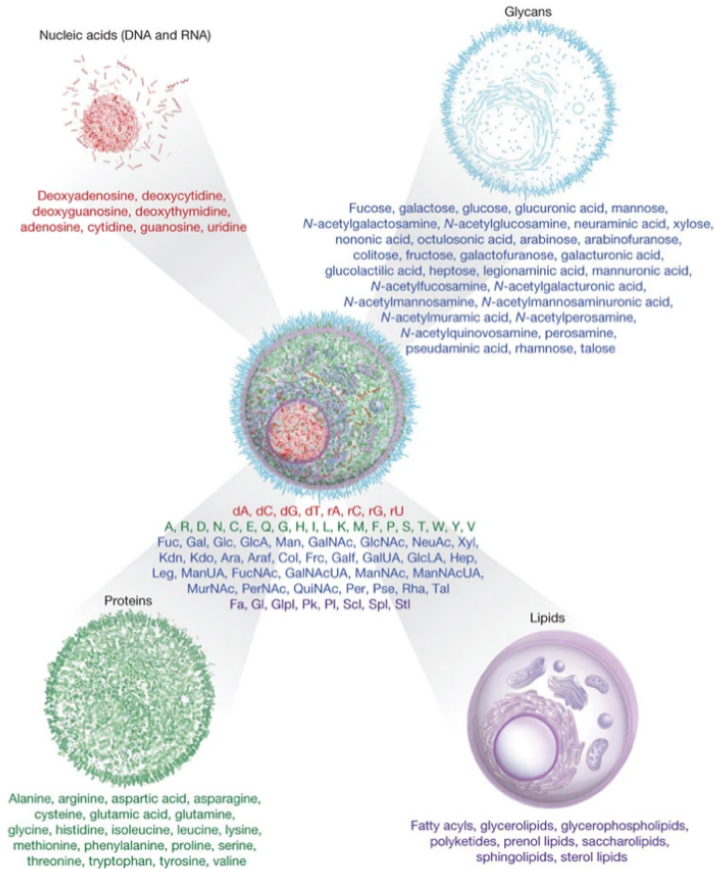
**Figure 9. The molecular building blocks of life** – *The four fundamental macromolecular components (lipids, glycans, nucleic acids and proteins) are built up by 68 molecules. Adapted from Marth with permission.*[156]

To get a better insight, cell-mimicking compartments have been created. The compartments show a high complexity and multifunctionality similar to living cells. They have distinct cell-like functionalities and are able to perform complex biochemical reactions and transformations.[158] Based on biomimicking compartments as platform, researchers could yield the information how metabolism, the fundamental prerequisite of living organisms, arose in organic frameworks. Overall, biomimicking compartments have great a potential in lots of interdisciplinary scientific fields in biotechnology, medicine and material science.[138, 159, 160] Besides treating diseases, it is possible that such synthetic biomimicking platforms will enable to assemble alternative tissues and organs. So, necessary transplantations won't be longer dependent on finding the right donors.

The living cells were discovered two centuries ago and up to now, various different achievements have been made that will bring the researchers' ambitious dreams closer of designing and creating cell mimics.[158] The main strategies for building up cell mimics and

biomimicking compartments in the microscale are: i) the "bottom-up" and ii) the "top-down" approaches. The "top-down" approach allows the manipulation and reengineering of the cells by using well-developed biotechnological tools.[161] This technique is based on the genetic modification of living cells (i.e. stem cell) to create so-called "minimal cells".[158, 162] In general, the "top-down" approach is suitable for designing fully functional cell mimics. The resulting artificial cell models are customized to the respective requested objective and fulfill different requirements. Their complexity is closer to the non-engineered cells than the compartments obtained from "bottom-up" approach. However, like in case of real cells, the high complexity can be a disadvantage as it is difficult to follow a distinct biochemical pathway.[162, 163]

The "bottom-up" approach starts with single components on the molecular level that are built up to consistent structures *in vitro*. Synthetic compounds such as lipids or polymers are assembled form the membrane of the micro-sized compartment which can be equipped with biological molecules for functionalization. Various different combinations have already been applied to create cell mimics that are able to accomplish biorelevant processes and biochemical reactions for defining structural parameters. Scientific disciplines using these cell-like compartments focus on designing simplified cell mimics to gain insights into the function of the very complex metabolism. In contrast to a living organism, where millions of actions take place, the "bottom-up" cell mimics undergo a limited number of processes that can be observed carefully and precisely in order to disclose basic working principles in biology.[145, 146, 164-166]

As this work focuses primarily on GPMVs as cell-mimicking platform, the basics and concept of lipid and poymer-basased GUVs are shortly summarized in the following.


## Building up GUVs

### Lipid-based GUVs

Lipidic GUVs have a size of at least 1 μm and the membrane is based on phospholipids forming a thin bilayer of approximately only 5 nm, similar to living cells. Latest research results have advanced lipid GUV systems including complex lipid compositions. Such GUVs exhibit controlled asymmetries and allow detailed studies of membrane protein structures and the corresponding functionality in cell-like model membranes.[167]

Besides phospholipids, minimal artificial cells incorporate additive biomolecules, such as DNA or proteins to perform elemental cellular functions. Two prominent technologies for producing such lipid-based artificial cells are "bottom-up" approaches, where membrane proteins extracted from living cells are reconstituted into GUVs. The compartments were formed by either the gentle hydration method (conventional method)[80, 168] or by microfluidic.[169-171]

Compared to the hydration method, microfluidic technology achieves the formation of very monodisperse, unilamellar giant lipid vesicles in higher concentrations and with a more efficient encapsulation rate.

**Polymer-based GUVs**

Up to now, several biopores have been reconstituted in polymer GUVs in order to allow controlled permeabilization towards ions and/or molecules. The conventional formation of lipid GUVs can be easily adapted to polymer GUV formation, if the differences in thermodynamic self-assembly of polymers have to be taken into account. Additionally, microfluidic double emulsion processes were successfully developed in order to produce polymer GUVs with diverse biofunctionalities including enzymes.[142]

However, lots of protein reconstitutions successfully implemented in lipid membranes, are not readily applicable to synthetic copolymer membranes; the different physicochemical properties of polymer membranes strongly affect the interactions between membrane and protein. Compared to lipid membranes, synthetic polymer membranes have a much higher molecular mass and a considerably thicker membrane with more limited flexibility and fluidity. These properties result in a length mismatch between the hydrophobic domain of the copolymer membrane and the membrane-spanning hydrophobic domain of the protein. Additionally, the polymer membrane is more fragile towards detergent-containing solutions, in which isolated membrane proteins are commonly stored in. To overcome this issue, hybrid GUVs were formed by phospholipid and block copolymers. The membrane consists of a lipid/polymer mixture that combines the biocompatibility and cell-membrane-resemblance of lipids with the robustness and chemical versatility of polymer membranes.[13, 79, 172]

# GPMVs as cell mimics

Synthetic GUVs represent the simplest cell-like platform due to limited complexity regarding internal composition. In contrast to GUVs, giant plasma membrane vesicles (GPMVs) are directly formed by cells and thus, contain most of the cellular components expect larger organelles, polymerized cytoskeletal elements or internal membranes. GPMVs are filled with cytoplasm and its membranes are rich in lipid and protein components corresponding to the plasma membrane of the donor cells.[173] GPMVs as non-living organisms, are probably the most innovative solution for creating "biological" cell-mimicking compartments, with partly identic cellular composition. Although GPMVs are the closest and most similar to cells up to today, they have been unnoticed as cell-mimics for years.

In this work, "bottom up" and "top-down" were combined to create GPMVs as cell-like compartments. This approach uses eucaryotic cells that have taken up non-natural occurring components for distinct functionality. These modified cells are then treated in order to produce very cell-like but not living microscale compartments bearing the synthetic components as well. Here, the complexity and functionality of GPMVs can be enhanced in a controlled manner by systematically increasing the number the components inside as it was performed with GUV modifications. Due to this, the construction of a cell-like compartment is continuously approximating real cells.

## GPMVs as promising cell-like compartment derived directly from cells

Naturally occurring vesicles produced by cells are an attractive alternative to synthetic compartments. For example, exosomes have a great potential for drug delivery systems as they achieve targeted delivery which still presents a challenge for other cell-mimicking vesicles.[174-176] However, the drawback of exosomes are their limitations regarding production and modification. Therefore vesicles formed from cellular oganelles with promising properties for additional modification have been investigated for their potential as exosome-mimics.[177, 178]

Additonally, GPMVs have been considered as promising alternative to exosomes and present the focus of this chapter. As the name indicates, GPMVs are derived from the plasma membrane of cells. GPMVs are naturally formed by cells if they are exposed to huge stress such as lack of food. In contrast to exosomes, the formation of GPMVs and the subsequent isolation from the donor cells have already been optimized for high yields under laboratory conditions. Here, GPMVs are systematically formed by treating the cells with very high salt concentrations, reducing agents or laser irradiation causing local delamination of the plasma membrane from

the underlying cytoskeleton.[179-181] The ensuing protrusions of the cell are then filled by a passive flow of the cytoplasma resulting in a GPMV.[182-184] GPMVs contain almost all cellular components expect larger organelles such as the nucleus or Golgi apparatus regarding the inner composition as well as the outer membrane structure.[181, 183, 185, 186]

GPMVs were used as platform for studying the compositional and structural characteristics of the plasma membrane before and after interactions with external compounds.[187-189] In addition, a detailed investigation of the properties of the membrane associated IgE-receptor complex was described.[190] Another research area also started dealing with the development and characterization of planar supported membranes received from GPMVs and exploited GPMVs as host-cell model for drug delivery.[182, 191] Studies regarding the high potential of GPMVs as artificial cells are still very rare.[184, 192] However, in fourth chapter of this work we describe a new promising strategy of using GPMVs as cell-mimicking systems in order to overcome the current challenges of designing ideal cell-like compartments.
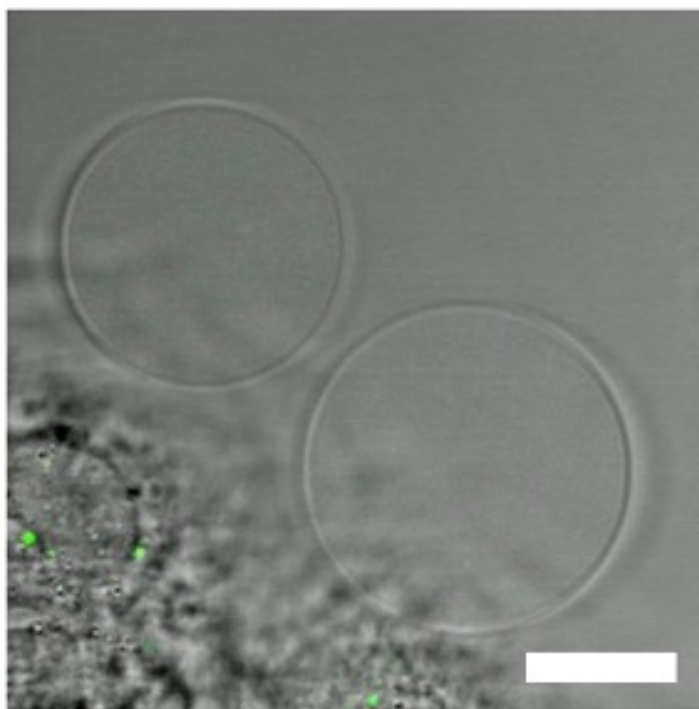


*Figure 10. GPMVs formed from Caco-2 cell line – Scale bar 15 μm.*

## Characterization of GPMVs

As GPMVs are vesicular structures in the micrometer range, they are easily visible under an optical microscope (Figure 10). Furthermore, it is possible to directly observe certain interactions of encapsulated solutes and/or structures in real-time. Light/fluorescence/confocal

laser scanning microscopy is a suitable technique to visualize cells forming GPMVs and follow GPMVs isolated from cells. In order to analyze fluorescently labelled nanoscale objects (peptides, polymersomes or nanoparticles) inside GPMVs, CLSM and flow cytometry (a light scattering technique)[193, 194] provide data in terms of GPMV size and fluorescent properties.[59] CLSM uses a spatial pinhole placed at the confocal plane of the lens for reconstructing the 3D architectures from images that are acquired with optical sectioning.

Membrane properties, such as permeability, elasticity, and surface charge are important parameters in many applications. Several methods have been applied to characterize GUVs but also GPMVs including various electron microscopy (EM) techniques, which allow direct visual inspection of the structures with high resolution. Here, an electron beam is driven through the sample and the resulting interactions are recorded. In contrast to the conventional transmission or scanning EM, cryo-EM provides information on size, morphology, and membrane thickness of the vesicular assemblies as for this method drying or staining of artifacts is not necessary.[59] In addition to microscopy techniques, Förster resonance energy transfer (FRET) yield quantitative information about dimerization propensities of fluorescent tagged proteins within the membrane. Further mechanical characteristics of GPMVs ca be analyzed by Atomic force microscopy (AFM) measurements.[195]

# Future perspectives

## Bioactive polymersomes

Triggerable permeability of catalytic polymersomes provides many opportunities for controlled activation of enzymatic reactions inside. One established approach is to insert OmpF in the membrane. OmpF is a very robust protein gate that is can be isolated fast from bacteria and allows an easy handling and modification. Furthermore, mutants of OmpF have been successfully expressed allowing diverse additonal modifications and functinalities. The modification of reconstituted OmpF mutants enables a molecule passage through the polymeric membrane controlled by stimuli-responsiveness of the mutant or of the molecular caps that have been selectively attached to the OmpF mutant. So far, OmpF has been modified with commercially available molecules or peptides, serving as molecular caps, that covalently bind to genetically engineered cysteine in the eyelet region. The drawback of this approach is the supplier-depended variety of potential linkers. Due to this, a refined strategy describing a more practicable preparation of stimuli-responsive molecules in the laboratory is needed. The new approach should be based on a more customizable solution where different factors can be taken into account during the designing process and the synthesis of molecule/linker for OmpF mutants. For example, it is important that the linker is of an appropriate size to block OmpF pores efficiently. For this reason, diverse structures of potential molecules such as coiling, or spatial orientation in aqueous media with a physiological pH, have to be respected. In order to apply this technique not only OmpF, but to other (more fragile) membrane proteins, it is also important to consider the water solubility of the product. For most proteins, harsh conditions like organic solvents, temperature, pH habe to avoided to protect the structure and functionality. Additionally, further potential applications of polymersomes with a controlled permeability should be considered. For example, polymersomes with encapsulated catalysts and with stimuli-responsive permeability present a smart system that allows a precisely initiated catalytic reaction and shows a promising potential in catalysis. Moreover, the encapsulation of polymersomes prolonges the activity of sensitive catalysts, such as enzymes, as the cargo is protected from the environment by the robust polymeric membrane.

## GPMVs

Due to their composition, GPMVs represent a very promising biomimicking platform with the closest similarity to real cells. However, most reported studies about GPMVs focused on their

structure and composition and not on their development as cell-mimicking compartments. Until today, there are still many open questions regarding the capability as cell-like templates and if a controlled modification of GPMVs is feasable. Therefore, it is essential to investigate the modification of GPMVs, meaning the equipment with external, not biological nanoobjects inside the cavity. One established sprocedure decribes the modification of GPMVs with different nanoscale objects that have been taken-up by cells and transfer subsequently into GPMVs during the formation process. Consequently, the next step is to study how GPMVs can be modified efficiently with non-cellular nanoobjects. Therefore, different impact factors playing an important role during the modification have factors have to be extracted and evaluated. Besides different physical and chemical properties of the nanoobjects, the impact of the cells forming the  GPMVs have to be investigated to observe first trends in optimizing GPMV modification.

*Chapter 2*

# AIM OF THE THESIS

In this work, biomimcking and bioactive compartments in the nano- and microscale are designed and modified to create i) catalytic polymersomes with stimuli-responsive membrane permeabilty and ii) GPMVs supplemented with NPs in high efficiency.

The first project, describes a new, chemistry-oriented strategy for triggerable activity of polymersomes (catalytic nanocompartments). Our aim is to chemically modify the membrane protein OmpF with a small organic linker and to subsequently reconstitute this OmpF as a pore into the polymeric membrane of the compartments. The linker is expected to block the diffusion of small molecules through the OmpF. However, in presence of a certain stimulus, the linker should be cleaved to open the OmpF pores. As the permeability is controlled by a stimuli-responsive membrane protein, the structure of the vesicles is preserved and allows diverse important applications, like artificial organelles or material for nanosensing. Our stategy to create such biohybrid polymersomes is based on the modification of the membrane protein OmpF serving as model protein. Additionally, our aim is to establish a technique for synthesizing customizable linkers suitable for all kinds of proteins. In order to produce a linker, completely soluble in water, we combine tools of organic chemistry synthesis with crosslinkers used commonly for bioconjugation as starting material. The requirement of the resutling linker was the application under protein-appropriate conditions without destroying the structure or functionality, meaning avoiding harsh organic solvents or pH values below or above physilogical conditions.

The aim of the second project is to investigate the potential of GPMVs as customizeable cell-like compartments. We are convinced that GPMVs are great candidates as cell mimics as they are directly formed from cells and thus, present the closest cell-mimicking compartments. In this work, we want to examine how GPMVs can be modified to obtain platforms applicable for the investigation of distinct cellular processes and highly complex biochemical reactions. Therefore, we collect new insights regarding the modification of GPMVs with NPs serving as a model for nanocompartments. Due to the fact that this research field is almost untouched, fundamental questions regarding: i) the effect of concentration, ii) the surface charge and iii) the size of such transferred nanoobjects were adressed and analyzed in detail. Those parameters

are thouroughly investigated via monitoring the distribution of different NPs inside at least 250 GPMVs per random sampling to yield representative results.

# *Chapter 3*

# MEMBRANE PROTEIN CHANNEL EQUIPPED WITH A CLEAVABLE LINKER TO ACTIVATE SENSITIVE CATALYSTS INSIDE POLYMERSOMES

*Significant progress in the functionalization of polymersomes has been obtained by embedding modified proteins into the membrane for stimuli-responsive permeability. Inside the polymersomes, enzymes are encapsulated and catalyze distinct reactions with molecules diffusing through the membrane. Due to the resulting triggerable activity, such bioinspired vesicles are promising tools for catalysis. In this chapter, we introduce here an efficient closing-opening method for polymersomes that contain sensitive catalysts and so achieve a controlled and extended catalytic activity. We developed a chemistry-oriented approach for modifying a membrane protein (OmpF) resulting in stimuli-responsive pore opening within the membrane of the polymeric compartments. We synthesized a diol-containing linker that selectively binds to the pores, blocking them. In the presence of an external stimulus (periodate), the linker is cleaved allowing the diffusion of substrate through the pores to the interior where the encapsulated enzyme catalyzes a reaction to colorimetric products. Besides the precise closing and opening of the pores controlling the catalytic activity, the oxidation by periodate guarantees the cleavage of the linker under mild conditions, where sensitive biomolecules like proteins and enzymes preserve their functionality.*

# Motivation and challenges ahead

Diverse stimuli-responsive polymersomes are specifically engineered to protect their cargo while supporting a triggered functionality when the stimulus is present in the environment.[27, 109, 126, 149, 196, 197] Due to this, such polymersomes, have an increasing potential for applications in catalysis as they are able to change their permeability upon the presence of a stimulus in their environment while preserving their architecture: the increased permeability favors the molecular flow through the synthetic membrane, which will trigger an *in situ* functionality, as for example by starting a specific reaction of the encapsulated active compounds.[129, 130] One strategy to generate stimuli-responsive polymersomes with preserved architecture is to take advantage of stimuli-responsive copolymers to form vesicles that shrink or swell upon an external signal (like protons, $CO_2$ or change in temperature).[66, 115, 198] A complementary strategy, which is "bioinspired" by the cell membrane known to contain a variety of membrane proteins that are essential for a molecular transport through, hinges on reconstitution of membrane proteins or small polypeptides into the polymeric membrane to achieve a desired permeability.[82, 129] For example, membrane protein channels, such as the outer membrane protein F (OmpF), enable the diffusion of molecules with a size up to the pore diameter, [74, 75, 90, 133] while others, such as aquaglyceroporin or gramicidin, only allow diffusion of specific molecules or ions.[79, 135] A step further in developing stimuli-responsive membrane permeabilization was achieved by modification of the membrane proteins such to become either a "valve" or a "gate". By attaching a pH-sensitive GALA polypeptide to OmpF, this one has been rendered a pH-triggerable valve, which served to open/close the polymersome when it has been inserted in the membrane.[199] Alternatively, when molecules were covalently bound to a double mutant of OmpF, this one became a gate when inserted into the membrane of polymersomes, the pores being closed and opened when the molecules were cleaved by upon the presence of a specific stimulus.[15] Furthermore, polymersomes equipped with stimuli-responsive OmpF gates and loaded with specific enzymes served for development of catalytic nanocompartments (CNCs) with triggered activity: only when the gate was open by the presence of a specific stimulus, which cleaved the molecules closing the pore, the enzymes encapsulated inside started to perform their biologic function as the substrates freely diffused through.[12, 15]

Here we enlarge the concept of CNCs with triggered activity by developing a chemistry-based strategy for modifying membrane protein channels to achieve stimuli-responsive opening of the pores inserted in the membrane of the compartments that allows the substrates to enter and start

the *in situ* reaction. We chemically modified a double mutant of OmpF under mild conditions by covalently binding a linker rationally designed and synthesized to render this channel porin a "gate" opening in the presence of periodate, an important oxidant for the selective oxidation of polysaccharides and glycopeptides.[200, 201] We chose OmpF as model of membrane protein channels as it is a well characterized porin in terms of structural and functional characteristics.[202] The linker was designed to bind to specific amino acids K89C R270C of OmpF, which are located at the pore opening, and to be cleavable by a particular, small molecule (periodate). We chose periodate as it serves for oxidative cleavage of the linker under mild conditions in aqueous solutions where membrane proteins are not affected and remain functional. Additionally, we were interested to synthesize a water soluble linker to enable applications without the use of organic solvents that are expected to affect membrane proteins.

# Modification of OmpF with a small organic compound for triggerable activation of catalytic polymersomes

OmpF monomer has the structure of hollow beta barrel, embedded in the membrane with a diameter of around 30 Å (Figure 11A), enabling diffusion of small (generally under 600 Da) water-soluble molecules in both directions.[203, 204] To achieve the chemical modification necessary to bind the linker, we used OmpF-M, a genetically modified porin that features two cysteine (Cys) residues opposing each other in the 'eyelet' region of the pore (OmpF double mutant K89C R270C, OmpF-M).[19, 20] The thiol groups of these Cys moieties are exposed and can be readily modified (Figure 11).
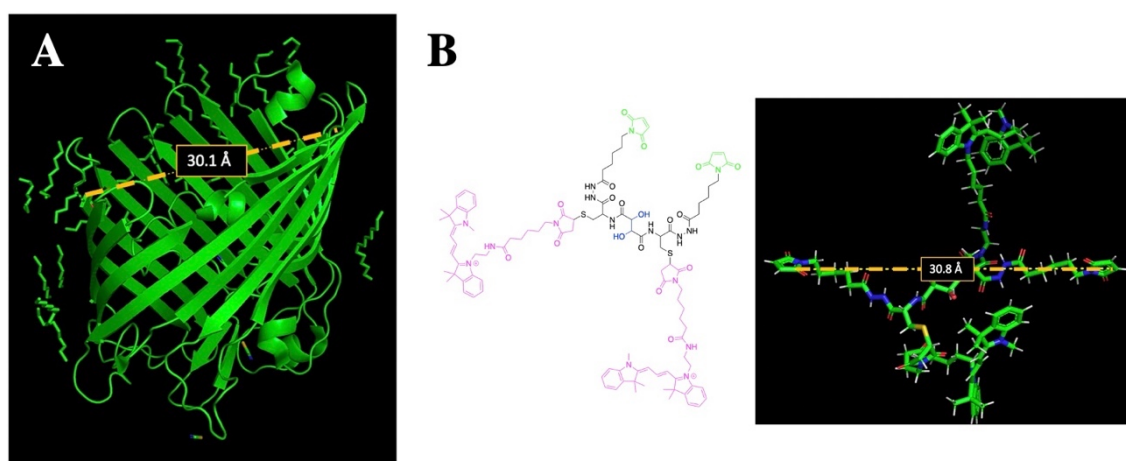


***Figure 11. OmpF structure and the linker design*** *– A) PyMol ribbon representation of OmpF-M secondary structure reveals a distance of about 30 Å between the side groups of the two Cys; B) Left: Chemical structure of the designed linker with maleimide groups indicated in green, fluorophores in pink and the diol unit in blue. Right: the linker length corresponds to the distance between the two opposing Cys of OmpF-M, as estimated by PyMol modeling.*

To block OmpF pores by covalent binding of an organic compound and induce a controlled opening by the presence of periodate, different requirements have to be considered in terms of the size and conformation of the linker, its accessibility and efficient cleavage for a stimuli-responsive opening of the OmpF pores. First, the steric size and conformation of the linker should efficiently block the pore and second, both ends of the linker should be bound to OmpF to minimize the freedom of rotation. Thus, we opted to synthesize a small organic compound to provide a more rigid structure compared to coiled macromolecules where the spatial orientation and folding is more difficult to predict.[205, 206] The length of the linker was designed

to span the diameter of the OmpF-M pore at the site of the two Cys moieties, i.e. approximately 30 Å, whereas a maleimide group at each linker end was inserted to favor the reaction with thiol side chain of the two cysteines (Figure 11B).[207] Third, an important factor to consider in the linker design was the periodate-responsiveness that would result in its oxidative cleavage to unblock of the OmpF 'gate'. Hence, we introduced a vicinal diol unit with a periodate-sensitive C-C bond in the middle of the symmetric linker (Figure 11B, in blue). Periodate oxidizes the diol into the corresponding carbonyl groups under mild conditions, at pH = 7 and room temperature.[208] Oxidation by periodate is predicted to produce two fragments able to rotate freely as they are bound only at one end to a Cys side chain: the periodate-triggered cleavage of the linker releases the OmpF pore obstruction. Finally, our linker design included two fluorophore (cyanine3 dye) side chains both to create a bulkier structure for a more efficient pore blocking and to allow detection by fluorescence-based techniques. Synthesis of the periodate-responsive linker was performed in three consecutive steps (Scheme 1). We started from the vicinal diol element of a disuccinimidyl derivative of tartaric acid and symmetrically built up the linker on both sides. To achieve a final linker length of approximately 30 Å, we coupled two cysteine molecules to the respective ends of the reactive ester, to which we then covalently attached cyanine3 maleimides via the thiol groups as fluorescent side chains. The two functional maleimide end groups of the linker were integrated using a compound combining maleimide with a small hydrocarbon chain and hydrazide as the second end functional group. The hydrazide moiety reacted selectively with the carboxylate group of the cysteine fragments resulting in the final linker with a length of 30 Å (Figure 11B).

In the first step, cysteine was coupled with disuccinimidyl tartrate (DST) by the simple reaction of amine groups with the NHS-activated tartaric acid (Scheme 1). This step was necessary to introduce the reactive thiol groups, which were subsequently involved in the second reaction step to couple the fluorescent cyanine3 maleimide molecules. The first intermediate (Compound 1) was only partially purified and then used further for the synthesis of Compound 2. Thus, the ^{1}H-NMR spectrum of the first intermediate showed the characteristic peaks of the coupled cysteine found in the range of 3.45-3.30 ppm and 4.65 ppm corresponding to the methylene (C$\underline{H}_2$-SH) and methine (NH-C$\underline{H}$) groups, together with the two protons (C$\underline{H}$-C$\underline{H}$) of the vicinal diol unit at 4.7-4.6 pm. Additionally, the spectrum indicated the presence of monofunctional product, cysteine and free N-hydroxy succinimide. The ^{13}C-NMR spectrum confirmed the presence of carbons around 180-170 ppm characteristic for carbonyl moieties from amides and carboxylic acids, the two carbons of the vicinal diol unit around 70 ppm, and the two carbon atoms of the cysteine connected to the tartaric acid by amide groups at around

50 ppm. Analysis by ESI-MS revealed a value of m/z= 179.05, which corresponds to double the protonated Compound 1 [M+2H]+ and could not be assigned to DST or cysteine. Compound 1 was used in the second reaction step aiming to induce its selective reaction with cyanine3 maleimide, resulting in Compound 2. The $^1$H-NMR spectrum of Compound 2 showed that possible impurities resulting from the synthesis of the first intermediate were efficiently removed during the purification step and did not lead to any other side products nor disrupt the reaction affording Compound 2 (Figure S1). In addition to the protons of the vicinal diol element of tartaric acid and the cysteine fragments, we observed peaks in the 9.00-5.50 ppm range, characteristic for the heterocyclic and aromatic rings, as well as for the extended conjugation of the double bonds of the cyanine3 dye. The singlet peak characteristic for the two protons of the maleimide groups was not identified in the spectrum, indicating the complete coupling of cyanine3 maleimide and consequently the formation of Compound 2. According to the $^{13}$C-NMR spectrum, the characteristic peaks of the carbon atoms from the carboxylic acids and amides were visible in the 180-170 ppm range. In addition, carbon peaks of cyanine3 dye were observed, including peak at 168 ppm representing carboxamides, C=C groups around 140 ppm, aromatic carbons around 120-110 ppm, aliphatic amines between 50-30 ppm, and the hydrocarbon chains in the 30-20 ppm range (Figure S2). Analysis of the product by MS (MALDI-TOF) revealed an m/z value of [M+2H]+ = 379.16, corresponding exactly to Compound 2. In the last synthesis step, the carboxylic acid groups of Compound 2 were activated by EDC to form the amine-reactive O-acyl isourea intermediate. Subsequently, the reaction with N-ε-maleimidocaproic acid hydrazide (EMCH) led to the formation of a symmetric bismaleimide linker, as confirmed by the NMR spectra (Figure S3 and Figure S4). In addition to the peaks that were already observed for Compound 2, the $^1$H-NMR spectrum showed peaks between 2.0-1.0 ppm, characteristic for protons of the two hydrocarbon chains that were introduced by reacting Compound 2 with EMCH. The hydrazide group of the crosslinker EMCH commonly generates a very broad peak between 4.5-3.5 ppm with an integral of 4, which was not found in the $^1$H-NMR spectrum of our final product. The $^{13}$C-NMR spectrum of the final linker indicated its large hydrocarbon backbone and showed the characteristic peaks of the two carboxamines carbons from the coupled maleimide groups around 165 ppm. Interestingly, the peaks of the aromatic carbons from the fluorophore were no longer detected. However, as the characteristic fluorescence of cyanine3 was still clearly visible when the linker was dissolved in the NMR-tube (Figure S4), we concluded that the absence represents an effect of a decreased solubility in CDCl3. Additionally, MALDI-TOF revealed an m/z value of [M+H]+ = 643.68, which corresponds exactly to the bismaleimide linker.
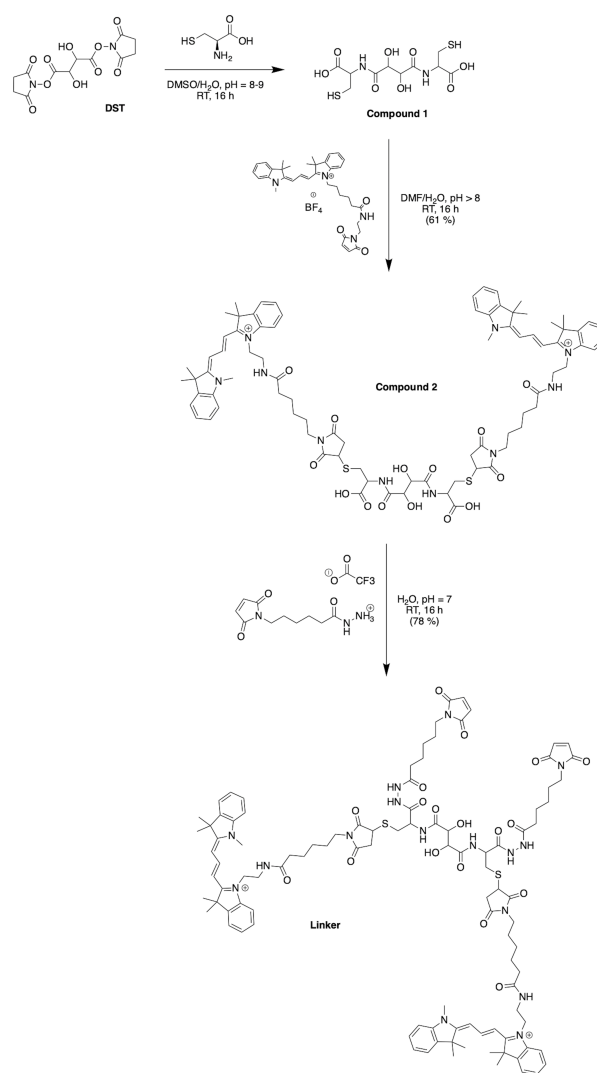
*Scheme 1. Route of synthesis of the periodate-sensitive linker*

Next, we reacted the linker dissolved in water with purified recombinant OmpF-M in order to attach the linker and close the OmpF pores. After the labeling reaction, linker-OmpF-M solution was heated to 95 °C to denature all intramolecular interactions except covalent bonds and then analyzed by SDS-PAGE (Figure S5). We observed a single fluorescent band running with the apparent molecular weight of monomeric OmpF-M (about 40 kDa[204], lanes 3, 4), which indicated a covalent binding of the fluorescent linker to OmpF-M. Therefore, an unspecific aggregation of the linker with the protein did not appear and the covalent binding was successful.

To establish whether the linker attachment to the OmpF-M was able to i) close efficiently the pore and ii) control the passage through the OmpF pore in a precise manner, we prepared several

types of polymersomes encapsulating laccase as model for a sensitive catalyst in their aqueous cavity: (i) CNCs without OmpF-M pores (CNC-noOmpF-M), (ii) CNCs with reconstituted linker-modified OmpF-M (CNC-linker-OmpF-M), (iii) CNCs with reconstituted OmpF-M lacking the linker modification (CNC-OmpF-M), and (iv) CNCs with wild-type OmpF inserted in their membranes (CNC-OmpF-WT). We used the film rehydration method[209] to form polymersomes from poly(2-methyl-2-oxazoline)-block-poly(dimethyl-siloxane)-block-poly(2-methyl-2-oxazo-line), $PMOXA_{11}$-b-$PDMS_{104}$-b-$PMOXA_{11}$. Such amphiphilic triblock copolymers (PMOXA-b-PDMS-b-PMOXA) are known to self-assemble into vesicles with membranes that are sufficiently flexible to integrate OmpF despite the hydrophobic mismatch.[82, 83, 210, 211] The average number of MOXA and DMS repeating units in $PMOXA_{11}$-b-$PDMS_{104}$-b-$PMOXA_{11}$ was assessed by proton nuclear magnetic resonance ($^1$H-NMR) spectroscopy (Figure S6). This method also allowed for obtaining the number-average molecular weight of this copolymer (Mn = 9800 g/mol), whereas a dispersity (Đ) of 1.23 was revealed by gel permeation chromatography (GPC) (Figure S7).



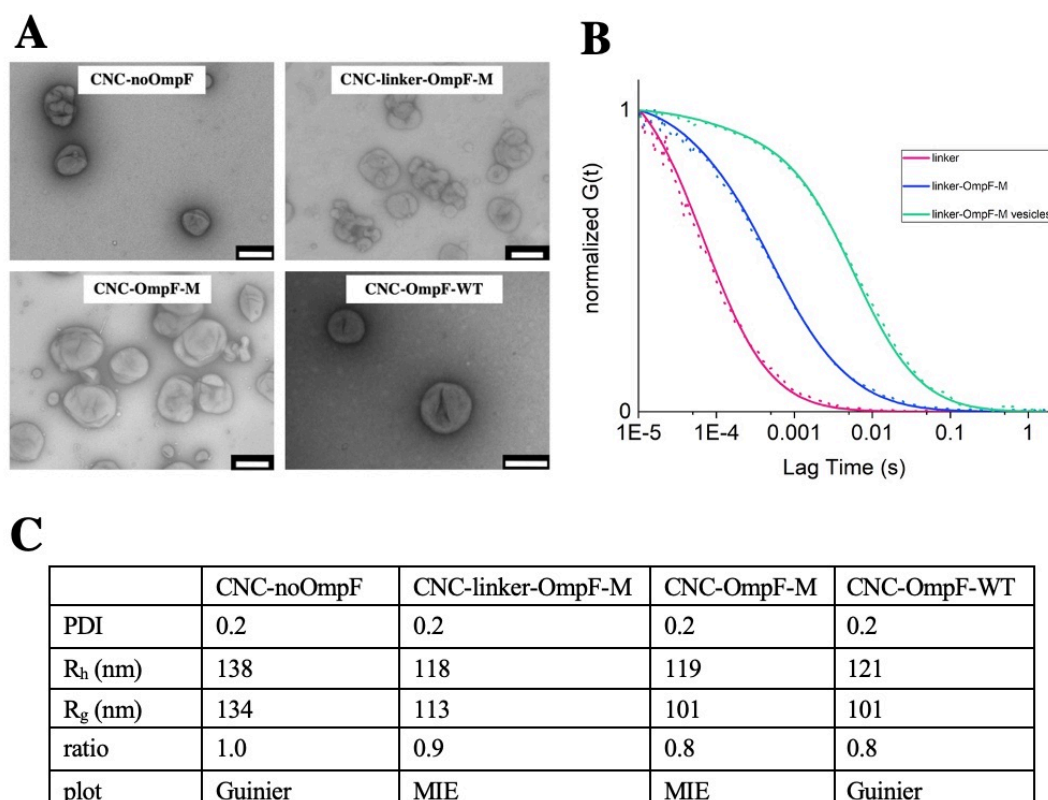|  | CNC-noOmpF | CNC-linker-OmpF-M | CNC-OmpF-M | CNC-OmpF-WT |
|---|---|---|---|---|
| PDI | 0.2 | 0.2 | 0.2 | 0.2 |
| $R_h$ (nm) | 138 | 118 | 119 | 121 |
| $R_g$ (nm) | 134 | 113 | 101 | 101 |
| ratio | 1.0 | 0.9 | 0.8 | 0.8 |
| plot | Guinier | MIE | MIE | Guinier |

*Figure 12. Characterization of the CNCs – A) TEM micrographs of CNCs without OmpF (CNC-noOmpF), CNCs with linker-OmpF-M (CNC-linker-OmpF-M) inserted in the membrane, CNCs with OmpF-M (CNC-OmpF-M), and OmpF wild type (CNC-OmpF-WT). Scalebars: 200 nm. B) B) FCS curves (line) and raw data (dots) of PBS solutions of the linker*

*(pink), free linker-OmpF-M in 1% OG (blue), and CNCs with linker-OmpF-M reconstituted in the membrane (green), C) Light scattering parameters of CNCs without OmpF pores (CNC-noOmpF), CNCs with inserted OmpF-M-linker (CNC-linker-OmpF-M), CNCs with inserted OmpF-M (CNC-OmpF-M), and CNCs with inserted wild-type OmpF (CNC-OmpF-WT). A ratio between the hydrodynamic radius ($R_h$) and radius of gyration ($R_g$) between 0.775 and 1 indicates a hollow sphere architecture for all types of CNCs. Polymersome size homogeneity was confirmed by dynamic light scattering with a PDI = 0.2.*

The size and architecture of CNCs were characterized by transmission electron microscopy (TEM), fluorescence correlation spectroscopy (FCS), and light scattering (LS) shown in Figure 12. All three techniques indicated hollow spheres with a diameter of around 200 nm with appropriate homogeneity (polydispersity index (PDI) = 0.2). The characteristic collapsed vesicle structures with a diameter of diameter of 200 nm are shown in Figure 12A. By extrapolating the data with Mie or Guinier plot (Figure 2C), we observed the radius of gyration ($R_g$) and radius of hydration ($R_h$) for all CNCs. CNC-linker-OmpF-M, CNC-OmpF-M and CNC-OmpF-WT were in a similar range of size with $R_h$ of around 120 nm and $R_g$ of 100-110 nm, while CNC-noOmpF were slightly bigger ($R_h$ = 138, $R_g$ = 134 nm). The calculated ratios of $R_h/R_g$ were found in the range between 0.8-1.0 presenting typical values for hollow spheres.

Owing to the fluorescent side chains of the linker, the backbone binding of the linker to OmpF-M has been assessed by FCS (Figure 12B). The autocorrelation curves revealed shifts in the diffusion times of linker-OmpF-M relative to free linker and linker-OmpF-M permeabilized CNCs relative to free linker-OmpF-M (Table S1). These characteristic increases in diffusion time confirmed a successful coupling of the linker to OmpF-M and a successful reconstitution of linker-OmpF-M in the polymeric membrane. In addition, we used brightness measurements to evaluate the number of linker molecules/OmpF pore. With the counts per molecules given in Table S1, we calculated that one linker molecule is bound per OmpF-M monomer and obtained the average number of 9 reconstituted linker-OmpF-M molecules per CNC.

We next assayed the *in situ* activity of encapsulated laccase in response to treating CNCs with $NaIO_4$. Laccase is expected to catalyze the oxidation of 2,6-dimethoxyphenol (DMP) to the corresponding radical species. The resulting orange radical can be detected spectrophotometrically at 470 nm.[212, 213] When DMP is added in the environment of CNCs, thus should diffuse through the OmpF pores to reach the enzyme, which is possible only when the linker-blocked OmpF-M pores are open as a result of the linker cleavage. The periodate-

triggered unblocking of OmpF-M pores in CNCs was evaluated by measuring the absorbance related to DMP oxidation for several hours (Figure 13). As controls, we monitored the enzymatic activity of CNCs with linker-modified OmpF-M pores in the absence of $NaIO_4$ (CNC-linker-OmpF-M) and of corresponding CNCs without OmpF pores (CNC-no-OmpF). To establish whether $NaIO_4$ cleaves the linker but does not affect the overall stability of the CNCs, CNC-no-OmpF was additionally treated with periodate (CNC-noOmpF-M with $NaIO_4$). The quenching with glucose after periodate treatment avoided false positive signals from periodate-induced oxidation reactions. The treatment of CNC-linker-OmpF-M with $NaIO_4$ led to a significantly higher absorbance at 470 nm as the DMP was able to diffuse into the cavity where it was oxidized to the colored product (Figure 3, pink curve). In the case of CNC-no-OmpF, the periodate treatment neither induced oxidation of DMP, nor damaged the CNCs (Figure 13, yellow curve), which would have otherwise led to a release of laccase and to an enzyme-catalyzed oxidation of DMP. Our spectrophotometric results clearly indicate that the linker closes OmpF efficiently and second, enables a stimuli-responsive opening of OmpF-M pores in the presence of periodate. Additionally, the increasing absorbance demonstrated that periodate did not unhinge the activity of encapsulated laccase.
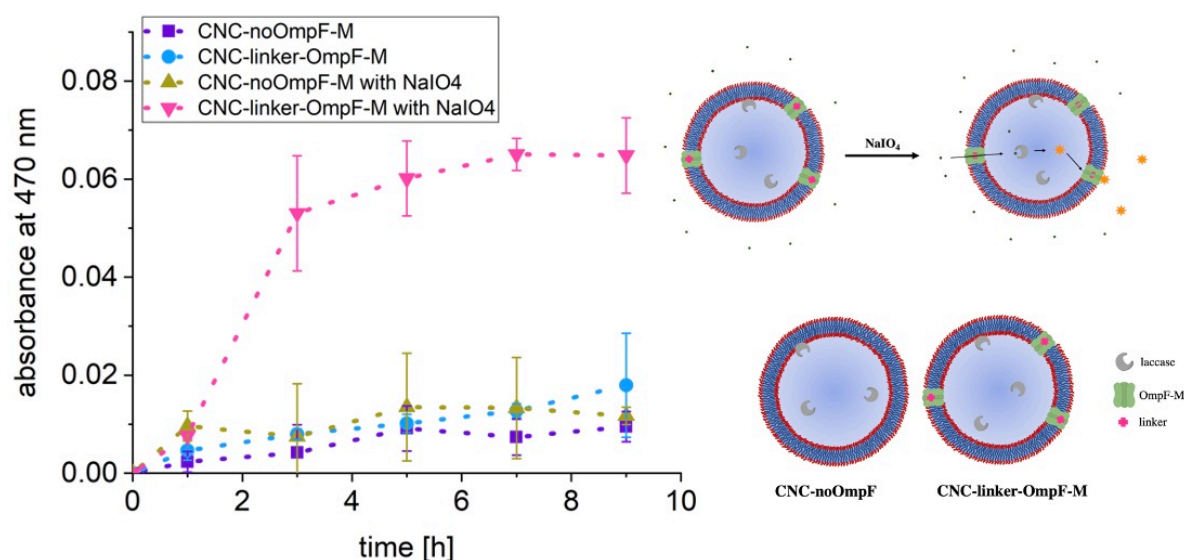


*Figure 13. Linker-based control of molecular passage through catalytic nanocompartments demonstrated by spectrophotometric assessment of laccase activity of CNCs in response to $NaIO_4$ – The increase in absorbance at 470 nm reflects laccase-catalyzed substrate conversion. Measurements were carried out at RT for 9 h at pH = 7.4. $NaIO_4$ cleaves the linker that blocks the passage of substrate through linker-OmpF-M pores in the closed state and thereby unblocks the pore. In the open state, DMP enters the compartment where it is oxidized in situ to a*

*detectable product by the confined laccase. The polymeric membrane separates the encapsulated laccase from the environment.*

We also measured the absorbance of CNCs over several days to evaluate how long the protection shield of polymersomes is protecting the encapsulated enzyme (Figure 14). The maximum activity of free laccase was reached after 8 h and continuously decreased over the following 12 h (Figure 14A). In contrast to this, enzymatic activity of laccase encapsulating CNCs whose membrane was permeable to DMP either by unmodified OmpF-M pores (CNC-OmpF-M) or by periodate-induced opening linker-OmpF-M pores (CNC-linker-OmpF-M), increased for several days (Figure 14B). Again, in the absence of OmpF pores (CNC-no-OmpF with NaIO$_4$), periodate treatment did not lead to the oxidation of DMP or damaged the CNCs as confirmed by TEM (Figure 14D).
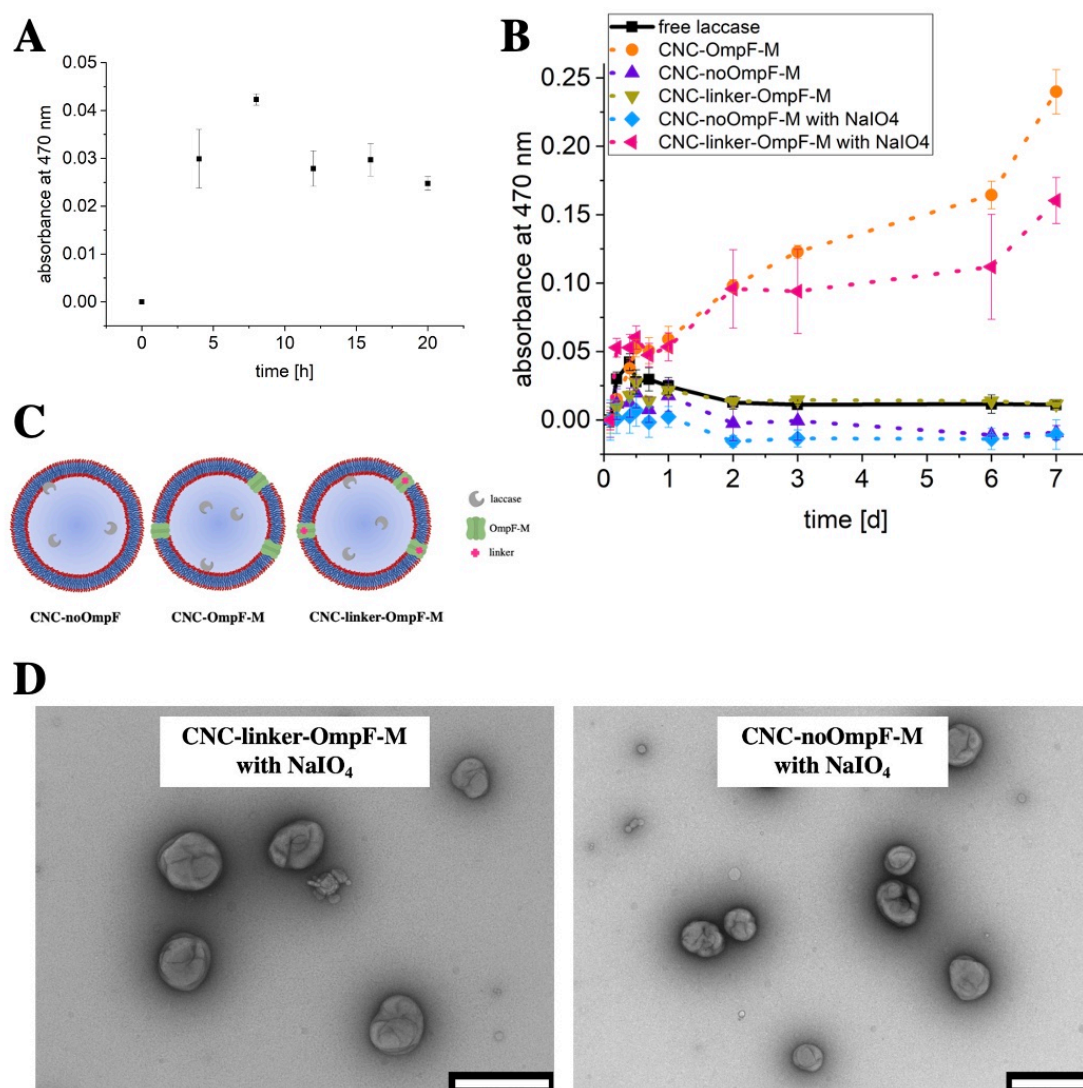


***Figure 14. Long-term laccase activity of CNCs in response to NaIO$_4$ (with standard deviation***

*calculated from three technical repeats), based on the increase in absorbance intensity of laccase-product with a characteristic absorbance at 470 nm* – Measurements were carried out at RT at pH 7.4: A) Activity of free laccase in PBS solution (with standard deviation) recorded over 20 h; B) Activity measured for one week of i) free laccase in PBS solution (without periodate treatment (black)), ii) CNC-OmpF-M (without periodate treatment (orange)), iii) CNC-noOmpF-M (without periodate treatment (purple)), iv) CNC-linker-OmpF-M (without periodate treatment (yellow)), v) CNC-noOmpF-M (without periodate treatment (blue)) and vi) CNC-linker-OmpF-M with periodate treatment (pink); C) Schematic representation of the three different polymersomes with encapsulated laccase. D) TEM micrographs of CNCs after periodate treatment. Scalebars: 500 nm.

For comparison, we also tested laccase activity of corresponding CNCs using 2,2'-azino-bis(3-ethylbenzothiazoline-6-sulfonic acid diammonium salt (ABTS) as substrate (Figure S8). These enzyme assays involving CNCs were performed over several months, indicating that CNCs were active over long time periods if stored at 4 °C. However, DMP in PBS solution exhibited notable lower autooxidation[212] over 9 h and thus was more suitable for our optimized long-term measurements of catalytic activity (Figure 14). Further evidence of the longevity of laccase encapsulating CNCs was provided by TEM micrographs recorded after eleven months (Figure S9). Long-term stability of CNCs represents a key aspect for further application of this system.

# Conclusion

Our CNC system allows the controlled activation of small catalysts and protects also sensitive catalysts from degradation by encapsulating them in stable polymeric nanocompartments. Due to i) efficient pore closing by a small organic linker and ii) due to precise pore-opening of the CNC by periodate, an improved spatio-temporal control has been achieved. Secondly, the catalytic reactions are induced under mild conditions (no organic solvents, pH = 7, RT) where other sensitive biomolecules stay intact. Moreover, through the cleavage of the stimuli-responsive linker, no modification to the CNC structure has been observed ensuring the full functionality of our system. Our approach in catalysis pave the way to a new molecular technology which might be extremely useful in multifunctional cluster activity when specific substrates or products need to be accessible at a precise time and space to be converted by the second catalyst to a desired molecule. We strongly believe that our novel approach for chemical OmpF modification with controllable functionality and improved properties could advance the development of sensitive catalysts based on CNCs for a broad range of applications including catalysis, food science and nanotechnology. For example, following titration experiments will provide more information regarding the sensitivity and selectivity of the linker towards periodate and will show if the CNCs are potential candidates as periodate sensors with appropriate properties such as lower detection limit.

# *Chapter 4*

# THE PROMISING POTENTIAL OF GPMVS AS CELL-MIMICKING PLATFORM

*Cellular model systems are essential platforms used across multiple research fields for exploring the fundaments of biology and biochemistry. Here, we present Giant Plasma Membrane Vesicles (GPMVs) as a platform of cell-like compartments that will facilitate the study of particles within a biorelevant environment and promote their further development. We studied how cellularly taken up nanoparticles (NPs) transfer into formed GPMVs and which are the molecular factors that play a role in successful transfer (size, concentration and surface charge along with three different cell lines: HepG2, HeLa, and Caco-2). We observed that, polystyrene (PS) carboxylated NPs with a size of 40 nm and 100 nm transferred successfully and efficiently into GPMVs derived from all cell lines. We then investigated the distribution of NPs inside formed GPMVs and established the average number of NPs/GPMVs and the percentage of all GPMVs with NPs in their cavity. Our results could pave the way for GPMVs usage as superior cell-like mimics in medically relevant applications.*

# Motivation and challenges ahead

The history of GPMVs (Giant Plasma Membrane Vesicles) starts in the first half of the 20th century where the formation of cell surface "blebs" was observed after treating a chick embryo heart with a variety of hypotonic and hypertonic solutions.[214] In 1948, the process of this formation, called potocytosis was described more accurately by using the phase microscope.[215] Later on, a method for isolating such plasma membrane vesicles (PMVs) from cells in higher amounts was developed. It was based on a great number of aldehydes and disulfide blocking agents that promoted the PMV formation and subsequent release from cells.[184] This pioneering procedure replaced the traditional techniques for the isolation of cell surface membrane fragments and enabled targeted studies and applications of PMVs (nowadays called GPMV: Giant Plasma Membrane Vesicle). The followed reports of those newly discovered GPMVs focused on studying the compositional and structural characteristics of their plasma membrane after formation from different cell lines.[181, 186, 216] Additionally, a detailed investigation of the properties of the membrane associated IgE-receptor complex was described.[217] So far, the most investigated field of GPMV studies used the vesicles as an innovative platform with realistic biological membrane composition without the cytoskeletal constraint found in living cells.[183,179, 218, 219] GPMVs are obtained directly from cells and include the cellular membrane and almost all cell components, except larger organelles, such as Golgi apparatus and the nucleus.[181, 184] In addition to that, the known mechanism of GPMV formation involves local delamination of the cytoskeleton.[185] Another research area also started dealing with the development and characterization of planar supported membranes received from GPMVs[220, 221] and exploited GPMVs as new tools for drug delivery.[222]

Here, we introduce GPMVs as the novel type for a complete, overall cell-mimicking compartment. The complexity of cells encourages the development of a huge variety of simplified cell model platforms, of which the features can be tailored to the respective requested objective to fulfill different requirements, e.g. cell-like membrane compositions. Until now, cell-mimicking structures have become indispensable strategies for investigating highly complex biological processes such as molecule transport through cell membrane, or specific reactions controlled by enzymes in cell organelles.[158]

With our study, we discovered a promsing new strategy of forming a new class of cell-mimicking systems in order to overcome the current challenges of designing ideal cell-like compartments. Here, we propose as cell-mimicking compartments the GPMVs and studied how they can be equipped with nanoparticles (NPs) during their formation process such to provide

a cytoplasm medium in which the NPs freely move. We selected GPMVs as cell-like compartments because they combine the advantage of having both a cytoplasm and cell membrane[185, 219] with a defined inner cavity volume and long-term stability without requiring cell cultivation. In addition, even though GPMVs are larger in size (in the lower μm range), their cell-identical composition supports them as promising platforms to study medically relevant exosomes. Cell-secreted exosomes are vesicles that contain plasma membrane proteins, cell-type-specific RNA and protein cargoes and play an important role in different biological processes such as intercellular signaling, stimulation or inactivation of T-cells.[223] Whilst exosomes attract a lot of attention with the focus on understanding different biological functions and on their applications in diagnostics and therapeutics, their development has stagnated due to their low production by cells and their inefficient isolation. In contrast to exosomes, GPMVs can be produced on a large scale, which turns them into valuable platforms in medical research.[14]

While we previously proved that GPMVs can be equipped with soft nanoassemblies, such as liposomes and polymersomes[14], here we go one step further and studied how hard NPs with different properties can transfer into GPMVs without affecting their properties and in which conditions this transfer can take place. We focused on different properties of NPs, such as surface chemistry, size and concentration that have the potential of influencing their transfer from cells into GPMVs. We selected three cell lines in order to understand whether the transfer of NPs is mediated by the cell type and to identify which precursor cell line results in the largest GPMV population. By using fluorescent NPs, we evaluated qualitatively and quantitatively the number of NPs transferred into subsequently formed GPMVs as a function of the cell line by a combination of confocal laser scanning microscopy (CLSM) and flow cytometry. Our study reveals that a balance between the properties of the NPs and the cell line is crucial for obtaining a maximal loading of GPMVs.

# Applying GPMVs as biomimicking platform

In order to study the transfer efficiency of nanoparticles (NPs) from cells into the cavity of GPMVs, it is essential to investigate precisely all effects influencing the cellular uptake - size, concentration and surface of NPs. We selected carboxylated polystyrene (PS) NPs as those presents a suitable model system for determining the factors of particle functionalization.[224] We studied the transfer of fluorescent NPs in sizes of 40 nm, 100 nm, 500 nm, that were added to the cells in different concentrations. Additionally, we studied how the surface modification of PS NPs could influence the cellular uptake and tested 100 nm sized particles functionalized with amine groups on the surface and NPs (100 nm) without any additional modification. The experiments were performed in parallel with three different cell types to investigate the cell-dependent behavior of the endocytotic pathway. Within the endosomal transport of endocytosis, the taken up NPs (cargos) are delivered in endosomes. Here, a sorting process occurs where the cargos are routed to different organelles. Cargoes can be sorted to recycling endosomal carriers bringing the cargos back to the plasma membrane.[225] We assume that the cargoes found in the recycling process near the plasma membrane are exactly those NPs, we can observe inside GPMVs.

HeLa cells were chosen for our experimental setup because of their role as model cell line for NP uptake studies.[224] HepG2 cell line were selected due to their lack of membrane protein caveolae1 which disables the NP entry by caveolae-dependent endocytosis.[226] As third cell line, we chose Caco-2 since they have been widely used as a model for the intestinal barrier. Due to its heterogenous structure, Caco-2 culture contains cells with slightly different properties. [227]

GPMVs are obtained directly from cells when they are exposed to chemical stress.[228] All three chosen cell lines were able to form GPMVs when treated with a "vesiculation solution" containing reducing agent dithiothreitol (DTT) and cross-linking agent paraformaldehyde (PFA), however with varying sizes and uniformity.

The cells have to uptake the respective NPs before the GPMV formation can be induced. By confocal laser scanning microscopy (CLSM) we investigated if these taken-up NPs have successfully been transferred into GPMVs and if they bear the potential for innovative tools in nanotechnology that retain the cell-like composition. The yielded GPMVs were observed by CLSM and we analyzed their average size by measuring the diameter of more than 250 GPMVs per cell line.

# Evaluating a possible transfer of polystyrene nanoparticles with different surface modifications into GPMVs

**Polystyrene nanoparticles in cell medium**

In order to evaluate the nanoparticle (NP) transfer into GPMVs, it is important to investigate the NP properties influencing the cellular uptake: NP size, charge, surface chemistry and the in which concentration the particles were added to the cells.

We first compared the impact of the NP's surface properties. We selected i) PS NPs with carboxylate groups on the surface or ii) with amine groups instead and iii) PS NPs without additional surface modifications. All NPs had a size of 100 nm. Carboxylated NPs are known to be nontoxic and to be readily taken up by all cells at sizes smaller than 200 nm.[224] Amine-modified NPs were chosen as the natural occurring complement of the carboxylate group in amino acids. The unmodified NPs were used to understand the general influence of functional groups on the NP surface for the transfer into GPMVs. We ensured that the same conditions for all performed trials with any NPs were maintained so that we could compare the results of each experiment accurately. The initial concentrations of the NPs were determined by nanoparticle tracking analysis (NTA). Furthermore, the NPs were analyzed by dynamic light scattering (DLS) and zeta potential both in solutions of aqueous phosphate-buffered saline (PBS) and cell medium (Table 1) to visualize the resulting different hydrophobicity and hydrophilicity in these media. In contrast to PBS, cell medium contains high concentrations of proteins from fetal bovine serum.[229, 230]

**Table 1.** *Measurements of 100 nm PS particles with different surface modifications (carboxylated, aminated, unmodified) in PBS and cell medium.*

|  | carboxylate-modified NP | | | amine-modified NP | | | non-modified NP | | |
|---|---|---|---|---|---|---|---|---|---|
|  | diameter [nm] | charge [mV] | PDI | diameter [nm] | charge [mV] | PDI | diameter [nm] | charge [mV] | PDI |
| 1x PBS pH 7.4 | 109.2±0.4 | -32.2±1.2 | 0.005±0.002 | 104.2±0.2 | +17.4±0.7 | 0.086±0.019 | 99.7±0.5 | -39.3±1.9 | 0.010±0.008 |
| medium pH 7.1-7.3 | 145.8±1.0 | -8.4±1.4 | 0.240±0.005 | 134.9±0.7 | -8.2±0.8 | 0.299±0.023 | 136.3±0.6 | -10.1±0.6 | 0.228±0.002 |

In cell medium, the NPs showed similar zeta potentials, stabilized to -8 mV and -10 mV. However, in PBS (pH 7.4) the carboxylated NPs and those without surface modifications were highly negatively charged; around -32 mV or more. The most extensive change in surface

charge was observed in case of aminated NPs. While having a positive charge in PBS, these NPs turned slightly negative in cell medium (-8 mV).

With regard to the size of NPs, we observed that the hydrodynamic radius all NPs was higher in cell medium (30-38 nm) than in PBS. In cell medium, the implied proteins adsorbed onto the NPs surface and formed a protein corona which induced in a bigger measured particle size, higher polydispersity index (PDI, Table 1) and change in zeta potential.[231] In case of the three different NPs, all zeta potentials shifted more towards zero while the hydrodynamic diameter increased slightly of ca. 36-38 nm. In general, the effect of a protein corona depends on its protein composition and the resulting strength of adsorption forces between the proteins and NP surface.[232-234] As a strong surface charge prevents NPs from aggregation, further characterization by transmission electron microscopy (TEM) of NPs in cell medium was essential to prove that no aggregations occurred in the medium (Figure 15) that could distort the performed DLS measurements or manipulate the following cellular uptake studies.
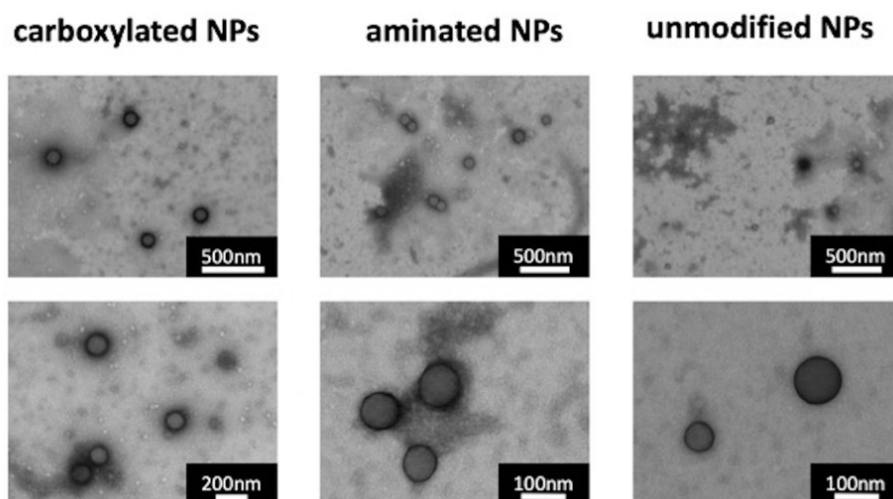


*Figure 15. TEM micrographs of carboxylated, aminated and unmodified NPs in cell medium – Scale bar of top images: 500 nm and for images below: 200 nm.*

**Effect of the surface modifications of PS NPs on their transfer into GPMVs**

For studying the impact of the NP's surface properties on the transfer into GPMVs, we treated three cell lines (HepG2, Caco-2 and HeLa) with different fluorescent PS NPs (carboxylated, aminated, without additional surface modifications) having a size of 100 nm. In the first step, the cells were incubated for 24 h with the selected NPs to induce the uptake. Then, the GPMV formation was promoted by treating the cells with a solution containing PFA and DTT

(vesiculation buffer). After 1-2 h, the GPMVs were isolated from cells by centrifugation (Figure 16).

By LSM, we investigated if the fluorescent NPs are located in the formed GPMVs. By comparing the NPs with different surface modification, we observed that only carboxylated NPS transferred from cells into GPMVs (Figure S14). Both the aminated NPs and those without additional functional groups were not found in GPMVs formed from any cell line. Moreover, Caco-2 cells especially, underwent serous changes in the morphology indicative for cell death after incubation with aminated NPs. At the highest concentration it was not possible any more to yield GPMVs from the treated cells. Regarding aminated NPs, it is known that a positive surface charge can increase the uptake as the resulting interaction with the negatively charged cell membrane is stronger. However, on the other hand previously published studies reported toxic effects towards cells caused by aminated NPs which is also in agreement with our observations where the irregular cellular morphology suggested to cell damages. Positively charged NPs having amine or cysteamine groups on the surface induced destabilization of the lysosomal membrane and damaged the mitochondria after entering the astrocytoma cell line 1321N1.[230] For endothelial cells, a positively charged NP surface led to a strong reduction in cell viability, whereas neutral and negatively charged nanoparticles were classified as highly biocompatible.[229] In addition, it had to be considered that the stability of the protein corona verified by DLS (Table 1) depended highly on adsorption forces between the surface charge of the NPs and the protein source. As a consequence, the individual charge of the functional groups on NPs still had to be taken into account during cellular uptake[233].
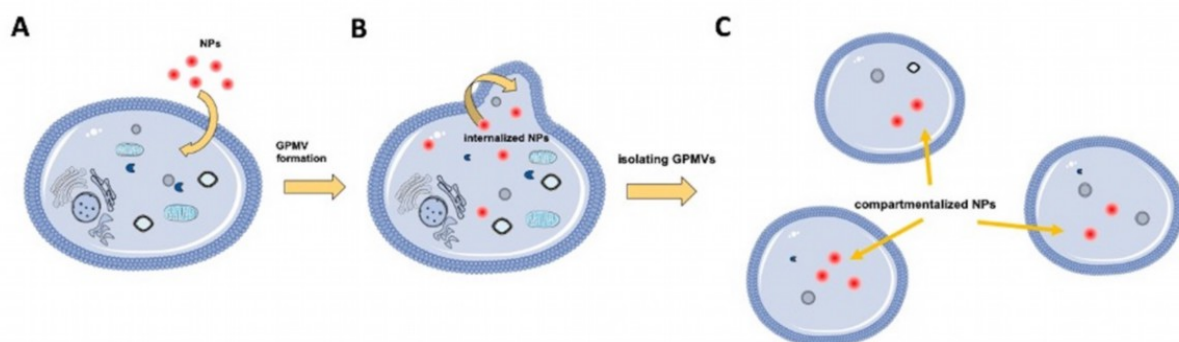


*Figure 16. General procedure for generating GPMVs from cells loaded with NPs – A) NPs are taken up by the cells within 24 h. B) NPs transfer into GPMVs during GPMV formation, induced by GPMV vesiculation solution. C) After 1-2 h the NP equipped GPMVs are formed and isolated from the cells.*

By comparing the two negatively charged NPs (carboxylated, unmodified) we investigated that not only the surface chemistry but also the biocompatibility of the NPs played a crucial role in the transfer process from cells into GPMVs. The carboxylated NPs have been often used for cell uptake studies as they are known to be nontoxic are known for their biocompatibility.[224] In contrast to this, the unmodified NPs were not found in GPMVs although these NPs also had a strong negatively charged surface.

The experiments demonstrated how strong the surface chemistry and biocompatibility affected the NP transfer into GPMVs. Positively charged aminated NPs induced an intrinsic cytotoxic effect on the cells, and simultaneously prevented their transfer signaling that such nanostructures are not biologically relevant for future biomedical studies. In general, the uptake of NPs by cells without causing cell death so that GPMVs can still be formed, was the fundamental precondition for a successful NP transfer into GPMVs. In contrast to synthetic GUVs, this kind of built-in sorting out system of not biocompatible nanomaterials occurred naturally in the case of GPMVs and presents a direct advantage over GUVs, where all kinds of nanoscale objects can be encapsulated with no feedback information on biorelevance.[13, 140] This described biocompatible-selectivity of GPMVs allowed the application as cell-mimicking platform while maintaining a strong resemblance to real cells.

As the carboxylated NPs were both non-toxic and successfully taken up and transferred into GPMVs, we selected them to establish the role of other molecular properties on the NPs transfer into GPMVs. We focused on the questions such as how different sizes and concentrations of carboxylated NPs influence the transfer into GPMVs.

# Crucial preconditions for the transfer of polystyrene carboxylated nanoparticles into GPMVs

**Analysis of empty GPMVs by CLSM**

In order to investigate if the transfer process of NPs into GPMVs has an impact on the size of the formed GPMVs, we first evaluated the average size of 250 GPMVs from each cell line (HepG2, Caco-2, HeLa) without NPs (Figure 17). The yielded GPMVs were isolated from the cells and observed by confocal laser scanning microscopy (CLSM) to measure the respective diamters of the GPMVs. HepG2 produced GPMVs in a range of ca. 5-14 μm. Caco-2 cells formed the biggest GPMVs on average with a size and with a large size distribution between 6 and 20 μm. The smallest, yet most uniform in size, GPMVs were obtained from HeLa cells (4-8 μm).
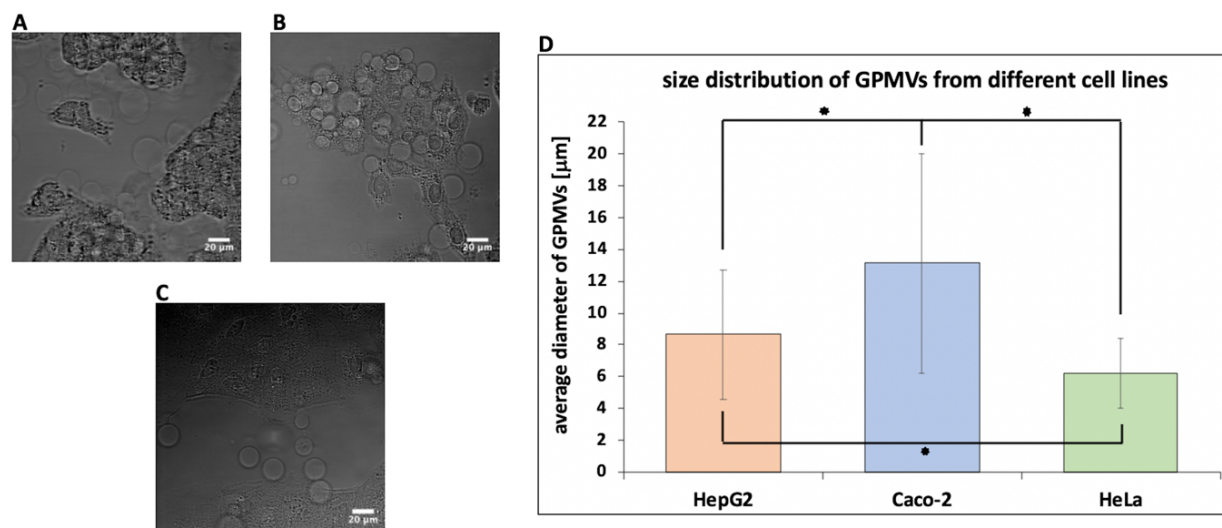


*Figure 17. HepG2, Caco-2 and HeLa cells form GPMVs – A) HepG2 cells after GPMV formation, B) Caco-2 cells after GPMV formation, C) HeLa cells after GPMV formation, D) average size of GPMVs generated by HepG2 (red), Caco-2 (blue) and HeLa cells (green) given as average diameter in μm with standard deviation. Significance level: p < 0.5 (\*).*

**Effect of size and cellular uptake of carboxylated PS NPs on transfer into GPMVs**

In the subsequent study, we determined an upper size limit of carboxylated NPs that still transferred into GPMVs using red fluorescent carboxylated PS NPs with different sizes (40 nm and 100 nm (Figure S15) and 500 nm (Figure S16)). The original concentrations of the particle

suspensions were analyzed by NTA (Table S3) to prepare dilutions at the same NP concentration ($4\times10^9$ particles/mL, $8\times10^9$ particles/mL, $1.6\times10^{10}$ particles/mL). First, the three cell lines (HepG2, Caco-2, HeLa) were treated with 500 nm particles to determine the upper limit of NP transfer. The resulting CLSM images showed only empty GPMVs after isolation from the cells indicating that particles of 500 nm in size were already above the maximum size limit for transferring NPs into GPMVs (Figure S16). In contrast to 500 nm particles, NPs of 40 nm and 100 nm in size were observed in the GPMVs formed by all three cell lines (Figure S15).

As mentioned above, the cellular uptake of the nanostructures into cells presented one important checkpoint in the investigation of the GPMV platforms. Therefore, the NP cell uptake was a crucial step we had to consider when optimizing the transfer of different particles into GPMVs. Due to this, flow cytometry analysis with each cell line treated with 40 nm or 100 nm carboxylated PS NPs at three different concentrations were performed ($4\times10^9$ particles/mL - $1.6\times10^{10}$ particles/mL, Figure S17-S20). In general, we observed a dose dependent increase in NP uptake in the case of all three cell lines. Regarding the selectivity, we observed that all cell lines favored the uptake of the smaller 40 nm NP over the larger 100 nm particles where significantly more 40 nm particles have been taken up at most tested concentrations compared to 100 nm NPs. The selectivity towards the different sizes was only negligible at the highest NP concentration tested ($1.6\times10^{10}$ particles/mL) for HepG2 cells and at the lowest NP concentration ($4\times10^9$ particles/mL) tested for Caco-2 cells.

The results will serve as a basis for determining the relationship between uptake and transfer of the NPs into GPMVs.


**Analysis of isolated GPMVs with transferred NPs by flow cytometry and CLSM**

After determining that the three cell types have efficiently taken up the NPs in a concentration dependent manner, we turned the focus towards investigating the appropriate technique for analyzing GPMVs as biomimicking platform. We started with a combination of both flow cytometry and CLSM to examine which method provided the most valuable information about the formed GPMVs and about the transferred NPs for a detailed analysis. The focus of this experiments was to clarify which of the two technique (flow cytometry or CLSM) provided the most appropriate analysis for the investigation of NP transfer into GPMVs. Based on the success with isolating GPMVs from HepG2 cell line in a previous study[14], we chose HepG2 as a model cell line to determine first if GPMVs are detected adequately by these two different measurement techniques and second, to identify and evaluate the information that were

provided by these two techniques. Therefore, we treated the HepG2 cells with different concentrations of 100 nm red fluorescent carboxylated PS particles ($4\times10^9$ particles/mL, $8\times10^9$ particles/mL and $1.6\times10^{10}$ particles/mL) in order to evaluate the dose-dependent NP transfer by flow cytometry and CLSM.
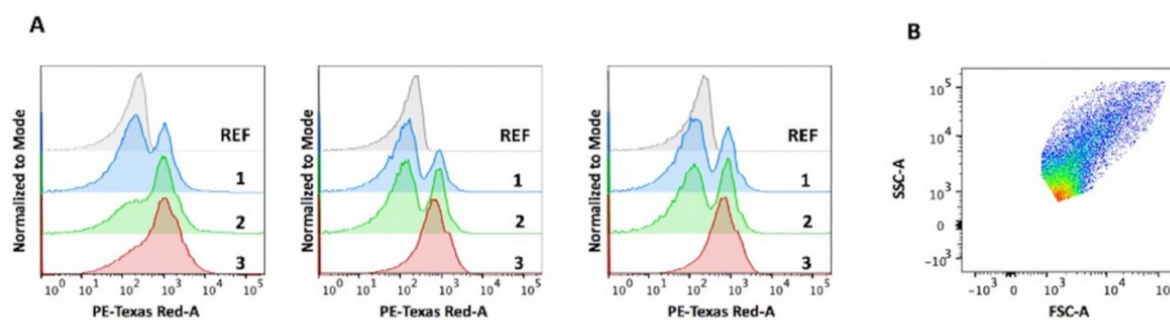


*Figure 18. Flow cytometry measurements of isolated GPMVs formed from HepG2 cells and loaded with increasing concentrations of 100 nm red fluorescent carboxylated PS NPs – A) three technical repeats of the measurements. The graphs of three self-standing flow cytometry measurements include the following peaks for GPMVs yielded from cells incubated with: REF no NPs (grey), 1: $4\times10^9$ particles/mL (blue), 2: $8\times10^9$ particles/mL (green), 3: $1.6\times10^{10}$ particles/mL (red). B) Flow cytometry analysis of GPMV size characterization by sideward and forward scattering analysis. The marked-out section represents GPMV populations used for analysis by flow cytometry.*

Flow cytometry analysis allowed a fast determination of the amount of GPMVs derived from HepG2. In addition, flow cytometry provided an analysis of the fluorescence of NP-equipped GPMVs, where we observed the effect of the NP concentration on the NP transfer ratio into GPMVs (Figure 18). Empty GPMVs served as a negative control (red peak) and the measurement series were repeated three times. The measurements showed clear the expected dose dependent increase in the NP loaded GPMV population. At the highest NP concentration, more than half of all GPMVs were loaded with NPs.

The visualization of the GPMVs from HepG2 by CLSM allowed us to track the red-fluorescent NPs inside all GPMVs. The NPs diffused freely inside the cytoplasm of the GPMVs. In contrast to flow cytometry, CLSM provided information about the size of each GPMV and about the distribution of transferred NPs and the average number of NPs/GPMV together with the mean size of the respective GPMVs (Figure S21-S26). Furthermore, we were able to distinguish by

CLSM if NPs are inside GPMVs or if interactions or aggregation between NPs and the membrane occurred.

As a result, we chose CLSM as the main imaging technique to establish and quantify the impact of size and concentration on the NP transfer process from three different cells (HepG2, Caco-2, HeLa) into GPMVs, since it allowed an exact localization of NPs. With CLSM it was possible to guarantee that only NPs freely diffusing within the cavity of the GPMVs were taken into the study without aggregation present or high affinity toward the GPMV membrane (Figure 19).
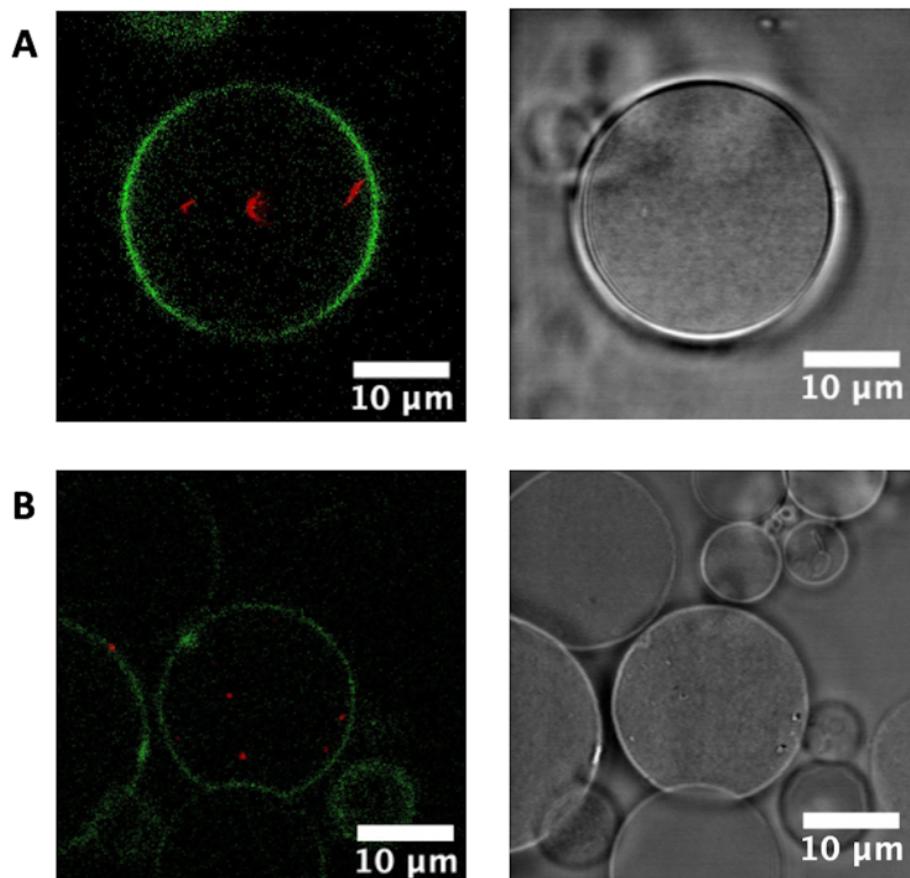


*Figure 19. GPMVs isolated from HepG2 cells – The membrane was stained fluorescent green either by A) CellMask$^{TM}$ or B) Lck-GFP-transfection[14]. Inside GPMVs, red fluorescent carboxylated PS NPs (100 nm) can be observed.*

**Effect of initial concentration of carboxylated PS NPs (40 nm, 100 nm) on their transfer to GPMVs**

We treated the three cell lines with 40 nm and 100 nm fluorescent carboxylated NPs particles in increasing concentrations ($4\times10^9$ particles/mL, $8\times10^9$ particles/mL, $1.6\times10^{10}$ particles/mL,

and $1.6 \times 10^{11}$ particles/mL) to quantify the impact of NP concentration on the transfer efficiency. After incubating the cells with NPs and subsequent GPMV formation, the transfer of 40 nm and 100 nm particles into GPMVs was visualized by CLSM (Figure S27 and Figure S28). We imaged more than 250 GPMVs in each experiment and summarized the observations regarding the average numbers of NPs/GPMV (Figure 20) and the percentage of GPMVs that showed NPs in the cavity as function of NP size and concentration GPMVs (Figure 21). One experiment covered the analysis of isolated GPMVs derived from one of the three cell lines treated with one type of NP size at each concentration, where we determined the number of NPs/GPMV along with the diameter of GPMVs using ImageJ. By collecting and summarizing all data, we received distribution graphs (Figure S21-S26), showing the diameter of GPMVs on the x-axis and the number of NPs inside GPMV on the y-axis. We investigated that the size of formed GPMVs has not been affected by the transfer process of NPs for any of the three cell lines, which further supported GPMVs as a platform to study NPs in a cell-like environment. In case of HepG2 cells, the formed GPMVs had a size of $8.7 \pm 4.1$ μm in the absence of NP uptake (Figure 17). The average size of GPMVs equipped with 40 nm sized NPs was $7.3 \pm 0.6$ μm and $7.3 \pm 0.2$ μm when equipped with 100 nm sized NPs. These results demonstrated that neither the transfer of NPs nor their size up to 100 nm affected the mean value of the diameter of GPMVs if NPs have transferred into the cavity.

For Caco-2 and HeLa cells, an impact of the NP transfer on the diameter was slightly more pronounced but still not significant. GPMVs formed by Caco-2 cells, showed an average size of $13.1 \pm 6.9$ μm in absence of NPs, while the 40 nm particle transfer resulted in GPMVs with a diameter of $7.9 \pm 0.4$ μm and $10.0 \pm 0.8$ μm for 100 nm. In case of HeLa cells, we obtained slightly bigger GPMVs if there were no NPs inside ($6.2 \pm 2.2$ μm) and when equipped with 40 nm particles the mean size of GPMVs decreased to $3.9 \pm 0.4$ mm, and $5.8 \pm 0.6$ μm for transfer of 100 nm NPs. Summarizing all data, we suggest that the transfer of NPs into GPMVs for Caco-2 and HeLa preserved the order of magnitude of the GPMVs size, but in contrast to HepG2, a higher degree of size change was observed.

With regard to the average number of NPs/GPMV (Figure 20), we observed that each cell line had a different average number of 40 nm and 100 nm particles per GPMV. For these experiments, the determined NPs represented the minimal number of NPs/GPMVs as the number was obtained by CLSM micrographs without a 3D staking. The NPs were freely moving inside GPMVs, so each micrograph presented a current snapshot of the NPs in the confocal plane of the microscope.
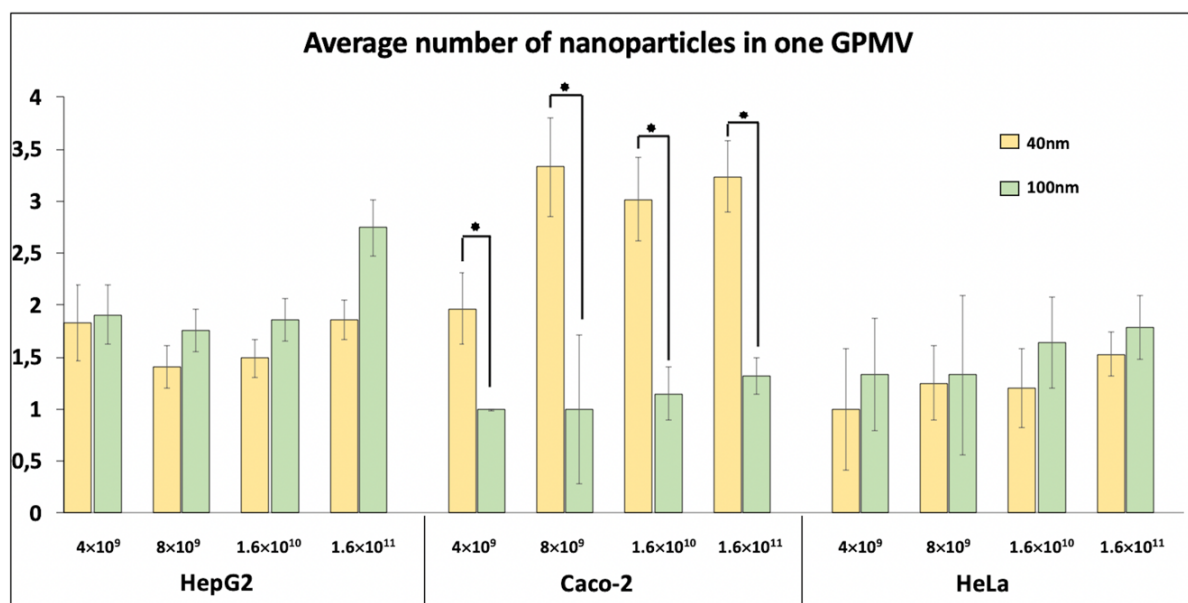
**Figure 20. *Average number of 40 nm (yellow) and 100 nm (green) NPs in 1 GPMV* –** *GPMVs were obtained from three cell lines HepG2, Caco-2 and HeLa. NPs were used at 4 different concentrations: $4\times10^9$ particles/mL, $8\times10^9$ particles/mL, $1.6\times10^{10}$ particles/mL, and $1.6\times10^{11}$ particles/mL. 250 GPMVs/cell line and for each type of NPs were observed by CLSM. Error bars are given as ± standard deviation, significance level: p < 0.5 (\*).*

Considering the size of NPs, we observed the highest difference of the average number of NPs/GPMV for the Caco-2 cells. At the maximum concentrations of the NPs, a number of 3.2±0.3 particles/GPMV was reached for 40 nm, and 1.3±0.2 particle/GPMV were obtained for 100 nm particles. In contrast to Caco-2, HepG2 and HeLa cell lines did not show a considerable effect of the NP size on the average number of NPs/GPMV. In GPMVs formed from HepG2, the number of 40 nm particles found per GPMV at highest concentration was 1.9±0.2, and 2.8±0.3 particles/GPMV in case of 100 nm. For HeLa cells, the average numbers of NPs were 1.5±0.2 (40 nm NPs) and 1.8±0.3 (100 nm NPs) per GPMV.

Even though it is possible to achieve a higher efficiency of NP encapsulation by microfluidic assembly, such resulting GUVs cannot keep up with the huge cell resemblance of GPMVs. For our study it was important to select GPMVs instead of GUVs as cell-mimicking platform since GPMVs contain both a cytoplasm and cell membrane. In comparison with NPs encapsulated in GUVs performing controlled reactions inside GPMVs[140], the average number of 1-3 NPs per GPMV presented a sufficient number of a successful nanoobject transfer with the future potential of mimicking cellular signaling pathways. As mentioned above, the numbers summarized in the graph, were maybe lower than the real numbers. Our counted values were

obtained by observing single plane projections of GPMVs, but the NPs were freely moving inside GPMVs. Besides that, there was no correlation between the number of NPs/GPMV and the size of GPMVs.

The percentage of GPMVs from each cell line that contained transferred NPs (loaded GPMVs) is shown as total numbers in Figure 21. In the case of HepG2 cells, the percentage of loaded GPMVs increased with the concentration of NPs which was also in in agreement with the above presented flow cytometry measurements suggesting that the percentage of cellularly taken up NPs correlated with the initial concentration used for cell incubation. The calculated values derived from recorded CLSM images (Figure 21), showed that by treating HepG2 cells with the highest NP concentration ($1.6 \times 10^{11}$ particles/mL), the number of formed GPMVs with NPs inside increased to 40-43 %. The percentage of the loaded GPMVs from HeLa cells exhibited a similar dependency on the NP concentration as compared to HepG2 cells. But in contrast to HepG2, the maximum percentage was lower: 20 % of the GPMVs were equipped with 40 nm, and 14 % with 100 nm particles. In case of Caco-2 cells, the number of resulting loaded GPMVs depended notably on the size of the transferred NPs. 35 % loaded GPMV population was achieved for the 40 nm NPs, but only 25 % for the 100 nm particles. In summary, the transfer efficiency of NPs was the greatest when transferring from HepG2 cells into the subsequently formed GPMVs. Here, almost 40 % of the GPMVs were successfully loaded in case of 40 nm particles at highest concentration, and 45 % in the case of 100 nm particles. In total, HeLa cells had the lowest transfer of the three cell lines with only 15-20 % loaded GPMVs at the highest concentration of NPs.

Comparing the cellular uptake studies of NPs in individual cell lines (Figure S17-S20) to the results of NP loaded GPMVs (average number of NP/GPMV and % of NP loaded GPMVs) we assumed that the NP to GPMV transfer was not only promoted by an efficient cell uptake. Addditionally, it depended on the "post-GPMV-behavior" of each cell-type. For example, while the uptake of 40 nm NPs was favored for HepG2 cells, we observed, however, that the transfer of 100 nm NPs from HepG2 into GPMVs was more favored. In case of Caco-2, 40 nm NPs were favored both in the cellular uptake of the NPs and in the NP transfer process into GPMVs. HeLa cells seemed to be not be as selective towards NP size. This indicated that for designing a GPMV platform, both first step (cellular uptake) and the transfer and isolation as second step were crucial. Again, this highlighted the advantage of a designed GPMV platform over synthetic or lipidic GUVs. In GPMVs, only biocompatible nanostructures, that were readily taken up and flow freely through the cytoplasm, transferred into the biomimicking microcompartment.
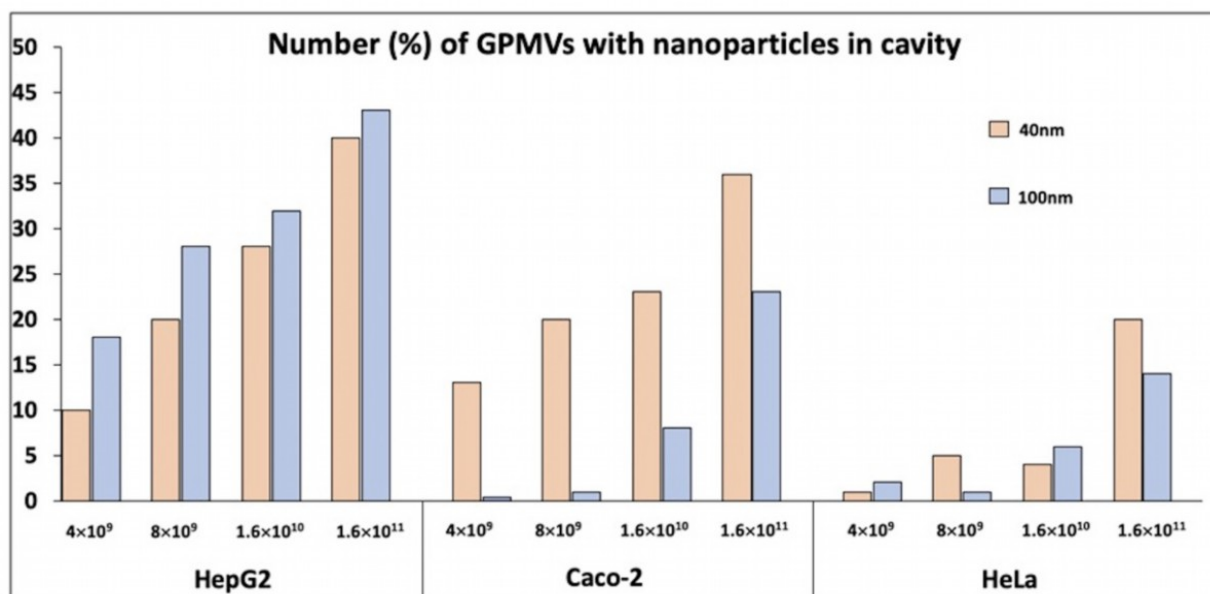
*Figure 21. Percentage of all GPMVs equipped with 40 nm (red) or 100 nm (blue) NPs in their cavity. – GPMVs were obtained from three cell lines HepG2, Caco-2, HeLa. NPs were used at four different concentrations: $4\times10^9$ particles/mL, $8\times10^9$ particles/mL, $1.6\times10^{10}$ particles/mL, and $1.6\times10^{11}$ particles/mL. 250 GPMVs/cell line for each type of NPs were observed by CLSM.*

Considering our results about the effect of concentration and size of carboxylated PS NPs, we were able to extract interesting characteristics for each cell line. The GPMVs formed from HepG2 and HeLa cells seemed to be dependent on the NP concentration, but independent on the size of the NPs as the transfer of 40 nm and 100 nm showed similar results regarding the average number of NPs/GPMV and percentage of NP-loaded GPMVs. In contrast to this, Caco-2 cells resulted in a more size dependent transfer of the NPs. Compared to 100 nm particles, the treatments with 40 nm particles achieved considerably higher values of the average number of NP/GPMV and of the percentage of NP loaded GPMVs.

# Conclusion

GPMVs present an innovative alternative to synthetic GUVs in applications as a biomimicking platform. GPMVs have a high potential for many different biologically relevant studies and are assumed to present the closest cell mimics. Our study highlighted their further medical potential. However, the lack of information regarding loading strategies with nanostructures limited the further development of GPMVs considering the multifaceted details of the NP transfer mechanisms. Additionally, the impacts of the respective cell line are complex and still not investigated completely. Therefore, our work aimed to start the investigation how the transfer on NPs into GPMVs could be optimized regarding different properties of NPs in order to designed cell-mimicking platforms that benefit from a cytoplasm medium and a cell membrane as boundary.

By comparing HepG2 and Caco-2 cells with HeLa as the model cell line for carboxylated PS NP uptake studies, we demonstrated that the NP transfer mechanism form the cells into GPMVs was cell dependent. With focus on the size of GPMVs, HeLa cells formed smaller but more uniform GPMVs while Caco-2 cells yielded larger GPMVs but having a bigger size distribution. The results regarding HepG2 cells having a lack of the membrane protein caveolae1, we observed that HepG2 are particularly well suited for GPMV formation, as the cells showed a high abundance of NP loaded GPMVs with no observable effect on the size of the GPMVs. HepG2 cells resulted GPMVs with a high average number of 40 nm and 100 nm particle loaded GPMVs. Caco-2 cells, already known for great adsorption skills (model for the intestinal barrier) seemed to be the best choice for 40 nm NPs, especially, since here the obtained average number of NPs/GPMV was the highest compared to HepG2 or HeLa.

In general, we suggest that a balance between the highest NP concentration (achieving the most efficient transfer of NPs into GPMVs) and the NPs' intrinsic toxicity is essentail. For optimizing GPMVs as cell-mimicking platform, we want to highlight the fact that biocompatibility of the nanostructures was already taken into account during the tranfer process as it was an important prerequisite for our system. Compared to synthetic GUVs, we have the possibility to prescreen all non-biorelevant nanostructures prior to loading in case of designing GPMVs as biomimicking platform. Therefore, GPMVs allowed us to study only nanostructures with high biomedical potential. We are convinced that our study provided an important guideline towards further modification and applications for GPMVs equipped with nanoassemblies. GPMVs allowed us to study the interactions of NPs or investigate distinct reactions of nanocompartments inside a close-to nature system. Our study will help promote the future

development of GPMVs such as an optimized strategy to separate modified GPMVs from non-modified. Potential approaches may include a technique resembling to FACS (Fluorescence Activated Cell Sorting) or use magnetic beads to achive appropriate separation in a magnetic field.

# CLOSING REMARKS AND OUTLOOK

Polymersomes allowing the modification with diverse biomolecules and compounds are described detailed in this work. Such bioactive nanocompartments have increasing potential in many different applications as their versatility is markedly expanded by the biomolecules that endow the polymersomes with specific molecular and cellular functions. In particular, polymersomes are of great interest because of the increased stability and biocompatibility.

Towards the development of bioactive polymersomes, we modified chemically OmpF as a biopore that showed triggerable permeability when reconstituted in the polymeric membrane. For the OmpF modification, we designed and synthetized a small organic linker that blocked the passage of molecules through the pore. In presence of periodate, the linker was cleaved and the diffusion through OmpF was established. Inside the polymersomes, laccase was encapsulated to catalyze the oxidation of an external substrate to a colored product and to visualize the pore opening. For closing the pore and for a controlled cleavage, different factors had to be taken into account during the linker design. The linker was designed to have the appropriate size to block the OmpF passage and at the same time to allow the anchoring of different functional groups. The linker was equipped with maleimide ends to enable the covalent binding to two engineered cysteine of OmpF (OmpF-M). In the middle of the linker structure, we needed a functional group where covalent bonds cleave upon a certain stimulus (periodate). In addition to this, we modified the linker with fluorophores to facilitate the detection and consequent measurements. For the synthesis of the linker, we used peptide crosslinkers commonly used for bioconjugation as starting materials. Such crosslinkers allowed mild reaction conditions and formed products with expected water solubility. In general, it is essential to work in aqueous solutions during the protein modification to prevent the protein structure and functionality. Furthermore, we applied organic chemistry techniques for high reaction yields and purifications. Our approach to the chemical modification of membrane proteins presents a first step towards the development of biomolecules with triggerable functionality and activity due to the guaranteed mild working conditions. A promising future study regarding the linker would be to investigate if after the oxidation (clevage of the linker) a subsequent reduction will merge the two linker residues together again. This would show the potential of the linker as a reversible blocking/unblocking tool of the OmpF pore. Another

chemistry-related protein modification could describe a synthesis of a linker that allows reversible activation without breaking chemical bonds and provides mild conditions. An advanced linker structure would be needed that e.g., undergoes different reversible spatial orientations leading to a blocking/unblocking of a membrane protein or activation/deactivation of a receptor. One opportunity would be light-sensitive compounds such as azobenzenes that changes from trans to cis conformation upon a certain wavelength.

In addition to synthetic biomimicking compartments, like GUVs, GPMVs represent an innovative platform for cell-mimics as such microscale compartments are derived formed from cells and include most of the cellular components (e.g., biological membrane and cytoplasm). Moreover, GPMVs can be produced fast and isolated in larger quantities by chemical treatment. Even though GPMVs are the closest cell-like compartments available on the market, the application of GPMVs as cell-mimicking platform in biological relevant studies remains a challenge.In our second study, we demonstrated that GPMVs were formed from different cell lines. Depending on the cell line, GPMVs have a size from 4 to 20 μm. By investigating the transfer of cellular taken up NPs into subsequent formed GPMVs, we were able to gather new insides and trends regarding the customizable modification of GPMVs with synthetic nanoscale objects. We studied the impact of different cell lines and NPs varying from surface modification, size and concentration on the NP transfer process. An interesting next step in this field would be the investigation of GPMVs as promising alternatives towards exosomes. As both platforms are directly formed from cells, they show similar compositions, but in contrast to exosomes, GPMV production and modification is more practicable and faster. Therefore, it would be very interesting to decrease the size of GPMVs in the nanoscale (more similar to exosomes) and investigate properties of GPMVs especially regarding targeted drug delivery where exosomes attract a lot of attention due to their great features.

# *Chapter 6*

# MATERIALS AND METHODS

## Chapter 3

### Materials

Disuccinimidyl tartrate (DST) and 3,3'-N-[ε-maleimidocaproic acid] hydrazide, trifluoroacetic acid salt EMCH were purchased from ThermoFisher, cyanine 3 maleimide from Lumiprobe. All other materials were purchased from Sigma Aldrich, except the $PMOXA_{11}$-b-$PDMS_{104}$-b-$PMOXA_{11}$ triblock copolymer which was previously synthesized in our group. All reagents were of the highest commercially available grade and were used without any further purification, unless stated otherwise.

### Methods

#### Synthesis of amphiphilic triblock copolymer

The amphiphilic block copolymer $PMOXA_{11}$-b-$PDMS_{104}$-b-$PMOXA_{11}$ was previously synthesized in our group according to reported protocols.[59, 93] Briefly, a hydroxyl-terminated bifunctional PDMS was reacted below -10 °C with trifluoromethanesulfonic anhydride in dry hexane, leading to the activated PDMS macroinitiator. After filtration under argon and removal of hexane under vacuum, dry chloroform was added as reaction solvent, in which dry 2-methyl-2-oxazoline (MOXA) reacted with the macroinitiator via symmetric cationic ring-opening polymerization. The hydroxyl-terminated triblock copolymer was obtained after quenching the polymerization reaction with a triethylamine/water mixture (1:4 v/v) and ultrafiltration in a 1:5 (v/v) water/ethanol mixture. A number-average molecular weight ($M_n$) of 8700 g mol$^{-1}$ and a chemical composition of $PMOXA_{12}$-b-$PDMS_{87}$-b-$PMOXA_{12}$ was obtained from the $^1$H-NMR spectrum of this triblock copolymer, whereas its dispersity (Đ) of 1.6 was revealed by gel permeation chromatography (GPC) in THF.[59] To decrease the dispersity of this copolymer and thereby better control the shape morphology of the self-assembled structures, an extraction from a1:1 (v/v) hexane/methanol mixture was performed and the copolymer fraction with a longer PDMS block was recovered from the hexane phase after solvent removal. After this additional step, the copolymer with a longer PDMS block was characterized by $^1$H NMR (Figure S6) and

SEC (Figure S7), obtaining the final chemical structure as PMOXA$_{11}$-b-PDMS$_{104}$-b-PMOXA$_{11}$ with $M_n$ = 9800 g mol$^{-1}$ (from $^1$H-NMR) and Đ = 1.23 (from SEC).

$^1$H NMR (500 MHz, CDCl$_3$) δ/ppm = 3.84 – 3.15 (bm, 8H), 2.30 – 1.96 (bm, 6H), 1.64 – 1. 53 (bm, 4H), 1.38 – 1.26 (bm, 4H), 0.50 – 0.60 (m, 4H), 0.20 – -0.10 (bs, 6H).

## Synthesis and characterization of the bismaleimide Linker

To obtain the thiol-reactive linker able to covalently bind to both thiol groups of the OmpF double mutant and block its pore, we have selected as diol-containing starting compound the disuccinimidyl-activated derivative of tartaric acid. Thus, **Compound 1** was first synthetized according to a general procedure used for crosslinking proteins with small modifications.[235] Briefly, disuccinimidyl tartrate (DST, 10.7 mg, 31 mmol, 1.0 eq.) was first dissolved in 100 µL DMSO in an Eppendorf tube (1.5 mL), and then a 0.24 M aqueous solution containing L-cysteine was added (284 µL, 68.2 mmol, 2.2 eq.). After the pH was adjusted to a value between 8 and 9 with 1 M NaOH (aqueous solution), the reaction mixture was shaken in the dark at RT for 16 h. The resulting suspension was centrifuged (13.400 rpm, 5 min). The solvenst were removed by rotary evaporator, and the resulting product was dried under vacuum for 3 days to give **Compound 1** as a white solid which was further used in the synthesis of **Compound 2**.



MF: C$_{10}$H$_{16}$N$_2$O$_8$S$_2$

MW: 356.36

ESI-MS m/z calcd for C$_{10}$H$_{16}$N$_2$O$_8$S$_2$ [M+2H]$^+$: 179.02; found: 179.05.
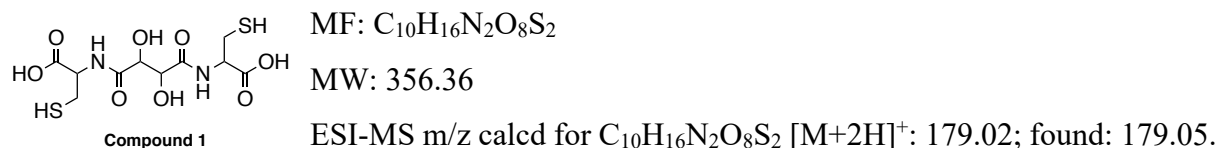
$^1$H-NMR (D$_2$O, 500 MHz): δ = 4.68 (d,), 4.65 ppm (d), 3.45-3.30 (dd, 4H) ppm.

$^{13}$C-NMR (D$_2$O, 126 MHz): δ = 176.49, 173.51, 162.97 (d, J = 35.5 Hz), 72.45, 72.35 (d, J = 7.0 Hz), 54.87, 53.49, 38.72, 37.55, 25.17 ppm.

The synthesis of **Compound 2** was adapted and modified from literature.[236] **Compound 1** (2.8 mg, 8.0 mmol, 1.0 eq.) was dissolved in 200 µL mixture of H$_2$O/DMF = 1/1 with a pH>8, whereas cyanine 3 maleimide (10.7 mg, 16.0 mmol, 2.0 eq.) was dissolved in 400 µL DMF. Both solutions were combined, and the resulting reaction mixture was shaken in the dark at RT for 16 h after adjusting the pH value back to 8 with 1 M NaOH. The solvent mixture was removed by adding an excess of toluene and subsequent rotary evaporation. To the crude product 10 mL H$_2$O with a pH>8 was added. The aqueous layer was extracted 3x with DCM. The organic phases were collected, and the solvent was evaporated to give **Compound 2** as pink solid (7.64 mg, 4.9 mmol, 61%).

Compound 2
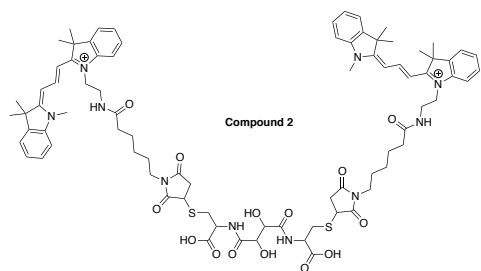
MF (cation): $C_{80}H_{104}N_{10}O_{14}S_2$

MW: 1515.87 (cation),

ESI-MS m/z calcd for $C_{82}H_{102}N_{10}O_{14}S_2$ [M+2H]$^+$: 379.18; found: 379.16.

$^1$H-NMR (500 MHz, CDCl3): δ = 11.35 (s, 2H), 8.38 (t, J = 13.4 Hz, 2H), 7.45 – 7.32 (m, 9H), 7.17 (d, J = 8.0 Hz, 2H), 7.12 (d, J = 8.0 Hz, 2H), 6.70 (t, J = 13.9 Hz, 4H), 6.41 (d, J = 13.1 Hz, 2H), 5.82 (d, J = 13.1 Hz, 2H), 4.17 (t, J = 7.6 Hz, 4H), 3.69 (s, 6H), 3.52 – 3.39 (m, 7H), 2.30 (t, J = 6.8 Hz, 4H), 2.23 (d, J = 10.4 Hz, 8H), 1.84 (p, J = 7.8 Hz, 4H), 1.80 – 1.75 (m, 4H), 1.72 (d, J = 5.5 Hz, 22H), 1.56 – 1.41 (m, 4H).

$^{13}$C-NMR (126 MHz, CDCl3): δ =174.73, 174.57, 174.04, 171.47, 168.05, 151.03, 143.03, 142.15, 140.97, 140.69, 138.71, 129.47, 129.34, 128.15, 126.04, 125.79, 122.43, 122.40, 111.80, 111.10, 104.46, 104.18, 77.67, 77.41, 77.16, 49.61, 49.32, 44.84, 39.84, 39.47, 36.74, 31.88, 28.50, 27.47, 26.05, 25.53.

The **Linker** was synthetized according to the general procedure used for chemical labelling with small modifications.[237] Briefly, 3,3'-N-[ε-Maleimidocaproic acid] hydrazide, trifluoroacetic acid salt (EMCH, 4.2 mg, 12.3 mmol, 2.5 eq.) was dissolved in 300 μL H$_2$O, whereas 1-Ethyl-3-(3-dimethylaminopropyl)-carbodiimide (EDC HCl, 4.7 mg, 24.5 mmol, 5 eq) in 100 μL H$_2$O. A solution of **Compound 2** (7.6 mg, 4.9 mmol, 1 eq.) was prepared in H$_2$O/DMF (1:1000, 3 mL). All three solutions were combined, and the pH was adjusted to 7 with 1 M NaOH. The reaction mixture was stirred in the dark at RT for 16 h. The crude product was purified by extraction with DCM (3x). The organic layers were combined, and the solvents were evaporated to yield the **Linker** as pink solid (8.0 mg, 3.8 mmol, 78 %).



Linker
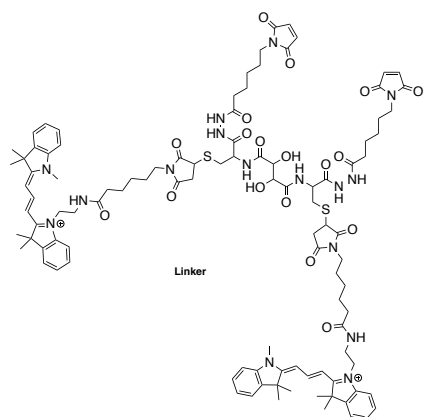
MF (cation): $C_{102}H_{128}N_{16}O_{18}S_2$

MW (cation): 1930.36

ESI-MS m/z calcd for $C_{102}H_{128}N_{16}O_{18}S_2$ [M+H]$^+$: 643.64; found: 643.68.

$^1$H-NMR (500 MHz, CDCl3): δ 7.71 (d, J = 16.0 Hz, 1H), 7.58 – 7.49 (m, 3H), 7.46 – 7.30 (m, 9H), 6.87 – 6.67 (m, 2H), 6.46 (d, J = 16.0 Hz, 2H), 6.15 (t, J = 1.3 Hz, 2H), 5.62 – 5.53 (m, 1H), 5.29 (s, 9H), 4.51 – 4.39 (m, 6H), 4.22 – 3.96 (m, 1H), 3.75 – 3.58 (m, 4H), 3.52 – 3.29 (m, 3H), 2.95 (s, 1H), 2.88 (s, 1H), 2.41 – 2.10

(m, 4H), 1.99 – 1.85 (m, 15H), 1.72 (d, J = 5.9 Hz, 16H), 1.41 (s, 3H), 1.32 – 1.17 (m, 13H), 1.10 (s, 8H), 0.90 – 0.79 (m, 3H), 0.07 (s, 1H).

^{13}C-NMR (126 MHz, CDCl3): δ 167.20, 166.71, 145.43, 135.96, 134.29, 130.45, 128.94, 128.93, 128.16, 126.11, 117.54, 77.24, 62.52, 62.21, 59.53, 53.44, 38.15, 31.24, 29.71, 28.13, 18.29, 14.13, 1.02.

## OmpF expression, extraction

Both OmpF wild type and the OmpF-M double mutant (OmpF K89C/R270C) were expressed and purified following a published procedure.[199] Protein purity was evaluated on a 12 % SDS-PAGE gel, and the concentration measured spectrometrically at λ = 280 nm with Nanodrop (Witec Ag). Wild type and mutant OmpF were stored at 4 °C in 3 % OG at a concentration of around 3 mg/mL for several months. Before the reconstitution experiments, OmpF was dialysed against 1 L of 0.05 % OG in PBS for 16 h, then 2x against PBS for 2 h. After the dialysis, the protein concentration was adjusted to 2.0 mg/mL in PBS.

## Chemical modification of protein gate OmpF double mutant (OmpF-M)

OmpF-M was diluted with PBS solution containing 3 % OG to a concentration of 1 mg/mL (500 µL, 25 mM, 12.5 nmol). Next, a solution of the linker in MilliQ-$H_2O$ (7.5 mM) was added (2.5 µL, 19 nmol). The mixture was stirred overnight in the dark at RT. The OmpF-M labelled with the linker (linker-OmpF-M) was washed 12 times with 1 % OG in PBS in Amicon Ultra-0.5 mL centrifugal filters for protein purification and concentration, molecular cutoff 10 kDa (Millipore). The volume of linker-OmpF-M suspension was adjusted to 450 µL, transferred to a dialysis tubing with a 14 kDa molecular cutoff (Carl Roth), and dialyzed against 1 % OG solution in PBS, for 16 h, followed by 2x2 h dialysis against PBS. After dialysis, the protein concentration of linker-OmpF-M was measured spectrometrically at λ = 280 nm with Nanodrop (Witec Ag) and adjusted to 2.0 mg/mL.

## Characterization of linker-OmpF-M

2.5-5 µL of OmpF WT, OmpF-M and linker-OmpF-M were each mixed with 4 x laemmli loading buffer (2.5 µL) containing mercaptoethanol (0.7 mM). The volume was adjusted to 12.5 µL with 1 % OG solution and samples denatured at 95 °C for 5 min. Samples (10 µL) were loaded on a 4-20 % precast polyacrylamide gel (Mini-PROTEAN® TGX™) and ran at 200 V for 45 min (Figure S5). Before Coomassie staining, the gel was imaged by Bio-Rad GelDoc to observe the emitted fluorescence of the linker (fluorescence of cyanine3 maleimide: 550/580).

**Preparation of bioactive polymersomes with encapsulated laccase**

5 mg PMOXA$_{11}$-b-PDMS$_{104}$-b-PMOXA$_{11}$ triblock copolymer was dissolved in 186 µL EtOH. 154 µL of dialyzed OmpF (2.0 mg/mL) or dialyzed OG solution (3 %) as control, were added. After evaporating the solvents by a rotary evaporator (155 rpm, 40 °C, 175 mbar for 10 min, then vacuum for 15 min), the polymer films were rehydrated with 1 mL laccase from *Agaricus bisporus* dissolved in PBS (4.6 µg/mL). For self-assembling nanocompartments, the mixture was stirred overnight at RT. After extrusion (200 nm polycarbonate filters), the nanocompartments were purified by size exclusion chromatography (SEC) and subsequently incubated with Proteinkinase K (1 mg/mL, 1-2 µL per 100 µL) to remove non-encapsulated enzyme.

**Characterization of CNCs with protein gates**

The size and morphology of polymersomes were evaluated by using a combination of light scattering (SLS, DLS), transmission electron microscopy (TEM) and fluorescence correlation spectroscopy (FCS). Quantification of reconstituted linker-OmpF-M was carried out by FCS measurements. With all three techniques, we were able to confirm the vesicular, hollow sphere structure of the CNCs with a size of around 200 nm. Additionally, we calculated the value for R$_h$ by using the diffusion time of FCS measurements from the BODIPY stained vesicles (Table S1). With a diffusion time of around 6000 µs, we received a R$_h$ of 92.1 nm resulting in a polymersome diameter of 184.2 nm, which is also in agreement with the results from TEM and LS (Figure 2). Cryo-TEM images of vesicles formed by the triblock copolymer PMOXA$_{11}$-b-PDMS$_{104}$-b-PMOXA$_{11}$ further showed a membrane thickness of around 15 nm (Figure S10).

To exclude unspecific binding of linker-OmpF-M to the CNC membrane, FCS measurements were performed with linker-OmpF-M added to preformed, CNC-noOmpF (Figure S11, Table S1). Although FCS measurements revealed an increased diffusion time compared to the free linker, the shift of fitted autocorrelation curves was less pronounced than that observed for linker-OmpF-M reconstituted into CNCs. In addition, to confirm that the detergent (1 % OG) used to solubilize linker-OmpF-M did not disrupt CNCs, we added hydrophobic BODIPY 630/650-X to stain the nanocompartment membrane and measure the vesicle diffusion time by FCS.

*DLS/SLS* - Light scattering experiments were performed using an ALV goniometer (ALV GmbH, Germany) equipped with an ALV He−Ne laser (JDS Uniphase, wavelength λ =

632.8 nm). The solutions after film rehydration method (10 µL of suspended nanocompartments in 990 µL PBS) were measured in a 10 mm cylindrical quartz cell at angles ranging from 35° to 135° at 293 K with angular steps of 5°. ALV/Static and Dynamic FIT and PLOT program version 4.31 10/10 were used for data analysis. Static light scattering data were processed according to the MIE and Guinier plotting models.

*TEM* Nanocompartments solutions were diluted in a ratio of 1:3 with PBS. 5 µL aliquots were deposited on a carbon-coated copper grid and negatively stained with 2 % uranyl acetate solution and deposited on a carbon-coated copper grid. The samples were examined with a transmission electron microscope (Philips CM-100) operated at 80 kV.

*Cryo-TEM* - Aliquots of the samples (4 µL) were deposited on a holey carbon-coated grid (Lacey, Tedpella, USA), and vitrified into liquid ethane at -178 °C using a Leica GP plunger (Leica, Austria). The frozen samples were examined with a Talos electron microscope (FEI, USA) operated at 200 kV.

*NTA* - NTA measurements were performed using a NanoSight NS3000 equipped with a blue (488 nm) and green laser (532 nm). The samples were diluted at 1:1000 in PBS to avoid interferences. The CNCs were excited with the blue laser and their emission was detected by using appropriate filters. The average particle concentration was calculated through the Stokes−Einstein equation related to a sphere, and their hydrodynamic radius distribution was analysed by NanoSight's single particle tracking system.

*FCS* - FCS measurements were carried out using a confocal laser scanning microscope (ZEISS ZEISS LSM 880, inverted microscope ZEISS Axio Observer, Carl Zeiss, Germany) equipped with a water immersion objective (C-Apochromate 40x/1.2W korr FCS M27) using the Zen Black software. A HeNe laser (561 nm or 633 nm) was used to excite the samples. The measurements were carried out at room temperature using a sample volume of 20 µL. Measurements were recorded over 10 s, and each measurement was repeated 30 times. The diffusion times of the free dye (100 nM cyanine3 maleimide), the linker and the different types of CNCs were measured independently. The autocorrelation function was calculated using a software correlator and fitted with a one component fit. Less than 10% of the correlation curves could not be fitted and were excluded from the analysis. Correlation curves that could not be fitted were excluded (<10%).

For determining the specific binding of the linker to OmpF-M and the reconstitition of linker-OmpF-M in the polymeric membrane, experimental auto correlation curves were fitted using a two-component model including the triplet state (Eq. 1).

Eq.                                                                                              1:

$$(\tau)_{\text{fit}} = 1 + \left(1 + \frac{T}{1-T}e^{-\frac{\tau}{\tau_{\text{trip}}}}\right)\frac{1}{N}\left[\frac{f_1}{1+\frac{\tau}{\tau_{D1}}}\frac{1}{\sqrt{1+R^2\frac{\tau}{\tau_{D1}}}}\right] + \left(1 + \frac{T}{1-T}e^{-\frac{\tau}{\tau_{\text{trip}}}}\right)\frac{1}{N}\left[\frac{f_2}{1+\frac{\tau}{\tau_{D2}}}\frac{1}{\sqrt{1+R^2\frac{\tau}{\tau_{D2}}}}\right]$$

$\tau_D$ represents the diffusion time, T the fraction of fluorophores in triplet state with triplet time $\tau_{\text{trip}}$, N is the number of particles and R the structural parameter.

R and $\tau_D$ of free dye (cyanine 3 maleimide) and the free linker were determined independently, experimental auto correlation curves were fitted using a one component model including triplet state (Eq. 2).

Eq. 2:

$$G(\tau)_{\text{fit}} = 1 + \left(1 + \frac{T}{1-T}e^{-\frac{\tau}{\tau_{\text{trip}}}}\right)\frac{1}{N}\left[\frac{1}{1+\frac{\tau}{\tau_D}}\frac{1}{\sqrt{1+R^2\frac{\tau}{\tau_D}}}\right]$$

$\tau_D$ represents the diffusion time, T the fraction of fluorophores in triplet state with triplet time $\tau_{\text{trip}}$, N is the number of particles and R the structural parameter.


**Enzyme encapsulation efficiency**

The concentration of non-encapsulated laccase (laccase from *Agaricus bisporus* MW: 65,000 g/mol[238], confirmed by SDS PAGE, Figure S12) was determined from the fraction of laccase in solution eluted from size exclusion (SEC) purification of CNC-noOmpF. Based on the BCA calibration curve (Figure S12) performed according to the supplier's protocol (Thermo Fisher Scientific, U.S.A.), we determined the initial concentration of the laccase in solution (4.60 µg/mL) and subsequently quantified the amount of enzyme that was not encapsulated in the CNCs (total volume 0.85 mL, $2.6 \times 10^{11} \pm 1.6 \times 10^{10}$ vesicles/mL, measured by NTA; see Table S2). The difference between the amount of laccase added for the formation of the CNCs and the amount of enzyme that was not encapsulated (3.70 µg), corresponded to the amount of laccase encapsulated in our CNCs-noOmpF. Dividing the total number of encapsulated laccase molecules by the number of vesicles yielded a value of 8-9 encapsulated laccase molecules per vesicle.


**How to open linker-OmpF-M**

To 100 µL of CNCs without OmpF and CNCs with linker-OmpF-M inserted in their membrane, $NaIO_4$ dissolved in MilliQ-$H_2O$ (0.3 M, 10 µL, 1 eq.) was added and incubated at 37° C for 24 h. An excess of glucose dihydrate dissolved in MilliQ-$H_2O$

(0.6 M, 25 µL, 5 eq.) was added to quench $NaIO_4$. We added approximately $2x10^{10}$ CNCs to an aqueous solution of $NaIO_4$ to a final periodate concentration of 30 mM in 110 µL, corresponding to $1.6x10^{-7}$ mmol or $3.5 x10^{-5}$ mg periodate per vesicle. The mixture was incubated at 37° C for 24 h. Subsequently, CNCs were purified by SEC and incubated with proteinase K (1 mg/mL, 2 µL per 100 µL) to remove the free laccase.

**Enzymatic assay with DMP**

CNCs (5 µL) without $NaIO_4$-treatment or CNCs incubated with $NaIO_4$ and glucose (20 µL due to dilution after SEC purification) per well were added to 2,6-dimethoxyphenol (DMP) in PBS (20 mM, 10 µL) at pH 7.4 (total volume 210 µL) in a 96-well plate. The absorbance at 470 nm was measured with a Spectramax M5e microplate reader (Molecular Devices). The activity was measured for free laccase in solution (1 pg, corresponding to the amount of laccase in 1x109 CNCs, 5 µL sample), for CNCs equipped with wild-type OmpF or double mutant OmpF-M, CNCs without inserted OmpF (before and after $NaIO_4$-treatment) and CNCs with linker-OmpF-M inserted in the membrane (before and after $NaIO_4$-treatment). The concentration of all CNC samples in PBS solution was determined by NTA (Table S2) to perform the assays at comparable enzyme concentrations.

**Enzymatic assay with ABTS**

Corresponding laccase activity measurements were carried out using 2,2'-azinobis [3-ethylbenzothiazoline-6-sulfonic acid]-diammonium salt (ABTS) as substrate. The oxidation product was monitored by determining the increase of absorbance at 420 nm using a Spectramax M5e microplate reader (Molecular Devices).

# Chapter 4

**Materials**

All materials were purchased from Sigma Aldrich, except CellMask™ Green Plasma Membrane Stain, Gibco™ Collagen I coated plate 6 well, FluoSpheres™ Carboxylate Mircospheres red fluorescent (580/605) 2-5 % solid (0.04 μm, 0.1 μm, 0.5 μm) were purchased from ThermoFisher. Red fluorescent polystyrene latex particles were purchased from Magsphere. Orange fluorescent (575/540) amine-modified polystyrene latex beads (0.1 μm, 2.5 % solid) were purchased from Merck.

**Methods**

**CellMask™ Green staining, solid-sphere particle uptake and packaging**

Cells were either cultured at a density of $5 \times 10^4$ cells per well in a μ-Slide 8 well, or at a density of $6 \times 10^6$ in a 6 well, in 200 μL or 500 μL cell medium respectively. The cells were grown as uniform monolayer with appropriate morphology and with at least 70% confluency. In case of HepG2 and HeLa cells, the medium was DMEM growth medium (High Glucose Dulbecco's Modified Eagle Medium (DMEM)), supplemented 10 % fetal calf serum, penicillin (100 units/mL) and streptomycin (100 μg/mL)). In case of Caco-2, the cell medium was Eagle's Minimum Essential Medium (EMEM) supplemented with 1X NEAA (non-essential amino acids), 2 mM glutamine, 10 % fetal calf serum, penicillin (100 units/mL) and streptomycin (100 μg/mL). After incubation for 24 h at 37 ºC, 5% $CO_2$ the medium was removed and 200 μL or 500 μL of FluoSpheres™ Carboxylate-Modified Microspheres, 2 % solids diluted to $4 \times 10^9$ particles/mL, $8 \times 10^9$ particles/mL, $1.6 \times 10^{10}$ particles/mL, and $1.6 \times 10^{11}$ particles/mL in DMEM/EMEM growth medium were added to the cells. Cells were incubated for an additional 24 h in DMEM/EMEM growth medium, then washed five times with 200 μL (8 well chambers) or 3 mL (6 well) DMEM/EMEM growth medium. After the final wash step, the DMEM/EMEM growth medium was removed and CellMask™ Green diluted 1:1000 in DMEM/EMEM growth medium was added. After incubation for 10 min the medium was removed, and the cells were washed 3 times with 200 μL (8 well chambers) or 3 mL (6 well chambers) cell medium. Then vesiculation buffer (1 mL solution of 10mM HEPES (4-(2-hydroxyethyl)-1-piperazineethanesulfonic acid), 150 mM NaCl, 2 mM $CaCl_2$, pH 7.4, 18 μL of 4 % (wt/vol) PFA solution, 2 μL of 1 M DTT) was added (200 μL for 8 well chambers, or 500 μL for 6 well chambers). The cells were imaged after incubation with vesiculation buffer for 1-2 h.

## GFP transfection

Cells were plated as described above in 8 or 6 well plates. 1 min after culturing the cells, 10 µL of CellLight® Plasma Membrane-GFP BacMam 2.0 was added for cells cultured in the 8 wells plates and 25 µL for cells cultured in 6 well plates. Subsequently, cells were incubated for 24 h at 37 ºC, and 5 % $CO_2$ to allow attachment to the surface.

## Isolation of GPMVs

The supernatant (500 µL) from 6 well cell culture plates was transferred to an Eppendorf tube and centrifuged at 0.1 rpm for 10 min to pellet and remove cells. The supernatant containing the GPMVs was transferred to plasma activated 2 well microscopy chambers (Nunc™ Lab-Tek™ Chamber Slide System, Thermo Fisher Scientific).

## CLSM

CLSM measurements were performed using a confocal laser scanning microscope (ZEISS LSM 880, inverted microscope ZEISS Axio Observer, Carl Zeiss, Germany) equipped with a water immersion objective (C-Apochromate 40x/1.2W korr FCS M27) using the Zen Black software. Samples containing CellMask™ Green Plasma Membrane Stain, GFP or the aminated NPs were excited with an argon laser at 488 nm by setting the detector range to 499-521 nm. To measure the fluorescence of Fluospheres™ Carboxylate Mircospheres, a diode-pumped solid-state 561-10 laser (DPSS) at 561 nm was used as excitation source and the detector range set to 572-704 nm. Respectively, nanocompartment beam splitters (MBS) of 488 and 561 were used. Each sample was scanned unidirectionally using 1024×1024 pixels with a Bit Depth of 16 Bit. Images were processed using ImageJ software.

## Flow cytometry analysis of GPMVs

The cells were grown in 6 well plates as described above and the GPMVs were subsequently isolated as described above for CLSM studies. Flow cytometry analysis was performed using a BD LSR Fortessa Analyzer. Doublets were excluded using FSC-A and FSC-H detectors. The GPMVs were excited at 541 nm, and the emission was detected using the Texas-Red Channel (BP filter 620/10). 100 000 events were recorded for each sample in "slow" flow through mode. The data was processed using Flow Jo VX software (TreeStar, Ashland, OR).

**Flow cytometry analysis of cells**

For cellular uptake studies cells were grown and incubated with NPs in 6 wells as described above. Cells were washed five times with cell medium, trypsinized, resuspended in 1 mL cell medium, centrifuged and then suspended in 500 µL PBS. Flow cytometry analysis was performed using a BD FACS Canto II flow cytometer (BD Bioscience, USA). Doublets were excluded using FSC and SSC detectors, single cells were excited at 561 nm and the emission was detected in FL5 (610/20; Texas-Red Channel). A total of 10,000 single cells for each sample were analyzed and data processed using Flow Jo VX software (TreeStar, Ashland, OR).

**NTA**

NTA measurements were performed using a NanoSight NS3000 equipped with a blue (488 nm) and red laser (642 nm). The NPs were excited with red laser and their emission was detected by using appropriate filter for 642 nm. The average particle concentration was calculated through the Stokes-Einstein equation related to a sphere and their hydrodynamic radius distribution was analyzed by NanoSight's single particle tracking system

**TEM**

A suspension of 100 nm beads ($1\times10^9$ particles/mL) in cell medium was used for TEM imaging studies. These samples were negatively stained with 1.5 % uranyl acetate solution and deposited on carbon-coated copper grids. A transmission electron microscope (Philips Morgagni 268D) at 293 K was used.

**DLS**

The measurements of hydrodynamic diameter ($R_h$) of NPs were performed on a Zetasizer Nano ZSP at 25 °C. The measure angle is 173 ° and the data was analyzed by intensity distribution. A suspension of 450 µL of with a concentration of $1.6\times10^{11}$ particles/mL was used for the measurements.

# APPENDIX – SUPPLEMENTARY INFORMATION

## Chapter 3
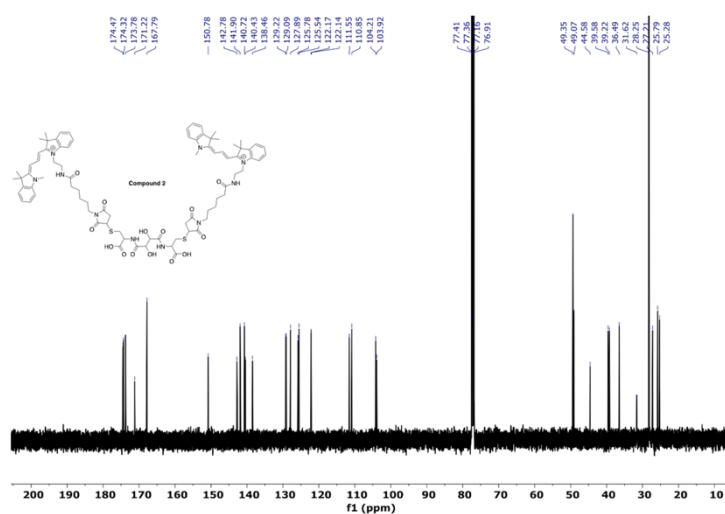


***Figure S1.*** *$^{1}$H-NMR spectrum of Compound 2 in CDCl$_3$ at 500 MHz.*
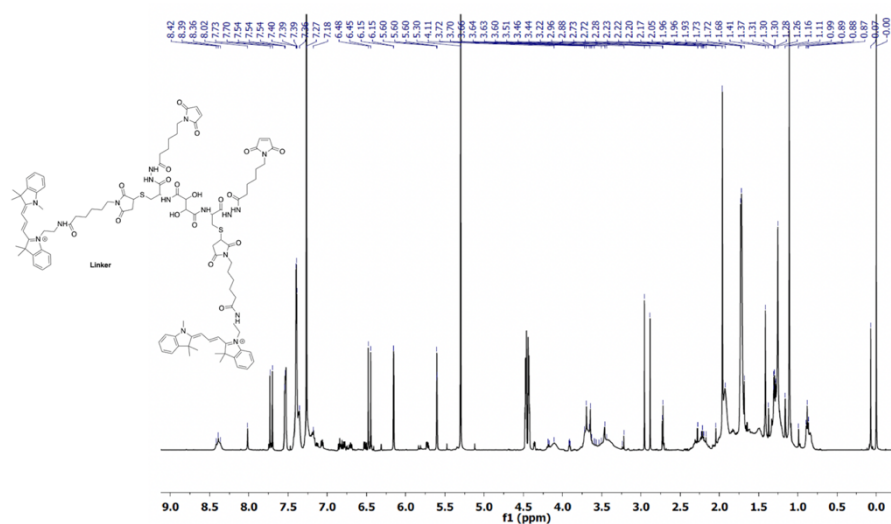


***Figure S2.*** *$^{13}$C-NMR spectrum of Compound 2 in CDCl$_3$ at 126 MHz.*
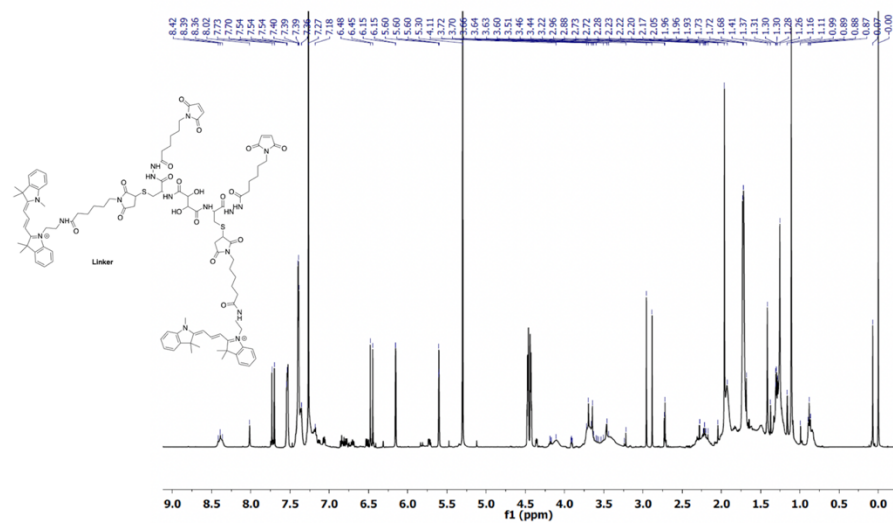
***Figure S3.*** *¹H-NMR spectrum of the bismaleimide linker in CDCl₃ at 500 MHz.*
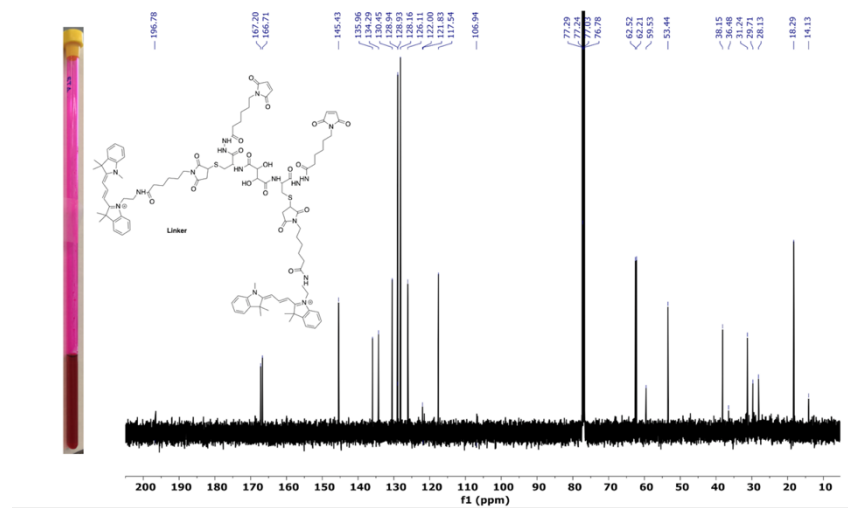


***Figure S4.*** *¹³C-NMR spectrum of the bismaleimide linker in CDCl₃ at 126 MHz and the image of the corresponding dissolved linker in the NMR-tube.*
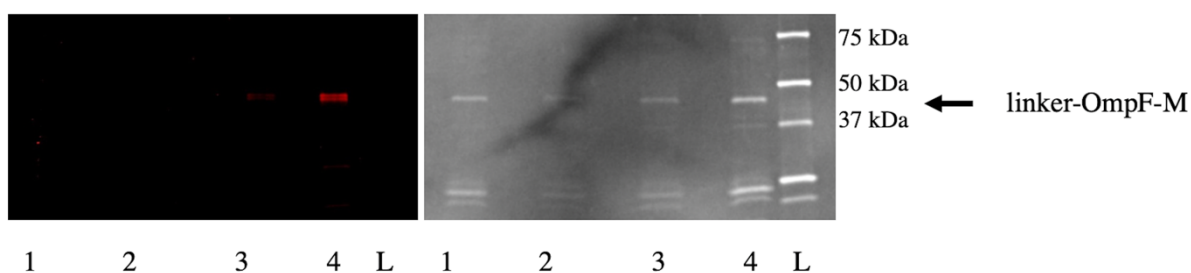
**Figure S5.** *SDS PAGE of OmpF-M (left, fluorogram, right, Coomassie-stained): L: Protein ladder; 1,2: unlabelled OmpF-M, at 1/1 (1) and 2/1 (2) ratio (v/v) with loading buffer. 3, 4: OmpF-M labelled with the linker comprising fluorescent cyanine 3 (550/580). MW of OmpF around 40 kDa.*

**Table S1.** *Fluorescence correlation parameters of the free fluorophore cyanine3 maleimide, free linker, CNCs with OmpF-M-linker inserted in the membrane, stand-alone OmpF-M-linker, and OmpF-M-linker added to empty polymersomes before and after staining the polymersomes with BODIPY 630/650-X.*

|  | Counts per molecule [kHz] | Diffusion time [μs] |
|---|---|---|
| Cyanine3 maleimide | 1.7 | 61 |
| Linker | 2.3 | 70 |
| OmpF-M-Linker vesicles | 28.3 | 4530 |
| Linker-OmpF-M | 3.1 | 452 |
| Vesicles ANDlinker-OmpF-M without BODIPY | 7.0 | 452 |
| Vesicles AND linker-OmpF-M with BODIPY | 138.3 | 6000 |
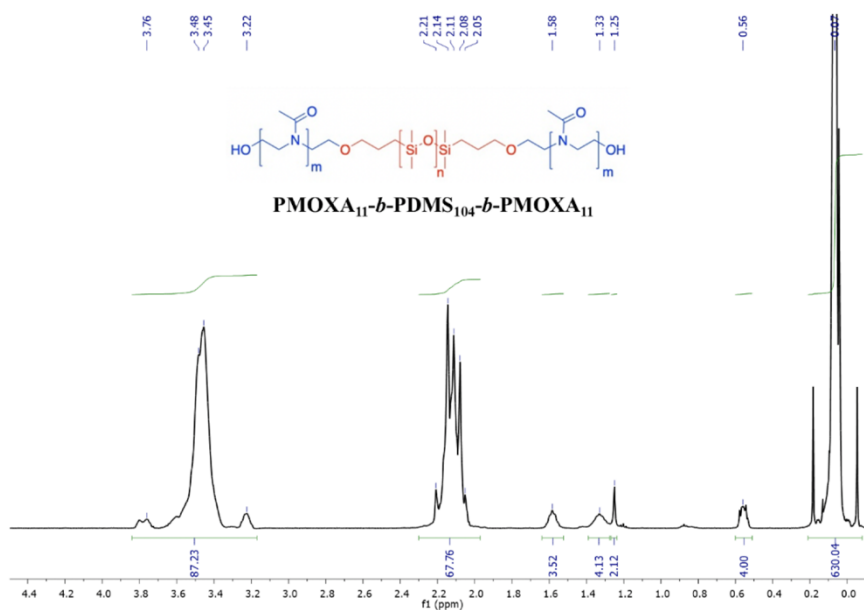
**Figure S6.** *¹H-NMR spectrum of poly(2-methyl-2-oxazoline)-b-poly(dimethylsiloxane)-b-poly(2-methyl-2-oxazoline) triblock copolymer (PMOXA$_{11}$-b-PDMS$_{104}$-b-PMOXA$_{11}$) in CDCl$_3$ at 500 MHz.*
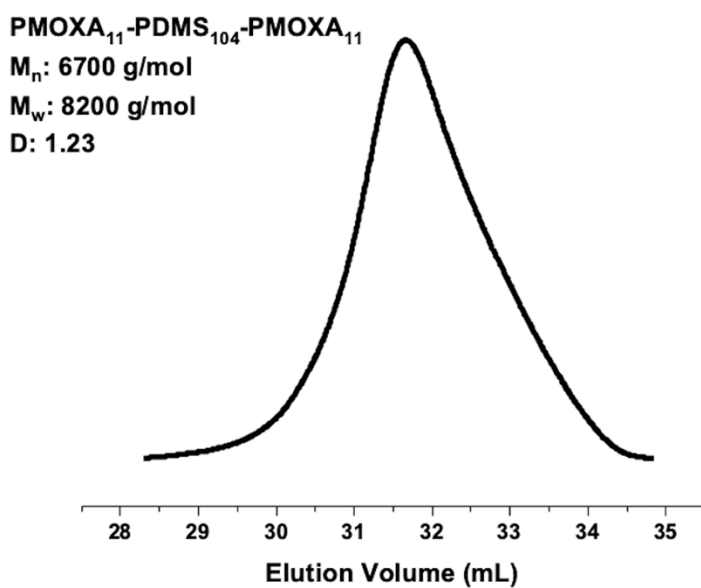


**Figure S7.** *Elugram (GPC) of PMOXA$_{11}$-b-PDMS$_{104}$-b-PMOXA$_{11}$ in DMF.*

***Table S2.*** *Data from NTA measurements of CNC-noOmpF, CNC-linker-OmpF-M, CNC-OmpF-M), and CNC-OmpF-WT samples diluted 1:1000 in PBS.*

|  | CNC-noOmpF | CNC-linker-OmpF-M | CNC-OmpF-M | CNC-OmpF-WT |
|---|---|---|---|---|
| diameter (nm) | 202±47 | 192±42 | 182±42 | 215±49 |
| concentration (particles/mL) | $2.6 \times 10^8 \pm$ $1.6 \times 10^7$ | $1.8 \times 10^8 \pm$ $4.5 \times 10^6$ | $3.1 \times 10^8 \pm$ $1.7 \times 10^7$ | $3.8 \times 10^8 \pm$ $2.4 \times 10^7$ |
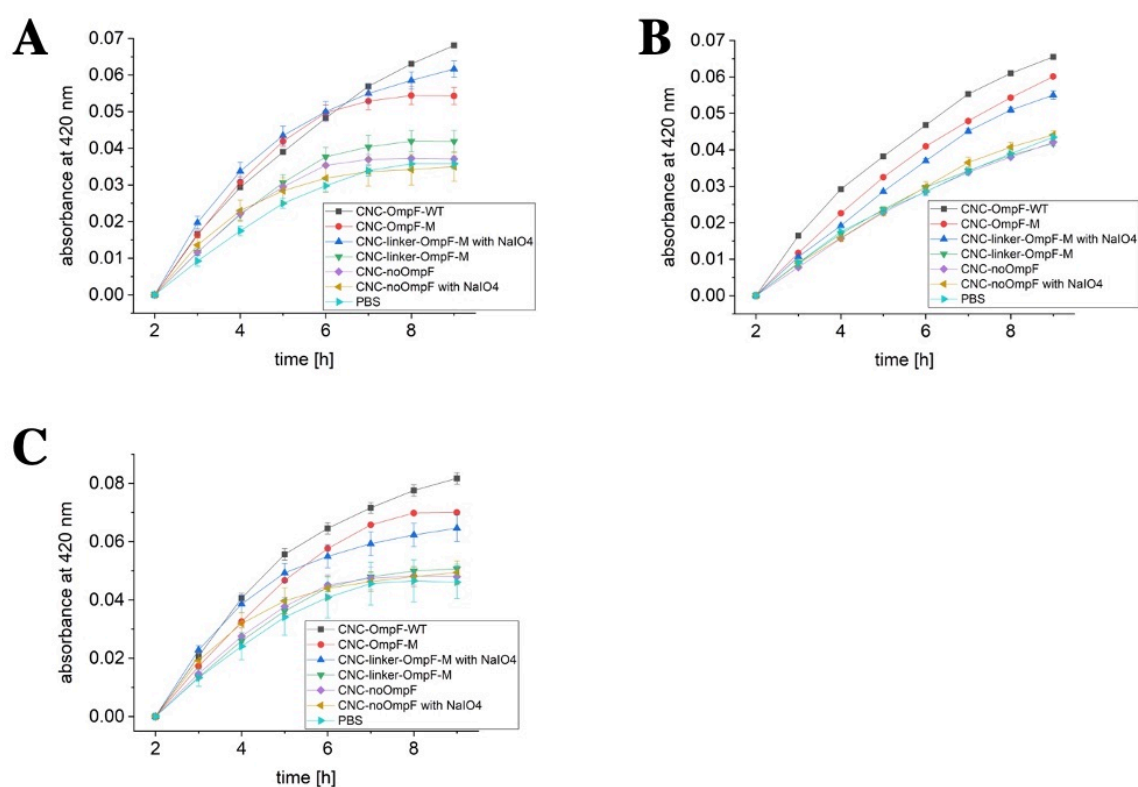


***Figure S8.*** *Laccase activity of CNCs in response to NaIO₄ (with standard deviation). Measurements were carried out over 9 h at RT, pH 7.4: ABTS in PBS with CNC-OmpF-WT (black), ABTS in PBS with CNC-OmpF-M (red), ABTS in PBS CNC-linker-OmpF-M in the presence (green) and absence of NaIO₄ (blue), CNC-noOmpF without (purple) and with NaIO₄ (yellow), and ATBS in PBS: A)-C) represent 3 independent CNC preparations.*
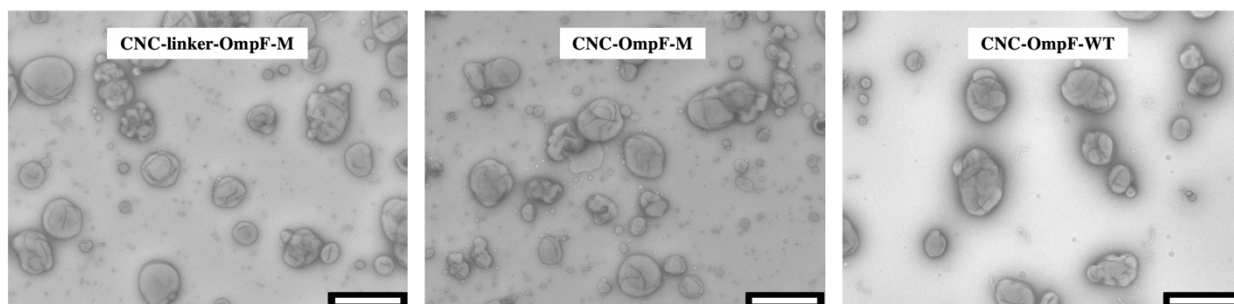
**Figure S9.** *TEM micrographs of different CNCs encapsulating laccase 11 month after preparation. Left, with linker-OmpF-M inserted in the membrane (CNC-linker-OmpF-M), middle, with inserted OmpF-M (CNC-OmpF-M), right, with inserted wild-type OmpF (CNC-OmpF-WT). Scalebars: 500 nm*
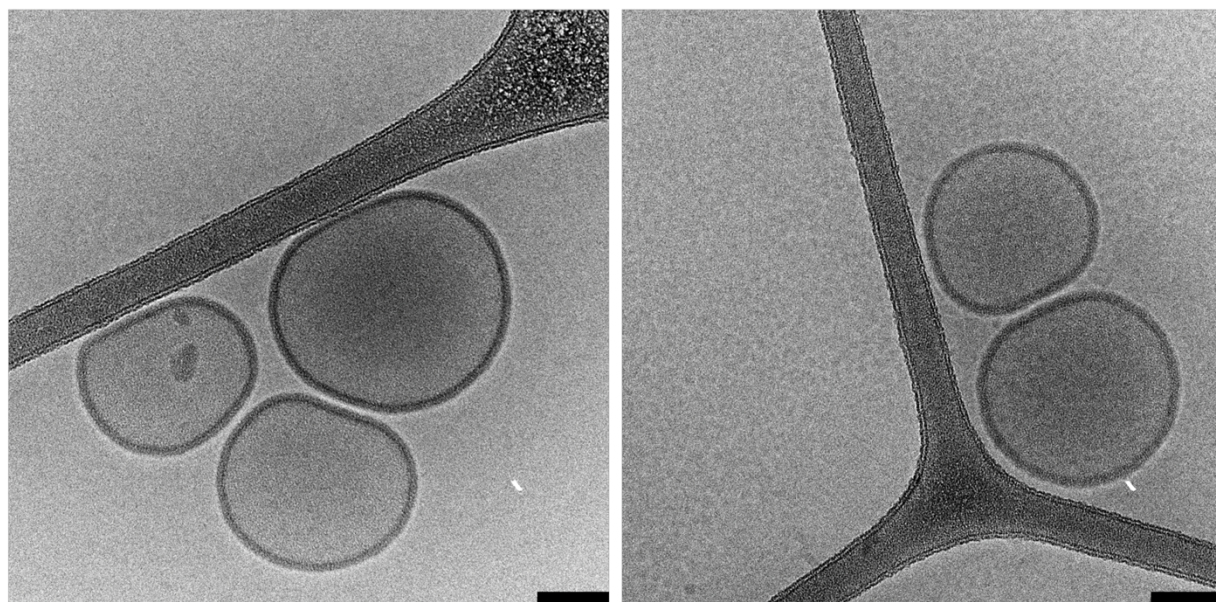


**Figure S10.** *Cryo-TEM micrographs of polymersomes self-assembled from PMOXA$_{11}$-b-PDMS$_{104}$-b-PMOXA$_{11}$. Scale bars: 100 nm*
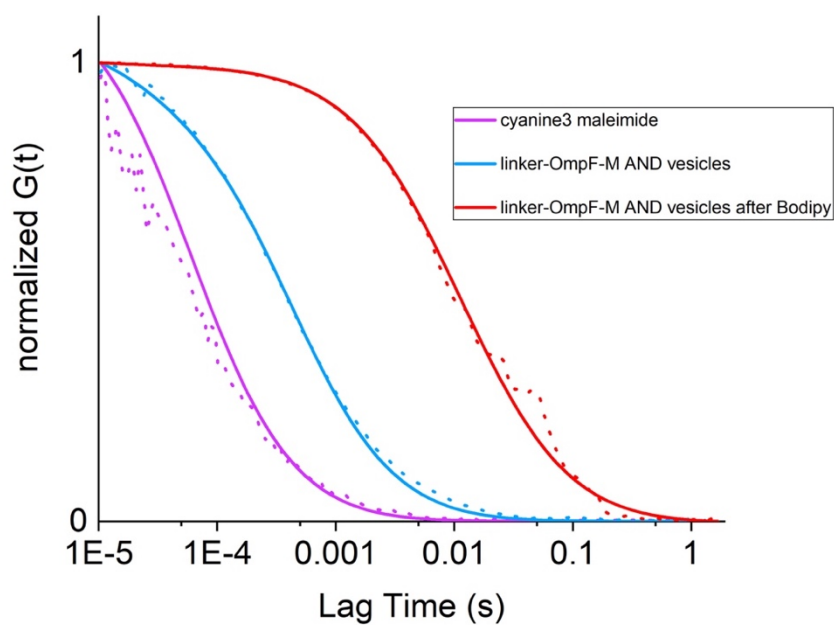
**Figure S11.** *FCS curves (line) and raw data (dots) of PBS solutions of cyanine 3 maleimide (pink), OmpF-M-linker in 1% OG mixed with empty polymersomes before (blue), and after stained with BODIPY 630/650-X (red).*
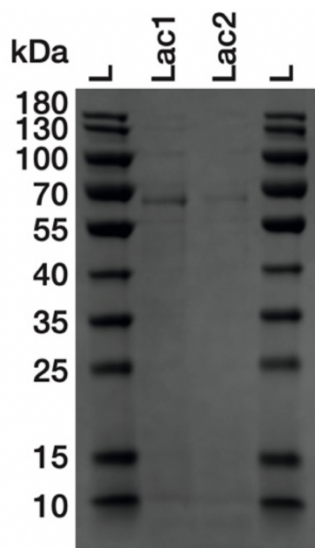


**Figure S12.** *SDS PAGE of laccase: L: Protein ladder; Lac1: 10 μg laccase, Lac2: 5 μg laccase.*
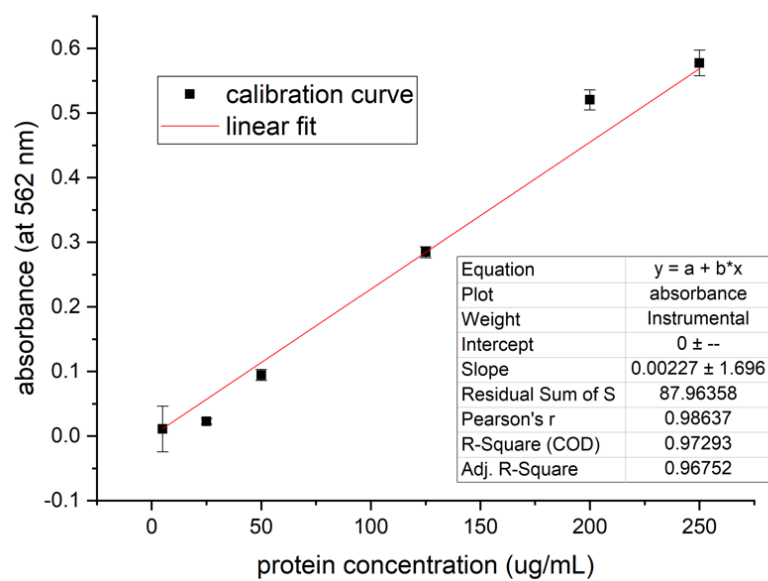
**Figure S13.** *Calibartion curve for BCA assay performed according to the supplier's protocol (Thermo Fisher Scientific, U.S.A.)*

# Chapter 4

*Table S3*. *Original concentrations of purchased NP suspensions in particles/mL.*

|  | Original concentration of suspension (particles/mL) |
|---|---|
| FluoSpheres$^{TM}$ 40 nm | $1 \times 10^{13}$ |
| FluoSpheres$^{TM}$ 100 nm | $8 \times 10^{12}$ |
| FluoSpheres$^{TM}$ 500 nm | $2 \times 10^{11}$ |
| amine-modified PS NPs 100 nm | $2 \times 10^{11}$ |
| red-fluorescent PS NPs 100 nm | $8 \times 10^{12}$ |
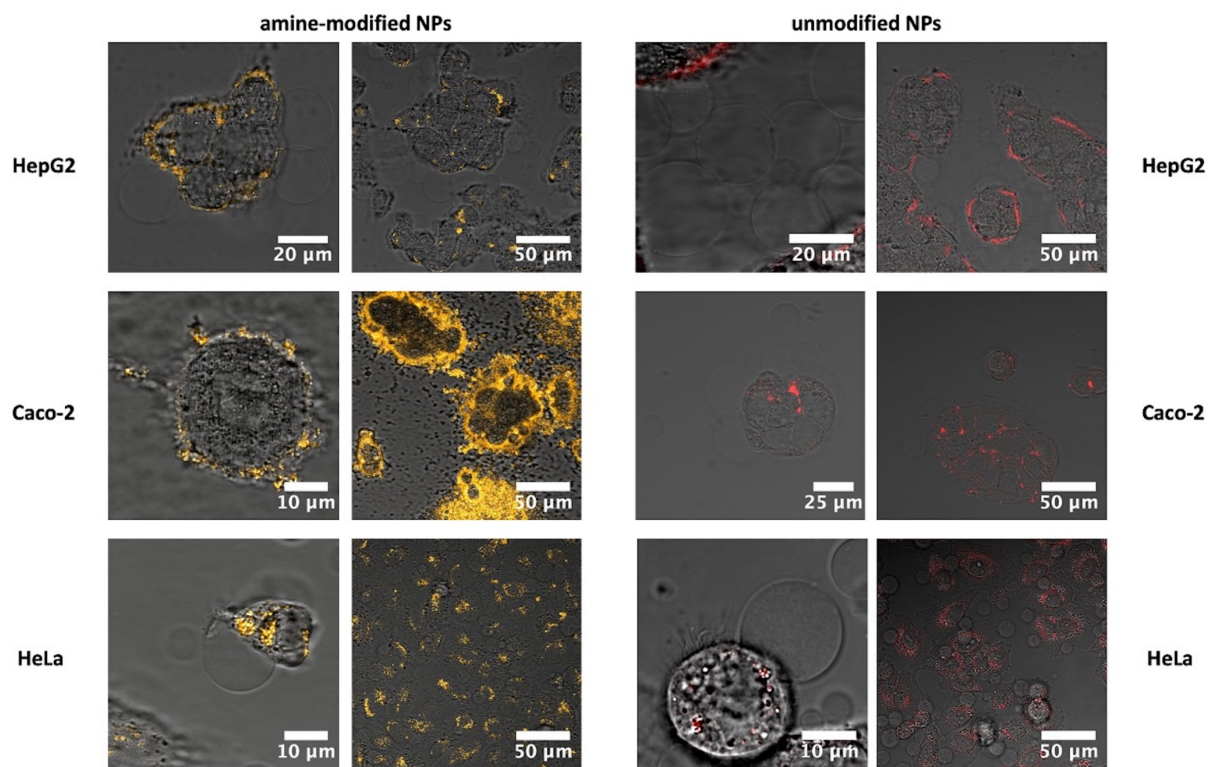
***Figure S14****. Formation of GPMVs from HepG2, Caco-2 and HeLa cells after incubation with 100 nm fluorescent aminated NPs (yellow) or unmodified NPs (red) with initial concentrations between $4{\times}10^9$ particles/mL and $1.6{\times}10^{11}$ particles/mL.*
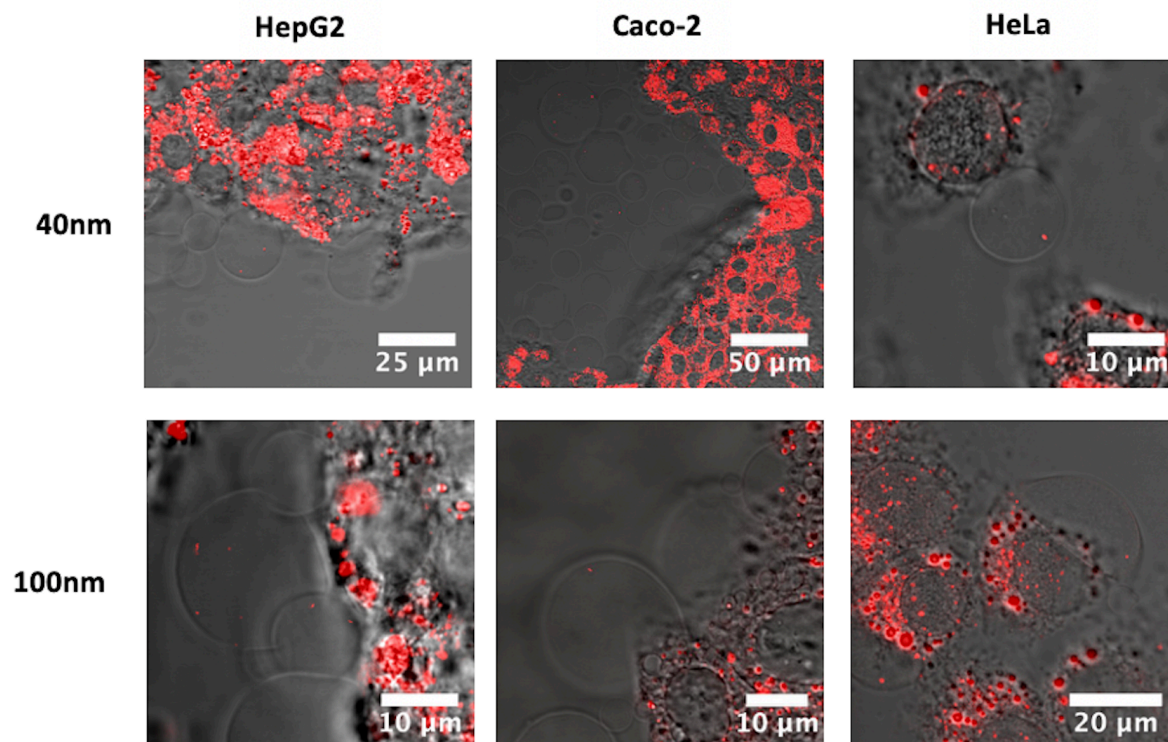
***Figure S15.*** *GPMVs formed from HepG2, HeLa and Caco-2 cells with transferred, red fluorescent carboxylated NPs inside their cavities. The NPs are of 40 nm or 100 nm size with initial concentrations between $4{\times}10^9$ particles/mL and $1.6{\times}10^{11}$ particles/mL.*
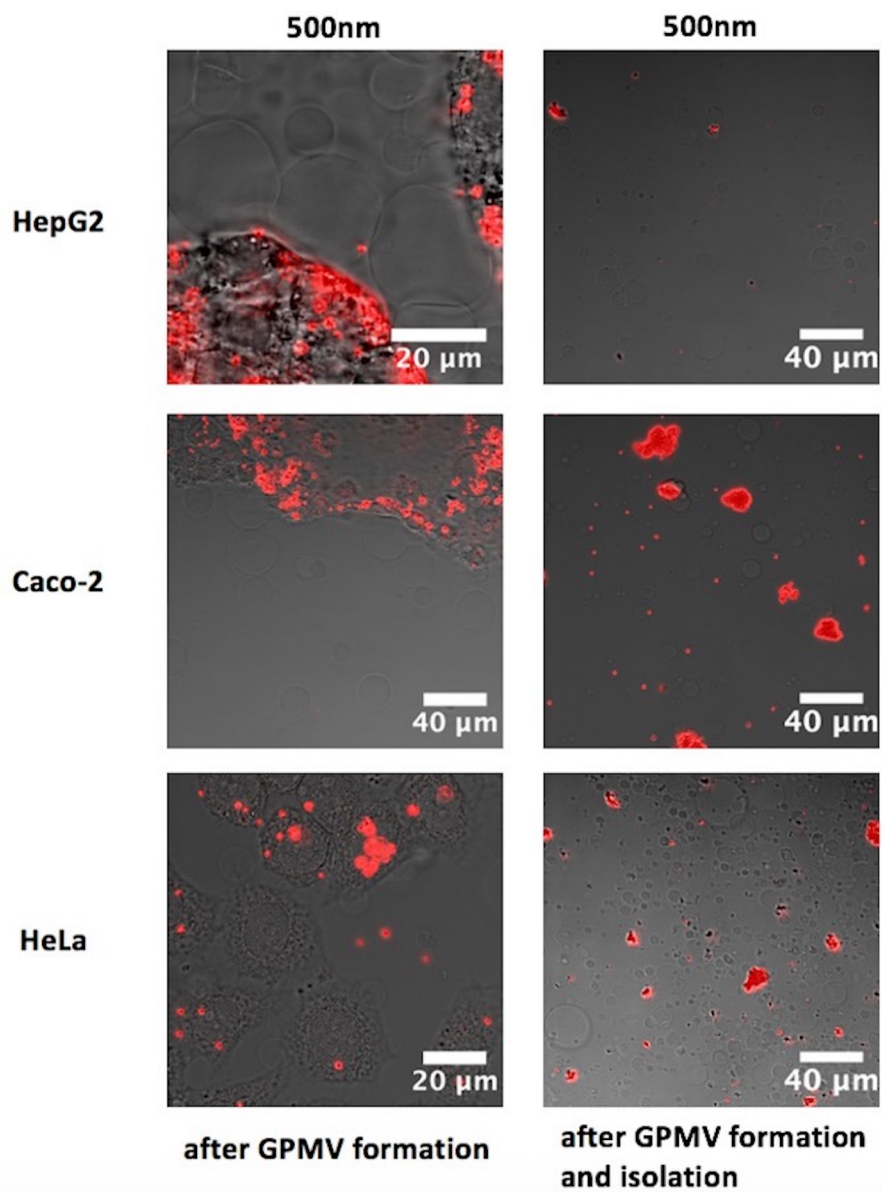
**Figure S16.** *GPMVs formed from HepG2, Caco-2 and HeLa cell lines treated with red fluorescent carboxylated NPs (500 nm with initial concentrations between $4 \times 10^9$ particles/mL and $1.6 \times 10^{11}$ particles/mL). No transfer of the 500 nm particles could be observed.*
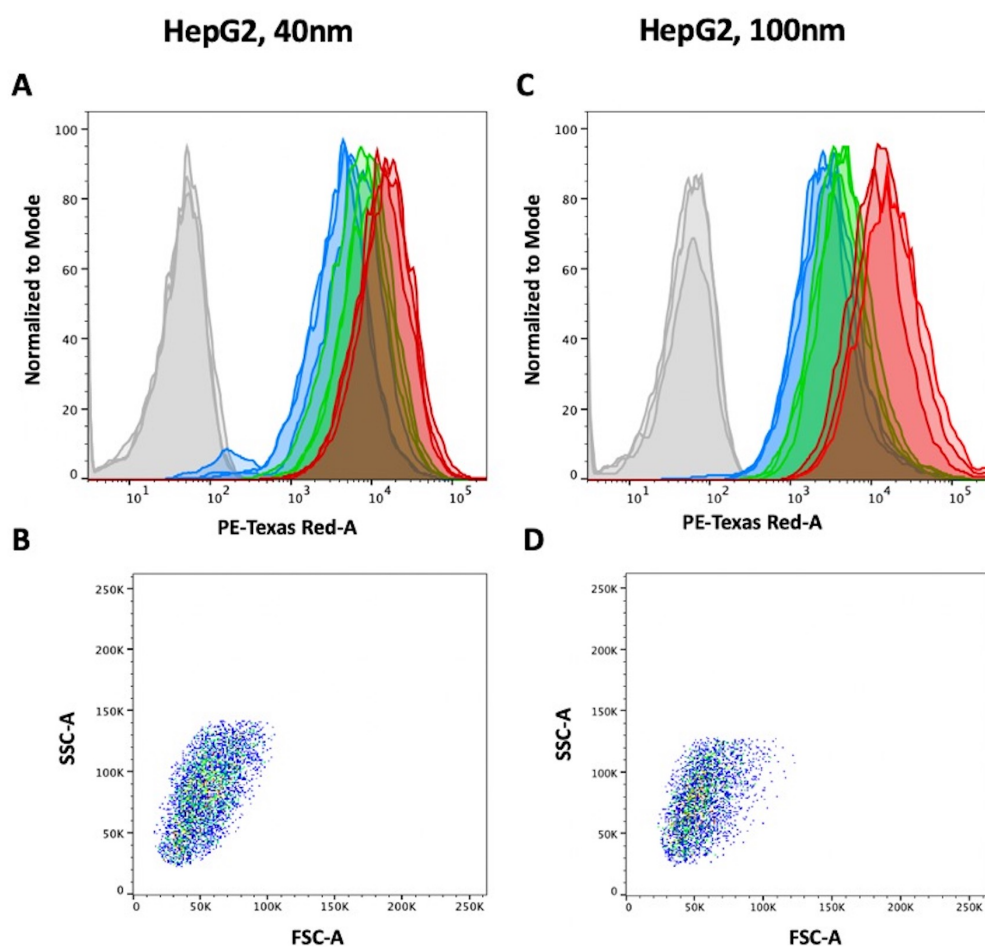
***Figure S17***. *Flow cytometry analysis of HepG2 cells with uptaken NPs: A) cellular uptake depending on the concentration of 40 nm red fluorescent carboxylated PS NPs. REF no NPs (grey), 1: $4\times10^9$ particles/mL (blue), 2: $8\times10^9$ particles/mL (green), 3: $1.6\times10^{10}$ particles/mL (red). B) flow cytometry analysis of HepG2 cell size characterization by sideward (SSC) and forward scattering (FSC) analysis. The marked-out section represents the cell populations used for further NP uptake analysis by flow cytometry by PE-Texas Red A. C) cellular uptake depending on the concentration of 100 nm red fluorescent carboxylated PS NPs. REF no NPs (grey), 1: $4\times10^9$ particles/mL (blue), 2: $8\times10^9$ particles/mL (green), 3: $1.6\times10^{10}$ particles/mL (red). D) flow cytometry analysis 100 nm NPs, size characterization by sideward and forward scattering analysis. The marked-out section represents the cell populations used for analysis by flow cytometry.*
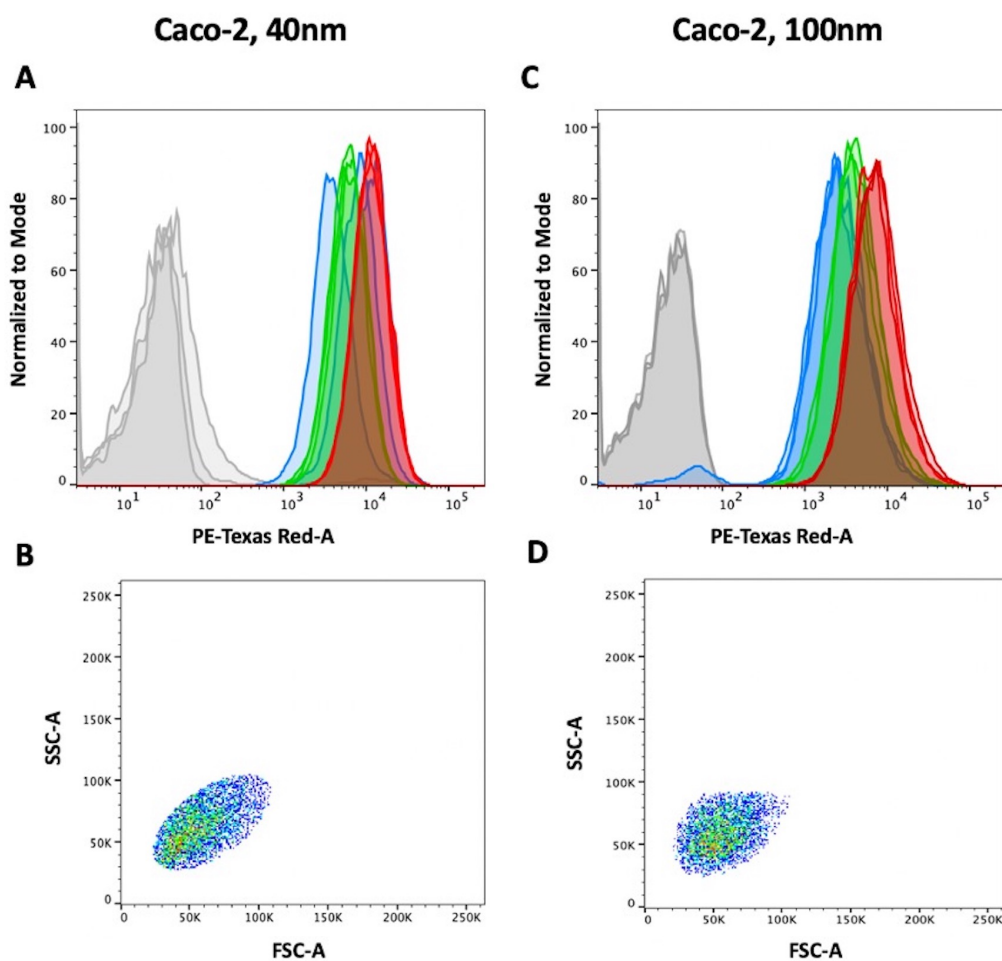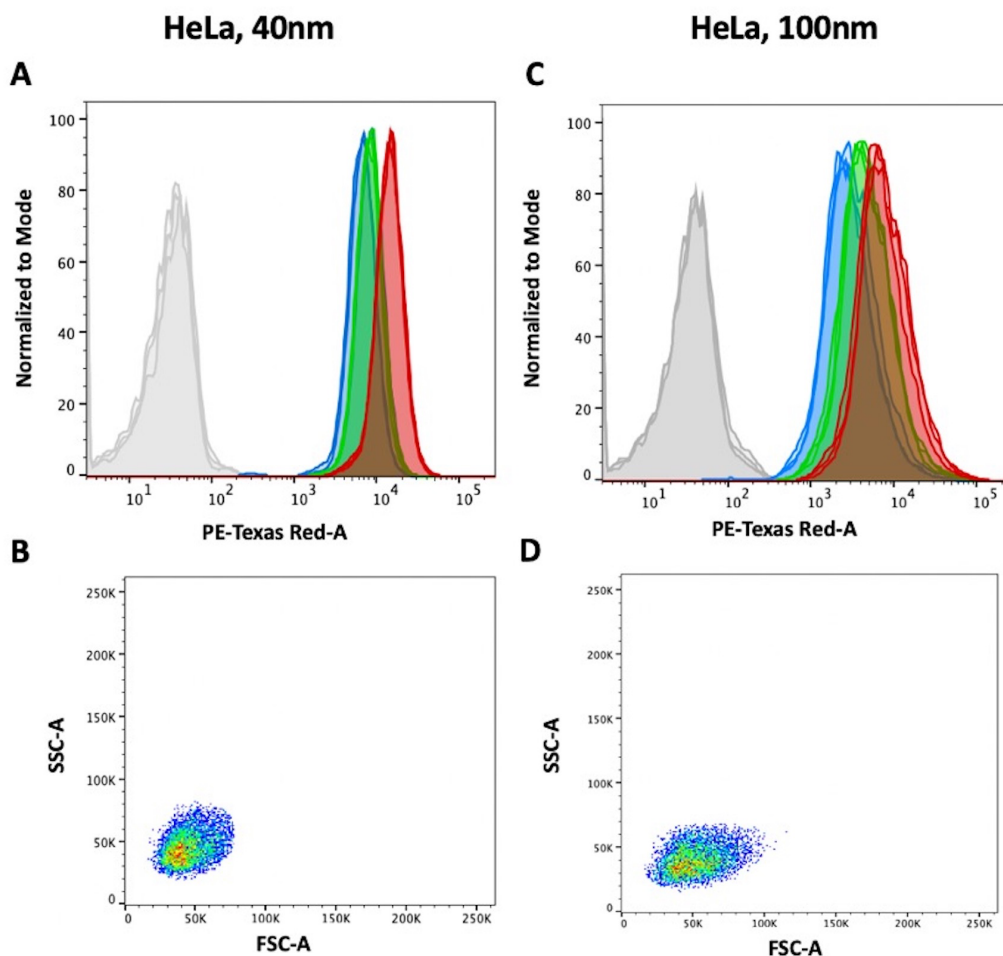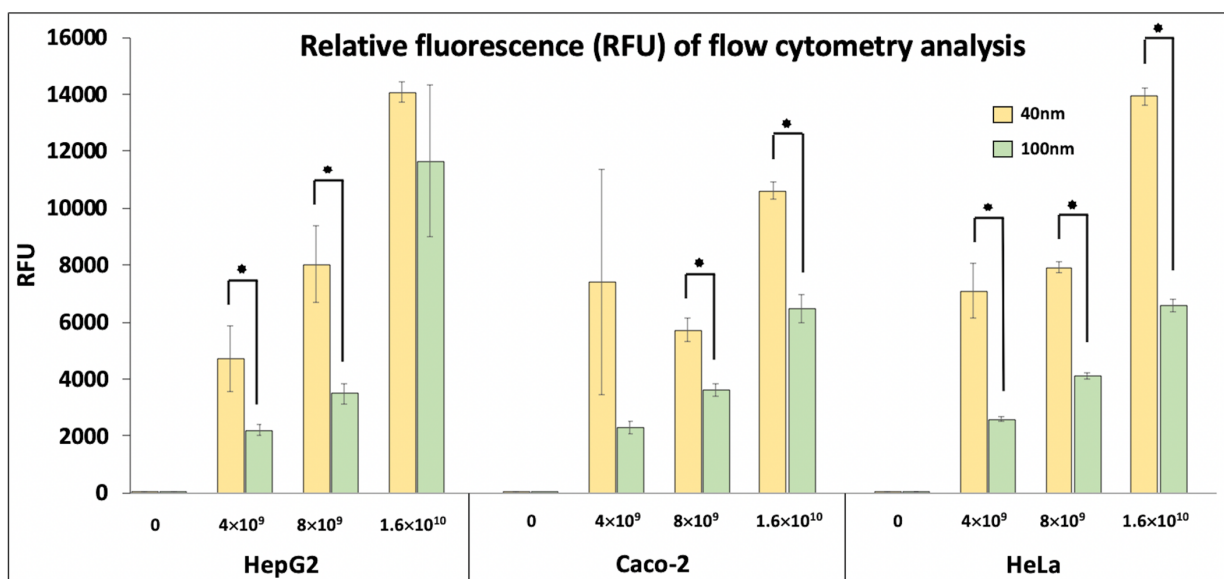
***Figure S18.*** *Flow cytometry analysis of Caco-2 cells with uptaken NPs: A) cellular uptake depending on the concentration of 40 nm red fluorescent carboxylated PS NPs. REF no NPs (grey), 1: $4\times10^9$ particles/mL (blue), 2: $8\times10^9$ particles/mL (green), 3: $1.6\times10^{10}$ particles/mL (red). B) flow cytometry analysis of Caco-2 cell size characterization by sideward (SSC) and forward scattering (FSC) analysis. The marked-out section represents the cell populations used for further NP uptake analysis by flow cytometry by PE-Texas Red A. C) cellular uptake depending on the concentration of 100 nm red fluorescent carboxylated PS NPs. REF no NPs (grey), 1: $4\times10^9$ particles/mL (blue), 2: $8\times10^9$ particles/mL (green), 3: $1.6\times10^{10}$ particles/mL (red). D) flow cytometry analysis 100 nm NPs, size characterization by sideward and forward scattering analysis. The marked-out section represents the cell populations used for analysis by flow cytometry.*

***Figure S19.*** *Flow cytometry analysis of HeLa cells with uptaken NPs: A) cellular uptake depending on the concentration of 40 nm red fluorescent carboxylated PS NPs. REF no NPs (grey), 1: $4\times10^9$ particles/mL (blue), 2: $8\times10^9$ particles/mL (green), 3: $1.6\times10^{10}$ particles/mL (red). B) flow cytometry analysis of HeLa cell size characterization by sideward (SSC) and forward scattering (FSC) analysis. The marked-out section represents the cell populations used for further NP uptake analysis by flow cytometry by PE-Texas Red A. C) cellular uptake depending on the concentration of 100 nm red fluorescent carboxylated PS NPs. REF no NPs (grey), 1: $4\times10^9$ particles/mL (blue), 2: $8\times10^9$ particles/mL (green), 3: $1.6\times10^{10}$ particles/mL (red). D) flow cytometry analysis 100 nm NPs, size characterization by sideward and forward scattering analysis. The marked-out section represents the cell populations used for analysis by flow cytometry.*

*Figure S20.* *Relative fluorescence (RFU) of flow cytometry analysis given in Figure S6-S8: HepG2, Caco-2 and HeLa cells without NPs and treated with 40 nm (yellow) and 100 nm (green) PS NPs at 3 different concentrations ($4\times10^9$ particles/mL, $8\times10^9$ particles/mL (green), $1.6\times10^{10}$ particles/mL). Error bars are given as ± standard deviation, significance level: $p < 0.5$ (\*).*
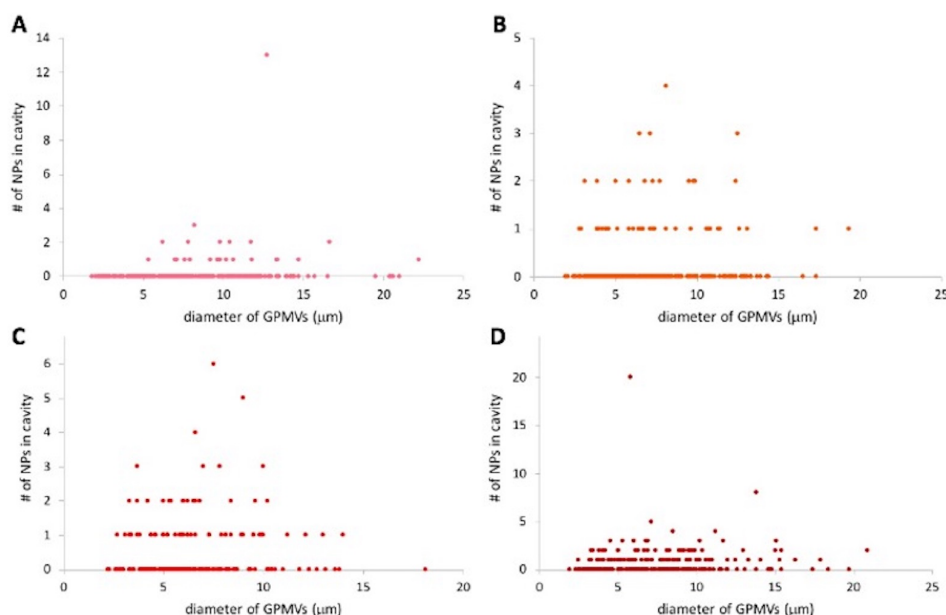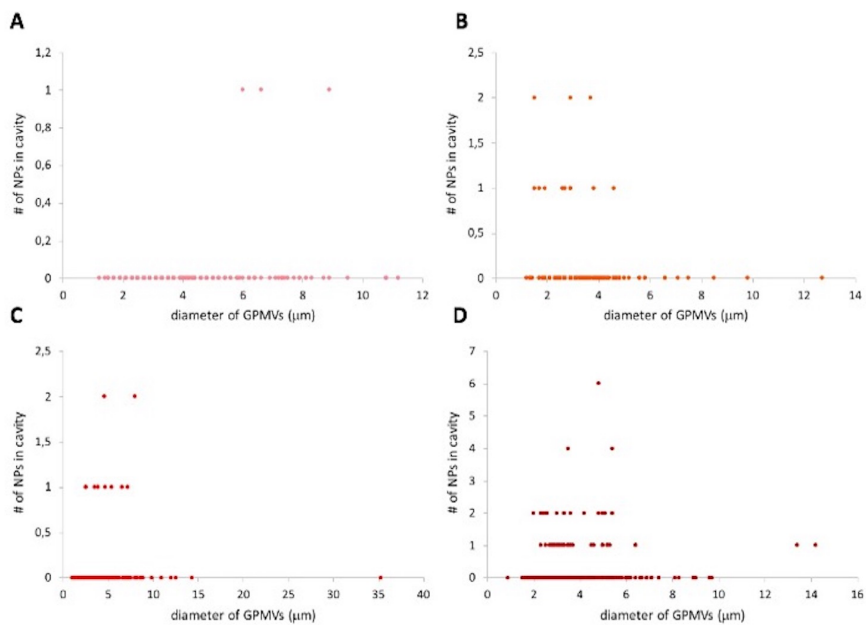


*Figure S21*. *Evaluation of single plane projections of GPMVs formed from HepG2 cells treated with 40 nm carboxylated NPs at different concentrations: A) $4\times10^9$ particles/mL, B) $8\times10^9$ particles/mL, C) $1.6\times10^{10}$ particles/mL, D) $1.6\times10^{11}$ particles/mL.*
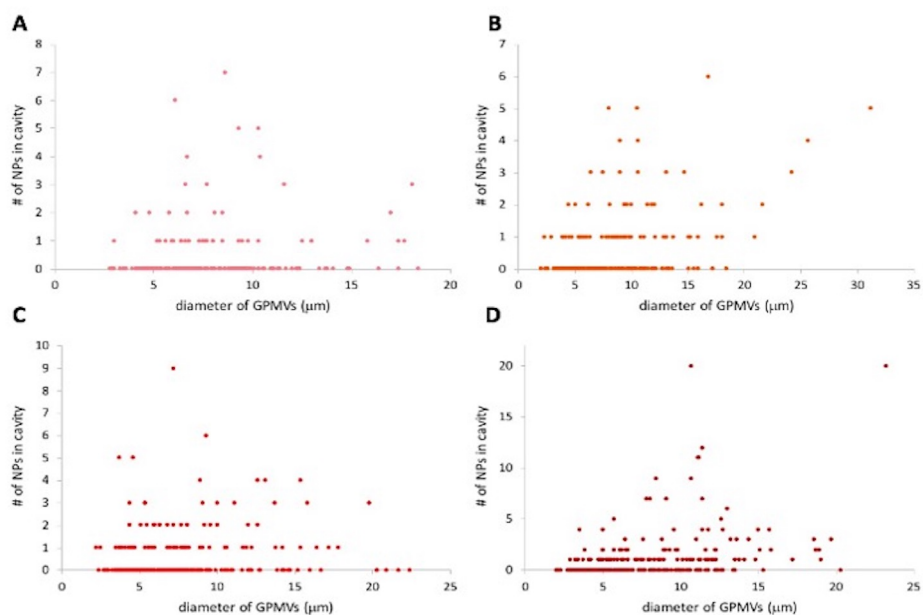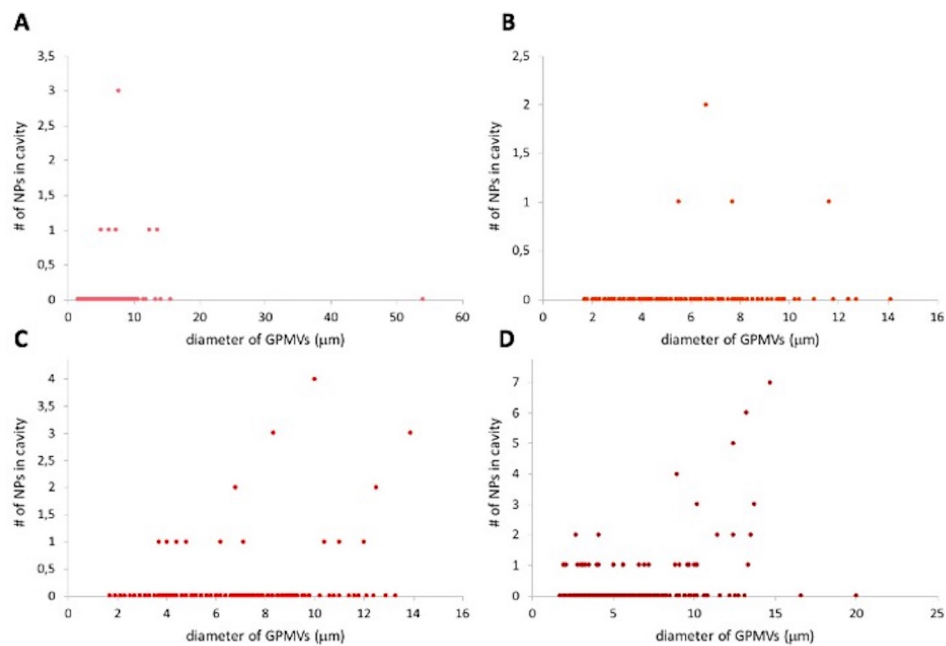
***Figure S22.*** *Evaluation of single plane projections of GPMVs formed from HepG2 cells treated with 100 nm carboxylated NPs at different concentrations: A) $4 \times 10^9$ particles/mL, B) $8 \times 10^9$ particles/mL, C) $1.6 \times 10^{10}$ particles/mL, D) $1.6 \times 10^{11}$ particles/mL.*
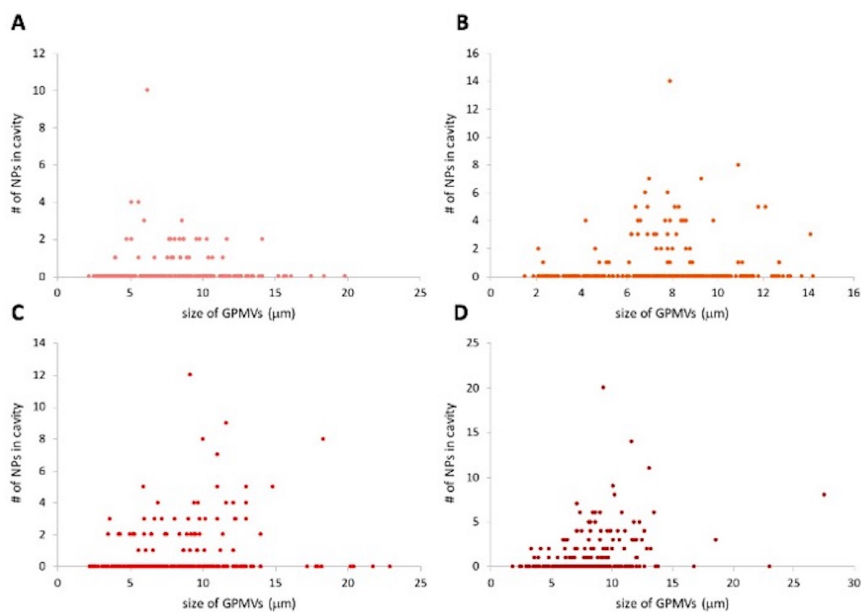


***Figure S23.*** *Evaluation of single plane projections of GPMVs formed from Caco-2 cells treated with 40 nm carboxylated NPs at different concentrations: A) $4 \times 10^9$ particles/mL, B) $8 \times 10^9$ particles/mL, C) $1.6 \times 10^{10}$ particles/mL, D) $1.6 \times 10^{11}$ particles/mL.*
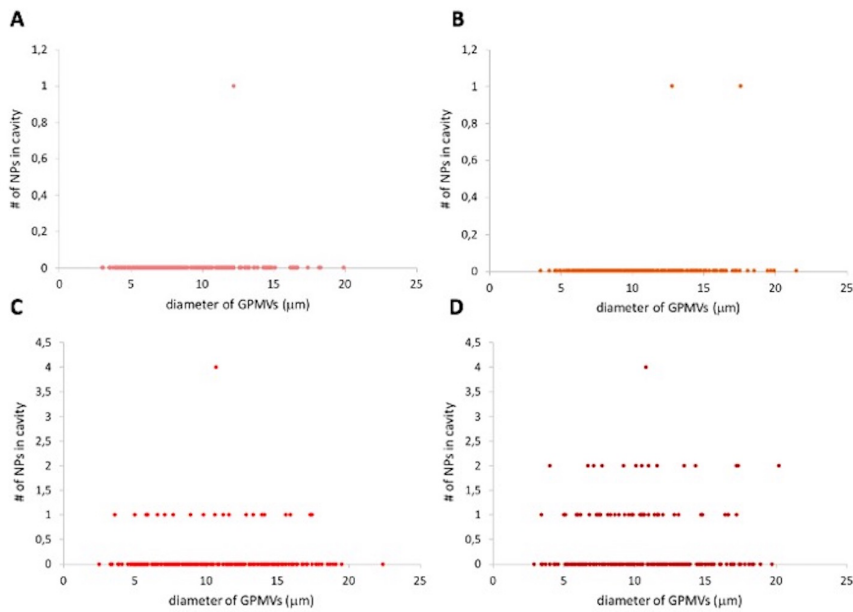
***Figure S24.*** *Evaluation of single plane projections of GPMVs formed from Caco-2 cells treated with 100 nm carboxylated NPs at different concentrations: A) $4 \times 10^9$ particles/mL, B) $8 \times 10^9$ particles/mL, C) $1.6 \times 10^{10}$ particles/mL, D) $1.6 \times 10^{11}$ particles/mL.*



***Figure S25.*** *Evaluation of single plane projections of GPMVs formed from HeLa cells treated with 40 nm carboxylated NPs at different concentrations: A) $4 \times 10^9$ particles/mL, B) $8 \times 10^9$ particles/mL, C) $1.6 \times 10^{10}$ particles/mL, D) $1.6 \times 10^{11}$ particles/mL.*

***Figure S26.*** *Evaluation of single plane projections of GPMVs formed from HeLa cells treated with 100 nm carboxylated NPs at different concentrations: A) 4×10⁹ particles/mL, B) 8×10⁹ particles/mL, C) 1.6×10¹⁰ particles/mL, D) 1.6×10¹¹ particles/mL.*
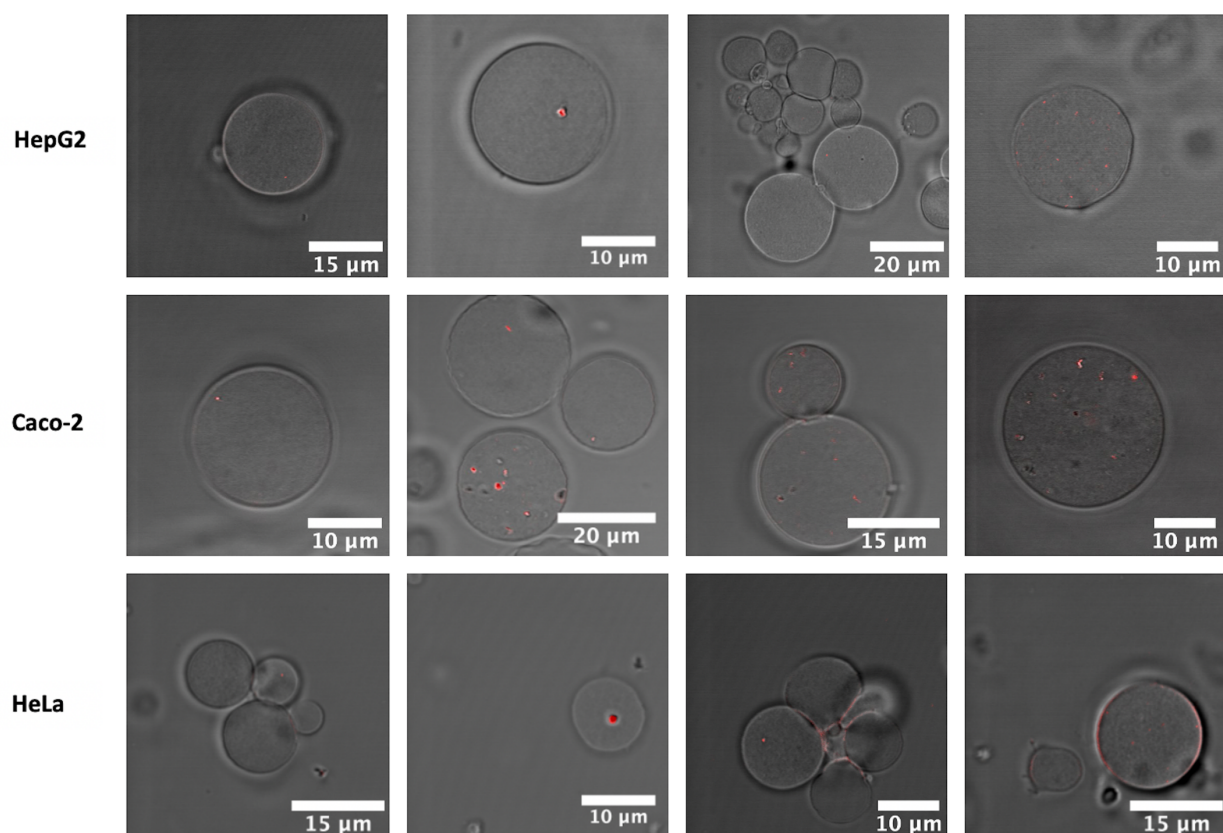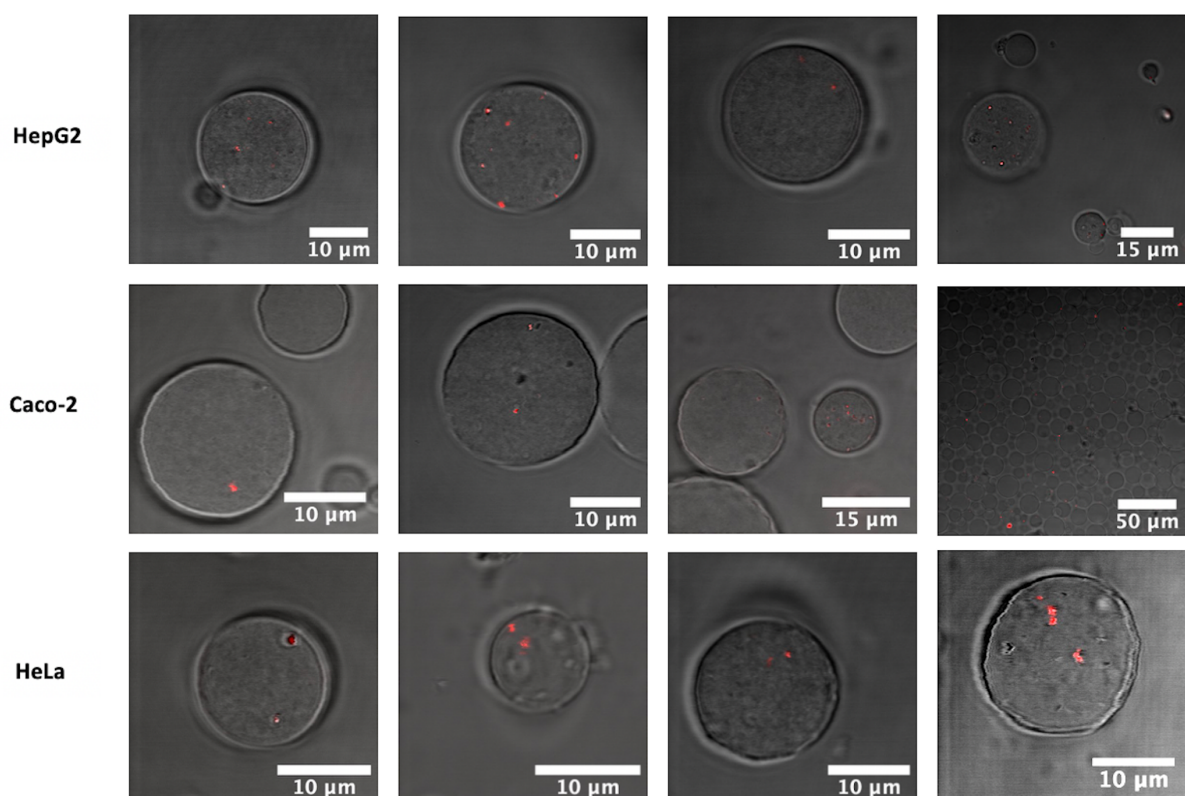
***Figure S27.*** *GPMVs formed from HepG2, Caco-2 and HeLa cell lines treated with 40 nm red fluorescent carboxylated NPs. From left to right the initial concentrations are $4\times10^9$ particles/mL, $8\times10^9$ particles/mL, $1.6\times10^{10}$ particles/mL and $1.6\times10^{11}$ particles/mL. After formation the GPMVs were isolated.*

**Figure S28.** *GPMVs formed from HepG2, Caco-2 and HeLa cell lines treated with 100 nm red fluorescent carboxylated NPs. From left to right the initial concentrations are $4\times10^9$ particles/mL, $8\times10^9$ particles/mL, $1.6\times10^{10}$ particles/mL and $1.6\times10^{11}$ particles/mL. After formation the GPMVs were isolated.*

# LIST OF ABBREVATIONS

| | |
|---|---|
| PS | phosphatidylserine |
| PE | phosphatidylethanolamine |
| PI | phosphatidylinositol |
| PC | phosphatidylcholine |
| SM | sphingomyeline |
| CRP | controlled/quasi- 'living' radical polymerization |
| ROP | ring-opening polymerization |
| PEM | polyelectrolyte multilayer |
| PAA | poly(acrylic acid) |
| PEO | poly(ethylene oxide) |
| PEG | poly(ethylene glycol) |
| PMOXA | poly(2-methyl-2-oxazoline) |
| PDMS | poly(dimethylsiloxane) |
| PB | polybutadiene |
| PS | polystyrene |
| PDEAEMA | poly(2-(diethylamino)ethyl methacrylate |
| PDMAEMA | poly(2-(dimethylamino)ethyl methacrylate |
| PAD | poly(N-amidiono)docecyl acrylamide |
| PSS | poly(styrene sulfonate) |
| PNIPAM | poly(N-isoproylacrylamide) |
| CMC | micellar concentration |
| GUV | giant unilammelar vesicles |
| GPMV | giant plasma membrane vesicle |
| DTT | dithiothreitol |
| PFA | paraformaldehyde |
| CNCs | catalytic nanocompartments |
| OmpF | outer membrane protein F |
| BR | bacteriorhodopsin |
| NTA | nanotracking particle analysis |
| PDI | polydispersity index |
| SLS | static light scattering |
| DLS | dynamic light scattering |
| Rg | radius of gyration |
| Rh | radius of hydration |
| CLSM | confocal laser scanning microscopy |
| FCS | fluorescence correlation spectroscopy |
| TEM | transmission electron microscopy |
| Cryo-TEM | cryogenetic transmission electron microscopy |
| EM | electron microscopy |
| FACS | fluorescence-activated cell sorter |
| ROS | reactive oxygen species |
| NP | nanoparticles |

| | |
|---|---|
| PBS | phosphate buffered saline |
| SRB | sulphorhodamine B |
| ABTS | 2,2′-azino-bis(3-ethylbenzothiazoline-6-sulfonic acid) diammonium salt |
| DMP | 2,6-dimethoxyphenol |
| BCA | bicinchoninic acid |
| OG | n-octyl-β-D-glucopyranoside |
| DMEM | high glucose dulbecco's modified eagle medium |
| EMEM | eagle's minimum essential medium |
| HEPES | 4-(2-hydroxyethyl)-1-piperazineethanesulfonic acid |
| DMSO | dimethyl sulfoxide |
| DMF | dimethylformamide |
| MeCN | acetonitrile |
| DST | disuccinimidyl tartrate |
| EMCH | 3,3'-N-[ε-maleimidocaproic acid] hydrazide, trifluoroacetic acid salt |
| EDC | 1-ethyl-3-(3-dimethylaminopropyl)-carbodiimide |
| DCM | dichloromethane |
| NMR | nuclear magnetic resonance |
| MS | mass spectrometry |
| Đ | polydispersity |
| GPC | Gel permeation chromatography |
| SDS-PAGE | sodium dodecyl sulfate polyacrylamide gel electrophoresis |
| SEC | size exclusion chromatography |
| RFU | relative fluorescence |

# LIST OF FIGURES AND TABLES

# REFERENCES

1.      Spector, A. A.; Yorek, M. A., Membrane lipid composition and cellular function. *Journal of Lipid Research* **1985,** *26* (9), 1015-1035.
2.      Phillips, R.; Ursell, T.; Wiggins, P.; Sens, P., Emerging roles for lipids in shaping membrane-protein function. *Nature* **2009,** *459* (7245), 379-85.
3.      Booth, P. J., Sane in the membrane: designing systems to modulate membrane proteins. *Curr Opin Struct Biol* **2005,** *15* (4), 435-40.
4.      Booth, P. J.; Riley, M. L.; Flitsch, S. L.; Templer, R. H.; Farooq, A.; Curran, A. R.; Chadborn, N.; Wright, P., Evidence That Bilayer Bending Rigidity Affects Membrane Protein Folding. *Biochemistry* **1997,** *36* (1), 197-203.
5.      Perozo, E.; Kloda, A.; Cortes, D. M.; Martinac, B., Physical principles underlying the transduction of bilayer deformation forces during mechanosensitive channel gating. *Nat Struct Biol* **2002,** *9* (9), 696-703.
6.      Pinot, M.; Chesnel, F.; Kubiak, J. Z.; Arnal, I.; Nedelec, F. J.; Gueroui, Z., Effects of Confinement on the Self-Organization of Microtubules and Motors. *Current Biology* **2009,** *19* (11), 954-960.
7.      Attard, G. S.; Templer, R. H.; Smith, W. S.; Hunt, A. N.; Jackowski, S., Modulation of CTP:phosphocholine cytidylyltransferase by membrane curvature elastic stress. *Proc Natl Acad Sci U S A* **2000,** *97* (16), 9032-9036.
8.      Working, E. B.; Andrews, A. C., The Structure of the Phospholipids. *Chemical Reviews* **1941,** *29* (2), 245-256.
9.      Dufourc, E. J., Sterols and membrane dynamics. *J Chem Biol* **2008,** *1* (1-4), 63-77.
10.     Uzman, A., Molecular biology of the cell (4th ed.): Alberts, B., Johnson, A., Lewis, J., Raff, M., Roberts, K., and Walter, P. *Biochemistry and Molecular Biology Education* **2003,** *31* (4), 212-214.
11.     Cournia, Z.; Allen, T. W.; Andricioaei, I.; Antonny, B.; Baum, D.; Brannigan, G.; Buchete, N. V.; Deckman, J. T.; Delemotte, L.; Del Val, C.; Friedman, R.; Gkeka, P.; Hege, H. C.; Hénin, J.; Kasimova, M. A.; Kolocouris, A.; Klein, M. L.; Khalid, S.; Lemieux, M. J.; Lindow, N.; Roy, M.; Selent, J.; Tarek, M.; Tofoleanu, F.; Vanni, S.; Urban, S.; Wales, D. J.; Smith, J. C.; Bondar, A. N., Membrane Protein Structure, Function, and Dynamics: a Perspective from Experiments and Theory. *J Membr Biol* **2015,** *248* (4), 611-40.
12.     Edlinger, C.; Einfalt, T.; Spulber, M.; Car, A.; Meier, W.; Palivan, C. G., Biomimetic Strategy To Reversibly Trigger Functionality of Catalytic Nanocompartments by the Insertion of pH-Responsive Biovalves. *Nano Lett* **2017,** *17* (9), 5790-5798.
13.     Garni, M.; Einfalt, T.; Goers, R.; Palivan, C. G.; Meier, W., Live Follow-Up of Enzymatic Reactions Inside the Cavities of Synthetic Giant Unilamellar Vesicles Equipped with Membrane Proteins Mimicking Cell Architecture. *ACS Synthetic Biology* **2018,** *7* (9), 2116-2125.
14.     Einfalt, T.; Garni, M.; Witzigmann, D.; Sieber, S.; Baltisberger, N.; Huwyler, J.; Meier, W.; Palivan, C. G., Bioinspired Molecular Factories with Architecture and In Vivo Functionalities as Cell Mimics. *Advanced Science* **2020,** *7* (4), 1901923.
15.     Einfalt, T.; Witzigmann, D.; Edlinger, C.; Sieber, S.; Goers, R.; Najer, A.; Spulber, M.; Onaca-Fischer, O.; Huwyler, J.; Palivan, C. G., Biomimetic artificial organelles with in vitro and in vivo activity triggered by reduction in microenvironment. *Nature Communications* **2018,** *9* (1), 1127.

16.    Li, J.; Wang, X.; Zhang, T.; Wang, C.; Huang, Z.; Luo, X.; Deng, Y., A review on phospholipids and their main applications in drug delivery systems. *Asian Journal of Pharmaceutical Sciences* **2015,** *10* (2), 81-98.

17.    Britannica, T. E. o. E., 15 Jan. 2009,  Accessed 2., "Phospholipid". *Encyclopedia Britannica* **2009**.

18.    Bitounis, D.; Fanciullino, R.; Iliadis, A.; Ciccolini, J., Optimizing Druggability through Liposomal Formulations: New Approaches to an Old Concept. *ISRN Pharmaceutics* **2012,** *2012*, 738432.

19.    Seddon, A. M.; Curnow, P.; Booth, P. J., Membrane proteins, lipids and detergents: not just a soap opera. *Biochim Biophys Acta* **2004,** *1666* (1-2), 105-17.

20.    Callan-Jones, A.; Sorre, B.; Bassereau, P., Curvature-driven lipid sorting in biomembranes. *Cold Spring Harb Perspect Biol* **2011,** *3* (2), a004648.

21.    Hatzakis, N. S.; Bhatia, V. K.; Larsen, J.; Madsen, K. L.; Bolinger, P.-Y.; Kunding, A. H.; Castillo, J.; Gether, U.; Hedegård, P.; Stamou, D., How curved membranes recruit amphipathic helices and protein anchoring motifs. *Nature Chemical Biology* **2009,** *5* (11), 835-841.

22.    Tonnesen, A.; Christensen, S. M.; Tkach, V.; Stamou, D., Geometrical membrane curvature as an allosteric regulator of membrane protein structure and function. *Biophysical journal* **2014,** *106* (1), 201-209.

23.    Sens, P.; Johannes, L.; Bassereau, P., Biophysical approaches to protein-induced membrane deformations in trafficking. *Current Opinion in Cell Biology* **2008,** *20* (4), 476-482.

24.    Messager, L.; Gaitzsch, J.; Chierico, L.; Battaglia, G., Novel aspects of encapsulation and delivery using polymersomes. *Current Opinion in Pharmacology* **2014,** *18*, 104-111.

25.    Rideau, E.; Dimova, R.; Schwille, P.; Wurm, F. R.; Landfester, K., Liposomes and polymersomes: a comparative review towards cell mimicking. *Chemical Society Reviews* **2018,** *47* (23), 8572-8610.

26.    Müller, S. S.; Wurm, F. R., Nanovesicles as Drug Delivery Vehicles: Liposomes and Polymersomes. In *Encyclopedia of Polymeric Nanomaterials*, Kobayashi, S.; Müllen, K., Eds. Springer Berlin Heidelberg: Berlin, Heidelberg, 2014; pp 1-6.

27.    Abdollahi, A.; Roghani-Mamaqani, H.; Razavi, B.; Salami-Kalajahi, M., The light-controlling of temperature-responsivity in stimuli-responsive polymers. *Polymer Chemistry* **2019,** *10* (42), 5686-5720.

28.    Kermagoret, A.; Gigmes, D., Combined nitroxide mediated radical polymerization techniques for block copolymer synthesis. *Tetrahedron* **2016,** *72* (48), 7672-7685.

29.    Moad, G., RAFT polymerization to form stimuli-responsive polymers. *Polymer Chemistry* **2017,** *8* (1), 177-219.

30.    Pan, X.; Fantin, M.; Yuan, F.; Matyjaszewski, K., Externally controlled atom transfer radical polymerization. *Chemical Society Reviews* **2018,** *47* (14), 5457-5490.

31.    Walsh, D. J.; Hyatt, M. G.; Miller, S. A.; Guironnet, D., Recent Trends in Catalytic Polymerizations. *ACS Catalysis* **2019,** *9* (12), 11153-11188.

32.    Baker, S. L.; Kaupbayeva, B.; Lathwal, S.; Das, S. R.; Russell, A. J.; Matyjaszewski, K., Atom Transfer Radical Polymerization for Biorelated Hybrid Materials. *Biomacromolecules* **2019,** *20* (12), 4272-4298.

33.    Skirtach, A. G.; Yashchenok, A. M.; Möhwald, H., Encapsulation, release and applications of LbL polyelectrolyte multilayer capsules. *Chemical Communications* **2011,** *47* (48), 12736-12746.

34.    del Mercato, L. L.; Ferraro, M. M.; Baldassarre, F.; Mancarella, S.; Greco, V.; Rinaldi, R.; Leporatti, S., Biological applications of LbL multilayer capsules: From drug delivery to sensing. *Advances in Colloid and Interface Science* **2014,** *207*, 139-154.

35.     Mauser, T.; Déjugnat, C.; Sukhorukov, G. B., Reversible pH-Dependent Properties of Multilayer Microcapsules Made of Weak Polyelectrolytes. *Macromolecular Rapid Communications* **2004,** *25* (20), 1781-1785.

36.     Vriezema, D. M.; Comellas Aragonès, M.; Elemans, J. A. A. W.; Cornelissen, J. J. L. M.; Rowan, A. E.; Nolte, R. J. M., Self-Assembled Nanoreactors. *Chemical Reviews* **2005,** *105* (4), 1445-1490.

37.     van Rijn, P.; Tutus, M.; Kathrein, C.; Zhu, L.; Wessling, M.; Schwaneberg, U.; Böker, A., Challenges and advances in the field of self-assembled membranes. *Chemical Society Reviews* **2013,** *42* (16), 6578-6592.

38.     Discher, B. M.; Won, Y.-Y.; Ege, D. S.; Lee, J. C. M.; Bates, F. S.; Discher, D. E.; Hammer, D. A., Polymersomes: Tough Vesicles Made from Diblock Copolymers. *Science* **1999,** *284* (5417), 1143.

39.     Marguet, M.; Bonduelle, C.; Lecommandoux, S., Multicompartmentalized polymeric systems: towards biomimetic cellular structure and function. *Chemical Society Reviews* **2013,** *42* (2), 512-529.

40.     Karayianni, M.; Pispas, S., Self-Assembly of Amphiphilic Block Copolymers in Selective Solvents. In *Fluorescence Studies of Polymer Containing Systems*, Procházka, K., Ed. Springer International Publishing: Cham, 2016; pp 27-63.

41.     Palivan, C. G.; Fischer-Onaca, O.; Delcea, M.; Itel, F.; Meier, W., Protein–polymer nanoreactors for medical applications. *Chemical Society Reviews* **2012,** *41* (7), 2800-2823.

42.     Discher, D. E.; Ahmed, F., Polymersomes. *Annu Rev Biomed Eng* **2006,** *8*, 323-41.

43.     Blanazs, A.; Armes, S. P.; Ryan, A. J., Self-Assembled Block Copolymer Aggregates: From Micelles to Vesicles and their Biological Applications. *Macromolecular Rapid Communications* **2009,** *30* (4-5), 267-277.

44.     Najer, A.; Wu, D.; Vasquez, D.; Palivan, C. G.; Meier, W., Polymer nanocompartments in broad-spectrum medical applications. *Nanomedicine (Lond)* **2013,** *8* (3), 425-47.

45.     Tanner, P.; Egli, S.; Balasubramanian, V.; Onaca, O.; Palivan, C. G.; Meier, W., Can polymeric vesicles that confine enzymatic reactions act as simplified organelles? *FEBS Lett* **2011,** *585* (11), 1699-706.

46.     Nicolas, J.; Mura, S.; Brambilla, D.; Mackiewicz, N.; Couvreur, P., Design, functionalization strategies and biomedical applications of targeted biodegradable/biocompatible polymer-based nanocarriers for drug delivery. *Chem Soc Rev* **2013,** *42* (3), 1147-235.

47.     Stuart, M. A. C.; Huck, W. T. S.; Genzer, J.; Müller, M.; Ober, C.; Stamm, M.; Sukhorukov, G. B.; Szleifer, I.; Tsukruk, V. V.; Urban, M.; Winnik, F.; Zauscher, S.; Luzinov, I.; Minko, S., Emerging applications of stimuli-responsive polymer materials. *Nature Materials* **2010,** *9* (2), 101-113.

48.     Sullivan, T. P.; Huck, W. T. S., Reactions on Monolayers: Organic Synthesis in Two Dimensions. *European Journal of Organic Chemistry* **2003,** *2003* (1), 17-29.

49.     Vericat, C.; Vela, M. E.; Benitez, G.; Carro, P.; Salvarezza, R. C., Self-assembled monolayers of thiols and dithiols on gold: new challenges for a well-known system. *Chemical Society Reviews* **2010,** *39* (5), 1805-1834.

50.     Allen, C.; Maysinger, D.; Eisenberg, A., Nano-engineering block copolymer aggregates for drug delivery. *Colloids and Surfaces B: Biointerfaces* **1999,** *16* (1), 3-27.

51.     Nicolai, T.; Colombani, O.; Chassenieux, C., Dynamic polymeric micelles versus frozen nanoparticles formed by block copolymers. *Soft Matter* **2010,** *6* (14), 3111-3118.

52.     Cho, H. K.; Cheong, I. W.; Lee, J. M.; Kim, J. H., Polymeric nanoparticles, micelles and polymersomes from amphiphilic block copolymer. *Korean Journal of Chemical Engineering* **2010,** *27* (3), 731-740.

53.      Palivan, C. G.;  Goers, R.;  Najer, A.;  Zhang, X.;  Car, A.; Meier, W., Bioinspired polymer vesicles and membranes for biological and medical applications. *Chemical Society Reviews* **2016,** *45* (2), 377-411.

54.      Lee, J. C.;  Bermudez, H.;  Discher, B. M.;  Sheehan, M. A.;  Won, Y. Y.;  Bates, F. S.; Discher, D. E., Preparation, stability, and in vitro performance of vesicles made with diblock copolymers. *Biotechnol Bioeng* **2001,** *73* (2), 135-45.

55.      Schatz, C.; Lecommandoux, S., Polysaccharide-Containing Block Copolymers: Synthesis, Properties and Applications of an Emerging Family of Glycoconjugates. *Macromolecular Rapid Communications* **2010,** *31* (19), 1664-1684.

56.      Lee, J. S.; Feijen, J., Polymersomes for drug delivery: design, formation and characterization. *J Control Release* **2012,** *161* (2), 473-83.

57.      Yildiz, M. E.;  Prud'homme, R. K.;  Robb, I.; Adamson, D. H., Formation and characterization of polymersomes made by a solvent injection method. *Polymers for Advanced Technologies* **2007,** *18* (6), 427-432.

58.      LoPresti, C.;  Lomas, H.;  Massignani, M.;  Smart, T.; Battaglia, G., Polymersomes: nature inspired nanometer sized compartments. *Journal of Materials Chemistry* **2009,** *19* (22), 3576-3590.

59.      Itel, F.;  Chami, M.;  Najer, A.;  Lörcher, S.;  Wu, D.;  Dinu, I. A.; Meier, W., Molecular Organization and Dynamics in Polymersome Membranes: A Lateral Diffusion Study. *Macromolecules* **2014,** *47* (21), 7588-7596.

60.      Stoenescu, R.;  Graff, A.; Meier, W., Asymmetric ABC-Triblock Copolymer Membranes Induce a Directed Insertion of Membrane Proteins. *Macromolecular Bioscience* **2004,** *4* (10), 930-935.

61.      Wittemann, A.;  Azzam, T.; Eisenberg, A., Biocompatible Polymer Vesicles from Biamphiphilic Triblock Copolymers and Their Interaction with Bovine Serum Albumin. *Langmuir* **2007,** *23* (4), 2224-2230.

62.      Braunecker, W. A.; Matyjaszewski, K., Controlled/living radical polymerization: Features, developments, and perspectives. *Progress in Polymer Science* **2007,** *32* (1), 93-146.

63.      Aoshima, S.; Kanaoka, S., A Renaissance in Living Cationic Polymerization. *Chemical Reviews* **2009,** *109* (11), 5245-5287.

64.      Dechy-Cabaret, O.;  Martin-Vaca, B.; Bourissou, D., Controlled Ring-Opening Polymerization of Lactide and Glycolide. *Chemical Reviews* **2004,** *104* (12), 6147-6176.

65.      Matyjaszewski, K., Atom Transfer Radical Polymerization: From Mechanisms to Applications. *Israel Journal of Chemistry* **2012,** *52* (3-4), 206-220.

66.      Yan, Q.;  Wang, J.;  Yin, Y.; Yuan, J., Breathing Polymersomes: CO2-Tuning Membrane Permeability for Size-Selective Release, Separation, and Reaction. *Angewandte Chemie International Edition* **2013,** *52* (19), 5070-5073.

67.      Iyisan, B.;  Kluge, J.;  Formanek, P.;  Voit, B.; Appelhans, D., Multifunctional and Dual-Responsive Polymersomes as Robust Nanocontainers: Design, Formation by Sequential Post-Conjugations, and pH-Controlled Drug Release. *Chemistry of Materials* **2016,** *28* (5), 1513-1525.

68.      Yu, S.;  Azzam, T.;  Rouiller, I.; Eisenberg, A., "Breathing" Vesicles. *Journal of the American Chemical Society* **2009,** *131* (30), 10557-10566.

69.      Qin, J.;  Liu, Q.;  Zhang, J.;  Chen, J.;  Chen, S.;  Zhao, Y.; Du, J., Rationally Separating the Corona and Membrane Functions of Polymer Vesicles for Enhanced T2 MRI and Drug Delivery. *ACS Applied Materials & Interfaces* **2015,** *7* (25), 14043-14052.

70.      Chiu, H. C.;  Lin, Y. W.;  Huang, Y. F.;  Chuang, C. K.; Chern, C. S., Polymer vesicles containing small vesicles within interior aqueous compartments and pH-responsive transmembrane channels. *Angew Chem Int Ed Engl* **2008,** *47* (10), 1875-8.

71.    Gaitzsch, J.; Appelhans, D.; Wang, L.; Battaglia, G.; Voit, B., Synthetic Bio-nanoreactor: Mechanical and Chemical Control of Polymersome Membrane Permeability. *Angewandte Chemie International Edition* **2012,** *51* (18), 4448-4451.

72.    Du, F.; Bobbala, S.; Yi, S.; Scott, E. A., Sequential intracellular release of water-soluble cargos from Shell-crosslinked polymersomes. *Journal of controlled release : official journal of the Controlled Release Society* **2018,** *282*, 90-100.

73.    Nardin, C.; Widmer, J.; Winterhalter, M.; Meier, W., Amphiphilic block copolymer nanocontainers as bioreactors. *The European Physical Journal E* **2001,** *4* (4), 403-410.

74.    Meyer, C. E.; Abram, S.-L.; Craciun, I.; Palivan, C. G., Biomolecule–polymer hybrid compartments: combining the best of both worlds. *Physical Chemistry Chemical Physics* **2020,** *22* (20), 11197-11218.

75.    Meyer, C. E.; Craciun, I.; Schoenenberger, C.-A.; Wehr, R.; Palivan, C. G., Catalytic polymersomes to produce strong and long-lasting bioluminescence. *Nanoscale* **2021,** *13* (1), 66-70.

76.    Kumar, M.; Habel, J. E. O.; Shen, Y.-x.; Meier, W. P.; Walz, T., High-Density Reconstitution of Functional Water Channels into Vesicular and Planar Block Copolymer Membranes. *Journal of the American Chemical Society* **2012,** *134* (45), 18631-18637.

77.    Muhammad, N.; Dworeck, T.; Fioroni, M.; Schwaneberg, U., Engineering of the E. coli outer membrane protein FhuA to overcome the hydrophobic mismatch in thick polymeric membranes. *J Nanobiotechnology* **2011,** *9*, 8.

78.    Graff, A.; Sauer, M.; Van Gelder, P.; Meier, W., Virus-assisted loading of polymer nanocontainer. *Proceedings of the National Academy of Sciences* **2002,** *99* (8), 5064.

79.    Lomora, M.; Garni, M.; Itel, F.; Tanner, P.; Spulber, M.; Palivan, C. G., Polymersomes with engineered ion selective permeability as stimuli-responsive nanocompartments with preserved architecture. *Biomaterials* **2015,** *53*, 406-414.

80.    Lomora, M.; Itel, F.; Dinu, I. A.; Palivan, C. G., Selective ion-permeable membranes by insertion of biopores into polymersomes. *Physical Chemistry Chemical Physics* **2015,** *17* (24), 15538-15546.

81.    Ihle, S.; Onaca, O.; Rigler, P.; Hauer, B.; Rodríguez-Ropero, F.; Fioroni, M.; Schwaneberg, U., Nanocompartments with a pH release system based on an engineered OmpF channel protein. *Soft Matter* **2011,** *7* (2), 532-539.

82.    Garni, M.; Thamboo, S.; Schoenenberger, C.-A.; Palivan, C. G., Biopores/membrane proteins in synthetic polymer membranes. *Biochimica et Biophysica Acta (BBA) - Biomembranes* **2017,** *1859* (4), 619-638.

83.    Itel, F.; Najer, A.; Palivan, C. G.; Meier, W., Dynamics of Membrane Proteins within Synthetic Polymer Membranes with Large Hydrophobic Mismatch. *Nano Letters* **2015,** *15* (6), 3871-3878.

84.    Gaitzsch, J.; Hirschi, S.; Freimann, S.; Fotiadis, D.; Meier, W., Directed Insertion of Light-Activated Proteorhodopsin into Asymmetric Polymersomes from an ABC Block Copolymer. *Nano Lett* **2019,** *19* (4), 2503-2508.

85.    Choi, H. J.; Montemagno, C. D., Artificial organelle: ATP synthesis from cellular mimetic polymersomes. *Nano Lett* **2005,** *5* (12), 2538-42.

86.    Wang, G.; Castiglione, K., Light-Driven Biocatalysis in Liposomes and Polymersomes: Where Are We Now? *Catalysts* **2019,** *9* (1).

87.    Lanyi, J. K.; Pohorille, A., Proton pumps: mechanism of action and applications. *Trends in Biotechnology* **2001,** *19* (4), 140-144.

88.    Matoori, S.; Leroux, J.-C., Twenty-five years of polymersomes: lost in translation? *Materials Horizons* **2020,** *7* (5), 1297-1309.

89.    Nardin, C.; Thoeni, S.; Widmer, J.; Winterhalter, M.; Meier, W., Nanoreactors based on (polymerized) ABA-triblock copolymer vesicles. *Chemical Communications* **2000,** (15), 1433-1434.

90.     Belluati, A.; Craciun, I.; Liu, J.; Palivan, C. G., Nanoscale Enzymatic Compartments in Tandem Support Cascade Reactions in Vitro. *Biomacromolecules* **2018,** *19* (10), 4023-4033.

91.     Axthelm, F.; Casse, O.; Koppenol, W. H.; Nauser, T.; Meier, W.; Palivan, C. G., Antioxidant nanoreactor based on superoxide dismutase encapsulated in superoxide-permeable vesicles. *J Phys Chem B* **2008,** *112* (28), 8211-7.

92.     Graff, A.; Fraysse-Ailhas, C.; Palivan, C. G.; Grzelakowski, M.; Friedrich, T.; Vebert, C.; Gescheidt, G.; Meier, W., Amphiphilic Copolymer Membranes Promote NADH:Ubiquinone Oxidoreductase Activity: Towards an Electron-Transfer Nanodevice. *Macromolecular Chemistry and Physics* **2010,** *211* (2), 229-238.

93.     Baumann, P.; Spulber, M.; Dinu, I. A.; Palivan, C. G., Cellular Trojan horse based polymer nanoreactors with light-sensitive activity. *J Phys Chem B* **2014,** *118* (31), 9361-70.

94.     Dobrunz, D.; Toma, A. C.; Tanner, P.; Pfohl, T.; Palivan, C. G., Polymer nanoreactors with dual functionality: simultaneous detoxification of peroxynitrite and oxygen transport. *Langmuir* **2012,** *28* (45), 15889-99.

95.     Tanner, P.; Onaca, O.; Balasubramanian, V.; Meier, W.; Palivan, C. G., Enzymatic Cascade Reactions inside Polymeric Nanocontainers: A Means to Combat Oxidative Stress. *Chemistry – A European Journal* **2011,** *17* (16), 4552-4560.

96.     Stauch, O.; Schubert, R.; Savin, G.; Burchard, W., Structure of artificial cytoskeleton containing liposomes in aqueous solution studied by static and dynamic light scattering. *Biomacromolecules* **2002,** *3* (3), 565-78.

97.     Anderson, W.; Kozak, D.; Coleman, V. A.; Jämting Å, K.; Trau, M., A comparative study of submicron particle sizing platforms: accuracy, precision and resolution analysis of polydisperse particle size distributions. *J Colloid Interface Sci* **2013,** *405*, 322-30.

98.     Patterson, G. H., Fluorescence microscopy below the diffraction limit. *Semin Cell Dev Biol* **2009,** *20* (8), 886-93.

99.     Najer, A.; Wu, D.; Bieri, A.; Brand, F.; Palivan, C. G.; Beck, H.-P.; Meier, W., Nanomimics of Host Cell Membranes Block Invasion and Expose Invasive Malaria Parasites. *ACS Nano* **2014,** *8* (12), 12560-12571.

100.    Najer, A.; Wu, D.; Nussbaumer, M. G.; Schwertz, G.; Schwab, A.; Witschel, M. C.; Schäfer, A.; Diederich, F.; Rottmann, M.; Palivan, C. G.; Beck, H.-P.; Meier, W., An amphiphilic graft copolymer-based nanoparticle platform for reduction-responsive anticancer and antimalarial drug delivery. *Nanoscale* **2016,** *8* (31), 14858-14869.

101.    Rigler, R.; Mets, Ü.; Widengren, J.; Kask, P., Fluorescence correlation spectroscopy with high count rate and low background: analysis of translational diffusion. *European Biophysics Journal* **1993,** *22* (3), 169-175.

102.    Dertinger, T.; Pacheco, V.; von der Hocht, I.; Hartmann, R.; Gregor, I.; Enderlein, J., Two-focus fluorescence correlation spectroscopy: a new tool for accurate and absolute diffusion measurements. *Chemphyschem* **2007,** *8* (3), 433-43.

103.    Baumann, P.; Spulber, M.; Fischer, O.; Car, A.; Meier, W., Investigation of Horseradish Peroxidase Kinetics in an "Organelle-Like" Environment. *Small* **2017,** *13* (17), 1603943.

104.    Onaca, O.; Sarkar, P.; Roccatano, D.; Friedrich, T.; Hauer, B.; Grzelakowski, M.; Güven, A.; Fioroni, M.; Schwaneberg, U., Functionalized Nanocompartments (Synthosomes) with a Reduction-Triggered Release System. *Angewandte Chemie International Edition* **2008,** *47* (37), 7029-7031.

105.    Deng, Z.; Hu, J.; Liu, S., Reactive Oxygen, Nitrogen, and Sulfur Species (RONSS)-Responsive Polymersomes for Triggered Drug Release. *Macromol Rapid Commun* **2017,** *38* (11).

106.    Zhang, L.; Gu, F. X.; Chan, J. M.; Wang, A. Z.; Langer, R. S.; Farokhzad, O. C., Nanoparticles in medicine: therapeutic applications and developments. *Clin Pharmacol Ther* **2008,** *83* (5), 761-9.

107.    Onaca, O.; Enea, R.; Hughes, D. W.; Meier, W., Stimuli-Responsive Polymersomes as Nanocarriers for Drug and Gene Delivery. *Macromolecular Bioscience* **2009,** *9* (2), 129-139.

108.    Meng, F.; Zhong, Z.; Feijen, J., Stimuli-Responsive Polymersomes for Programmed Drug Delivery. *Biomacromolecules* **2009,** *10* (2), 197-209.

109.    Reineke, T. M., Stimuli-Responsive Polymers for Biological Detection and Delivery. *ACS Macro Letters* **2016,** *5* (1), 14-18.

110.    Schumers, J. M.; Fustin, C. A.; Gohy, J. F., Light-responsive block copolymers. *Macromol Rapid Commun* **2010,** *31* (18), 1588-607.

111.    Jochum, F. D.; Theato, P., Temperature- and light-responsive smart polymer materials. *Chemical Society Reviews* **2013,** *42* (17), 7468-7483.

112.    Rodriguez, A. R.; Kramer, J. R.; Deming, T. J., Enzyme-triggered cargo release from methionine sulfoxide containing copolypeptide vesicles. *Biomacromolecules* **2013,** *14* (10), 3610-4.

113.    Kim, H.; Kang, Y. J.; Kang, S.; Kim, K. T., Monosaccharide-responsive release of insulin from polymersomes of polyboroxole block copolymers at neutral pH. *J Am Chem Soc* **2012,** *134* (9), 4030-3.

114.    Zhang, J.; Wei, H.; Tan, J.; Qiao, W.; Guan, Y.; Zhang, J., Thermo- and pH- dual responsive inorganic-organic hybrid hydrogels with tunable luminescence. *Science China Chemistry* **2018,** *61* (3), 328-335.

115.    Liu, F.; Kozlovskaya, V.; Medipelli, S.; Xue, B.; Ahmad, F.; Saeed, M.; Cropek, D.; Kharlampieva, E., Temperature-Sensitive Polymersomes for Controlled Delivery of Anticancer Drugs. *Chemistry of Materials* **2015,** *27* (23), 7945-7956.

116.    Du, Y.; Chen, W.; Zheng, M.; Meng, F.; Zhong, Z., pH-sensitive degradable chimaeric polymersomes for the intracellular release of doxorubicin hydrochloride. *Biomaterials* **2012,** *33* (29), 7291-7299.

117.    Zhan, F.; Chen, W.; Wang, Z.; Lu, W.; Cheng, R.; Deng, C.; Meng, F.; Liu, H.; Zhong, Z., Acid-Activatable Prodrug Nanogels for Efficient Intracellular Doxorubicin Release. *Biomacromolecules* **2011,** *12* (10), 3612-3620.

118.    Li, S.; Meng, F.; Wang, Z.; Zhong, Y.; Zheng, M.; Liu, H.; Zhong, Z., Biodegradable polymersomes with an ionizable membrane: Facile preparation, superior protein loading, and endosomal pH-responsive protein release. *European Journal of Pharmaceutics and Biopharmaceutics* **2012,** *82* (1), 103-111.

119.    Cheng, R.; Meng, F.; Ma, S.; Xu, H.; Liu, H.; Jing, X.; Zhong, Z., Reduction and temperature dual-responsive crosslinked polymersomes for targeted intracellular protein delivery. *Journal of Materials Chemistry* **2011,** *21* (47), 19013-19020.

120.    Xu, H.; Meng, F.; Zhong, Z., Reversibly crosslinked temperature-responsive nano-sized polymersomes: synthesis and triggered drug release. *Journal of Materials Chemistry* **2009,** *19* (24), 4183-4190.

121.    Hickey, R. J.; Haynes, A. S.; Kikkawa, J. M.; Park, S.-J., Controlling the Self-Assembly Structure of Magnetic Nanoparticles and Amphiphilic Block-Copolymers: From Micelles to Vesicles. *Journal of the American Chemical Society* **2011,** *133* (5), 1517-1525.

122.    Krack, M.; Hohenberg, H.; Kornowski, A.; Lindner, P.; Weller, H.; Förster, S., Nanoparticle-Loaded Magnetophoretic Vesicles. *Journal of the American Chemical Society* **2008,** *130* (23), 7315-7320.

123.    Egli, S.; Nussbaumer, M. G.; Balasubramanian, V.; Chami, M.; Bruns, N.; Palivan, C.; Meier, W., Biocompatible Functionalization of Polymersome Surfaces: A New Approach

to Surface Immobilization and Cell Targeting Using Polymersomes. *Journal of the American Chemical Society* **2011,** *133* (12), 4476-4483.

124.    Hu, X.; Zhang, Y.; Xie, Z.; Jing, X.; Bellotti, A.; Gu, Z., Stimuli-Responsive Polymersomes for Biomedical Applications. *Biomacromolecules* **2017,** *18* (3), 649-673.

125.    Hu, L.; Zhang, Q.; Li, X.; Serpe, M. J., Stimuli-responsive polymers for sensing and actuation. *Materials Horizons* **2019,** *6* (9), 1774-1793.

126.    Leong, J.; Teo, J. Y.; Aakalu, V. K.; Yang, Y. Y.; Kong, H., Engineering Polymersomes for Diagnostics and Therapy. *Advanced Healthcare Materials* **2018,** *7* (8), 1701276.

127.    Iyisan, B.; Landfester, K., Modular Approach for the Design of Smart Polymeric Nanocapsules. *Macromolecular Rapid Communications* **2019,** *40* (1), 1800577.

128.    Rifaie-Graham, O.; Apebende, E. A.; Bruns, N., Bio-Inspired Polymersome Nanoreactors. *Chimia (Aarau)* **2019,** *73* (1), 21-24.

129.    Zartner, L.; Muthwill, M. S.; Dinu, I. A.; Schoenenberger, C.-A.; Palivan, C. G., The rise of bio-inspired polymer compartments responding to pathology-related signals. *Journal of Materials Chemistry B* **2020,** *8* (29), 6252-6270.

130.    Idrissi, M. E.; Meyer, C. E.; Zartner, L.; Meier, W., Nanosensors based on polymer vesicles and planar membranes: a short review. *Journal of Nanobiotechnology* **2018,** *16* (1), 63.

131.    Goers, R.; Thoma, J.; Ritzmann, N.; Di Silvestro, A.; Alter, C.; Gunkel-Grabole, G.; Fotiadis, D.; Müller, D. J.; Meier, W., Optimized reconstitution of membrane proteins into synthetic membranes. *Communications Chemistry* **2018,** *1* (1), 35.

132.    Ke, W.; Li, J.; Mohammed, F.; Wang, Y.; Tou, K.; Liu, X.; Wen, P.; Kinoh, H.; Anraku, Y.; Chen, H.; Kataoka, K.; Ge, Z., Therapeutic Polymersome Nanoreactors with Tumor-Specific Activable Cascade Reactions for Cooperative Cancer Therapy. *ACS Nano* **2019,** *13* (2), 2357-2369.

133.    Belluati, A.; Craciun, I.; Palivan, C. G., Bioactive Catalytic Nanocompartments Integrated into Cell Physiology and Their Amplification of a Native Signaling Cascade. *ACS Nano* **2020,** *14* (9), 12101-12112.

134.    Meyer, C. E.; Liu, J.; Craciun, I.; Wu, D.; Wang, H.; Xie, M.; Fussenegger, M.; Palivan, C. G., Segregated Nanocompartments Containing Therapeutic Enzymes and Imaging Compounds within DNA-Zipped Polymersome Clusters for Advanced Nanotheranostic Platform. *Small* **2020,** *16* (27), 1906492.

135.    Zhang, X.; Lomora, M.; Einfalt, T.; Meier, W.; Klein, N.; Schneider, D.; Palivan, C. G., Active surfaces engineered by immobilizing protein-polymer nanoreactors for selectively detecting sugar alcohols. *Biomaterials* **2016,** *89*, 79-88.

136.    Tanner, P.; Balasubramanian, V.; Palivan, C. G., Aiding Nature's Organelles: Artificial Peroxisomes Play Their Role. *Nano Letters* **2013,** *13* (6), 2875-2883.

137.    Spulber, M.; Najer, A.; Winkelbach, K.; Glaied, O.; Waser, M.; Pieles, U.; Meier, W.; Bruns, N., Photoreaction of a hydroxyalkyphenone with the membrane of polymersomes: a versatile method to generate semipermeable nanoreactors. *J Am Chem Soc* **2013,** *135* (24), 9204-12.

138.    Peters, R. J. R. W.; Marguet, M.; Marais, S.; Fraaije, M. W.; van Hest, J. C. M.; Lecommandoux, S., Cascade Reactions in Multicompartmentalized Polymersomes. *Angewandte Chemie International Edition* **2014,** *53* (1), 146-150.

139.    Trantidou, T.; Friddin, M.; Elani, Y.; Brooks, N. J.; Law, R. V.; Seddon, J. M.; Ces, O., Engineering Compartmentalized Biomimetic Micro- and Nanocontainers. *ACS Nano* **2017,** *11* (7), 6549-6565.

140.    Thamboo, S.; Najer, A.; Belluati, A.; von Planta, C.; Wu, D.; Craciun, I.; Meier, W.; Palivan, C. G., Mimicking Cellular Signaling Pathways within Synthetic

Multicompartment Vesicles with Triggered Enzyme Activity and Induced Ion Channel Recruitment. *Advanced Functional Materials* **2019,** *29* (40), 1904267.

141.    Belluati, A.; Thamboo, S.; Najer, A.; Maffeis, V.; von Planta, C.; Craciun, I.; Palivan, C. G.; Meier, W., Multicompartment Polymer Vesicles with Artificial Organelles for Signal-Triggered Cascade Reactions Including Cytoskeleton Formation. *Advanced Functional Materials* **2020,** *30* (32), 2002949.

142.    dos Santos, E. C.; Belluati, A.; Necula, D.; Scherrer, D.; Meyer, C. E.; Wehr, R. P.; Lörtscher, E.; Palivan, C. G.; Meier, W., Combinatorial Strategy for Studying Biochemical Pathways in Double Emulsion Templated Cell-Sized Compartments. *Advanced Materials* **2020,** *32* (48), 2004804.

143.    Buchner, E.; Rapp, R., Alkoholische Gährung ohne Hefezellen. *Berichte der deutschen chemischen Gesellschaft* **1897,** *30* (3), 2668-2678.

144.    Stano, P.; Carrara, P.; Kuruma, Y.; Pereira de Souza, T.; Luisi, P. L., Compartmentalized reactions as a case of soft-matter biotechnology: synthesis of proteins and nucleic acids inside lipid vesicles. *Journal of Materials Chemistry* **2011,** *21* (47), 18887-18902.

145.    Adamala, K. P.; Martin-Alarcon, D. A.; Guthrie-Honea, K. R.; Boyden, E. S., Engineering genetic circuit interactions within and between synthetic minimal cells. *Nature Chemistry* **2017,** *9* (5), 431-439.

146.    Elani, Y.; Law, R. V.; Ces, O., Protein synthesis in artificial cells: using compartmentalisation for spatial organisation in vesicle bioreactors. *Physical Chemistry Chemical Physics* **2015,** *17* (24), 15534-15537.

147.    Kobori, S.; Ichihashi, N.; Kazuta, Y.; Yomo, T., A controllable gene expression system in liposomes that includes a positive feedback loop. *Mol Biosyst* **2013,** *9* (6), 1282-5.

148.    Xiao, Q.; Yadavalli, S. S.; Zhang, S.; Sherman, S. E.; Fiorin, E.; da Silva, L.; Wilson, D. A.; Hammer, D. A.; André, S.; Gabius, H.-J.; Klein, M. L.; Goulian, M.; Percec, V., Bioactive cell-like hybrids coassembled from (glyco)dendrimersomes with bacterial membranes. *Proceedings of the National Academy of Sciences* **2016,** *113* (9), E1134.

149.    Ashley, C. E.; Carnes, E. C.; Phillips, G. K.; Padilla, D.; Durfee, P. N.; Brown, P. A.; Hanna, T. N.; Liu, J.; Phillips, B.; Carter, M. B.; Carroll, N. J.; Jiang, X.; Dunphy, D. R.; Willman, C. L.; Petsev, D. N.; Evans, D. G.; Parikh, A. N.; Chackerian, B.; Wharton, W.; Peabody, D. S.; Brinker, C. J., The targeted delivery of multicomponent cargos to cancer cells by nanoporous particle-supported lipid bilayers. *Nature Materials* **2011,** *10* (5), 389-397.

150.    Kreft, O.; Prevot, M.; Möhwald, H.; Sukhorukov, G. B., Shell-in-Shell Microcapsules: A Novel Tool for Integrated, Spatially Confined Enzymatic Reactions. *Angewandte Chemie International Edition* **2007,** *46* (29), 5605-5608.

151.    Qiao, Y.; Li, M.; Booth, R.; Mann, S., Predatory behaviour in synthetic protocell communities. *Nat Chem* **2017,** *9* (2), 110-119.

152.    Nomura, S. M.; Tsumoto, K.; Hamada, T.; Akiyoshi, K.; Nakatani, Y.; Yoshikawa, K., Gene expression within cell-sized lipid vesicles. *Chembiochem* **2003,** *4* (11), 1172-5.

153.    Oberholzer, T.; Albrizio, M.; Luisi, P. L., Polymerase chain reaction in liposomes. *Chem Biol* **1995,** *2* (10), 677-82.

154.    Fischer, A.; Franco, A.; Oberholzer, T., Giant vesicles as microreactors for enzymatic mRNA synthesis. *Chembiochem* **2002,** *3* (5), 409-17.

155.    Godovac-Zimmermann, J.; Brown, L. R., Perspectives for mass spectrometry and functional proteomics. *Mass Spectrom Rev* **2001,** *20* (1), 1-57.

156.    Marth, J. D., A unified vision of the building blocks of life. *Nature Cell Biology* **2008,** *10* (9), 1015-1015.

157.    Rafelski, S. M.; Marshall, W. F., Building the cell: design principles of cellular architecture. *Nat Rev Mol Cell Biol* **2008,** *9* (8), 593-602.

158. Salehi-Reyhani, A.; Ces, O.; Elani, Y., Artificial cell mimics as simplified models for the study of cell biology. *Experimental Biology and Medicine* **2017,** *242* (13), 1309-1317.

159. Chang, T. M., Therapeutic applications of polymeric artificial cells. *Nat Rev Drug Discov* **2005,** *4* (3), 221-35.

160. Loiseau, E.; Schneider, J. A. M.; Keber, F. C.; Pelzl, C.; Massiera, G.; Salbreux, G.; Bausch, A. R., Shape remodeling and blebbing of active cytoskeletal vesicles. *Science Advances* **2016,** *2* (4), e1500465.

161. Xavier, J. C.; Patil, K. R.; Rocha, I., Systems biology perspectives on minimal and simpler cells. *Microbiol Mol Biol Rev* **2014,** *78* (3), 487-509.

162. Way, J. C.; Collins, J. J.; Keasling, J. D.; Silver, P. A., Integrating biological redesign: where synthetic biology came from and where it needs to go. *Cell* **2014,** *157* (1), 151-61.

163. Xu, C.; Hu, S.; Chen, X., Artificial cells: from basic science to applications. *Mater Today (Kidlington)* **2016,** *19* (9), 516-532.

164. Steinberg-Yfrach, G.; Rigaud, J.-L.; Durantini, E. N.; Moore, A. L.; Gust, D.; Moore, T. A., Light-driven production of ATP catalysed by F0F1-ATP synthase in an artificial photosynthetic membrane. *Nature* **1998,** *392* (6675), 479-482.

165. Lentini, R.; Santero, S. P.; Chizzolini, F.; Cecchi, D.; Fontana, J.; Marchioretto, M.; Del Bianco, C.; Terrell, J. L.; Spencer, A. C.; Martini, L.; Forlin, M.; Assfalg, M.; Serra, M. D.; Bentley, W. E.; Mansy, S. S., Integrating artificial with natural cells to translate chemical messages that direct E. coli behaviour. *Nature Communications* **2014,** *5* (1), 4012.

166. Elani, Y.; Law, R. V.; Ces, O., Vesicle-based artificial cells as chemical microreactors with spatially segregated reaction pathways. *Nature Communications* **2014,** *5* (1), 5305.

167. Witkowska, A.; Jablonski, L.; Jahn, R., A convenient protocol for generating giant unilamellar vesicles containing SNARE proteins using electroformation. *Scientific Reports* **2018,** *8* (1), 9422.

168. Lim, S. K.; De Hoog, H.-P.; Parikh, A. N.; Nallani, M.; Liedberg, B., Hybrid, Nanoscale Phospholipid/Block Copolymer Vesicles. *Polymers* **2013,** *5* (3).

169. Shum, H. C.; Kim, J.-W.; Weitz, D. A., Microfluidic Fabrication of Monodisperse Biocompatible and Biodegradable Polymersomes with Controlled Permeability. *Journal of the American Chemical Society* **2008,** *130* (29), 9543-9549.

170. Perro, A.; Nicolet, C.; Angly, J.; Lecommandoux, S.; Le Meins, J. F.; Colin, A., Mastering a double emulsion in a simple co-flow microfluidic to generate complex polymersomes. *Langmuir* **2011,** *27* (14), 9034-42.

171. Kamiya, K., Development of Artificial Cell Models Using Microfluidic Technology and Synthetic Biology. *Micromachines* **2020,** *11* (6).

172. Le Meins, J. F.; Schatz, C.; Lecommandoux, S.; Sandre, O., Hybrid polymer/lipid vesicles: state of the art and future perspectives. *Materials Today* **2013,** *16* (10), 397-402.

173. Gerstle, Z.; Desai, R.; Veatch, S. L., Chapter Eight - Giant Plasma Membrane Vesicles: An Experimental Tool for Probing the Effects of Drugs and Other Conditions on Membrane Domain Stability. In *Methods in Enzymology*, Eckenhoff, R. G.; Dmochowski, I. J., Eds. Academic Press: 2018; Vol. 603, pp 129-150.

174. Ha, D.; Yang, N.; Nadithe, V., Exosomes as therapeutic drug carriers and delivery vehicles across biological membranes: current perspectives and future challenges. *Acta Pharm Sin B* **2016,** *6* (4), 287-96.

175. Zhu, L.; Oh, J. M.; Gangadaran, P.; Kalimuthu, S.; Baek, S. H.; Jeong, S. Y.; Lee, S. W.; Lee, J.; Ahn, B. C., Targeting and Therapy of Glioblastoma in a Mouse Model Using Exosomes Derived From Natural Killer Cells. *Front Immunol* **2018,** *9*, 824.

176. Li, S. P.; Lin, Z. X.; Jiang, X. Y.; Yu, X. Y., Exosomal cargo-loading and synthetic exosome-mimics as potential therapeutic tools. *Acta Pharmacol Sin* **2018,** *39* (4), 542-551.

177.    Zhai, Y.; Su, J.; Ran, W.; Zhang, P.; Yin, Q.; Zhang, Z.; Yu, H.; Li, Y., Preparation and Application of Cell Membrane-Camouflaged Nanoparticles for Cancer Therapy. *Theranostics* **2017,** *7* (10), 2575-2592.

178.    Jeong, D.; Jo, W.; Yoon, J.; Kim, J.; Gianchandani, S.; Gho, Y. S.; Park, J., Nanovesicles engineered from ES cells for enhanced cell proliferation. *Biomaterials* **2014,** *35* (34), 9302-10.

179.    Del Piccolo, N.; Placone, J.; He, L.; Agudelo, S. C.; Hristova, K., Production of Plasma Membrane Vesicles with Chloride Salts and Their Utility as a Cell Membrane Mimetic for Biophysical Characterization of Membrane Protein Interactions. *Analytical Chemistry* **2012,** *84* (20), 8650-8655.

180.    Kelly, C. V.; Kober, M.-M. T.; Kinnunen, P.; Reis, D. A.; Orr, B. G.; Banaszak Holl, M. M., Pulsed-laser creation and characterization of giant plasma membrane vesicles from cells. *Journal of Biological Physics* **2009,** *35* (3), 279-295.

181.    Scott, R. E.; Maercklein, P. B., Plasma membrane vesiculation in 3T3 and SV3T3 cells. II. Factors affecting the process of vesiculation. *Journal of Cell Science* **1979,** *35* (1), 245.

182.    Gadok, A. K.; Busch, D. J.; Ferrati, S.; Li, B.; Smyth, H. D. C.; Stachowiak, J. C., Connectosomes for Direct Molecular Delivery to the Cellular Cytoplasm. *Journal of the American Chemical Society* **2016,** *138* (39), 12833-12840.

183.    Sezgin, E.; Kaiser, H.-J.; Baumgart, T.; Schwille, P.; Simons, K.; Levental, I., Elucidating membrane structure and protein behavior using giant plasma membrane vesicles. *Nature Protocols* **2012,** *7* (6), 1042-1051.

184.    Scott, R. E., Plasma membrane vesiculation: a new technique for isolation of plasma membranes. *Science* **1976,** *194* (4266), 743-745.

185.    Levental, K. R.; Levental, I., Chapter Two - Giant Plasma Membrane Vesicles: Models for Understanding Membrane Organization. In *Current Topics in Membranes*, Kenworthy, A. K., Ed. Academic Press: 2015; Vol. 75, pp 25-57.

186.    Levental, K. R.; Surma, M. A.; Skinkle, A. D.; Lorent, J. H.; Zhou, Y.; Klose, C.; Chang, J. T.; Hancock, J. F.; Levental, I., ω-3 polyunsaturated fatty acids direct differentiation of the membrane phenotype in mesenchymal stem cells to potentiate osteogenesis. *Science Advances* **2017,** *3* (11), eaao1193.

187.    Säälik, P.; Niinep, A.; Pae, J.; Hansen, M.; Lubenets, D.; Langel, Ü.; Pooga, M., Penetration without cells: membrane translocation of cell-penetrating peptides in the model giant plasma membrane vesicles. *J Control Release* **2011,** *153* (2), 117-25.

188.    Dubavik, A.; Sezgin, E.; Lesnyak, V.; Gaponik, N.; Schwille, P.; Eychmüller, A., Penetration of amphiphilic quantum dots through model and cellular plasma membranes. *ACS Nano* **2012,** *6* (3), 2150-6.

189.    Ge, M.; Gidwani, A.; Brown, H. A.; Holowka, D.; Baird, B.; Freed, J. H., Ordered and Disordered Phases Coexist in Plasma Membrane Vesicles of RBL-2H3 Mast Cells. An ESR Study. *Biophysical Journal* **2003,** *85* (2), 1278-1288.

190.    Holowka, D.; Baird, B., Structural studies on the membrane-bound immunoglobulin E-receptor complex. 1. Characterization of large plasma membrane vesicles from rat basophilic leukemia cells and insertion of amphipathic fluorescent probes. *Biochemistry* **1983,** *22* (14), 3466-74.

191.    Gadok, A. K.; Zhao, C.; Meriwether, A. I.; Ferrati, S.; Rowley, T. G.; Zoldan, J.; Smyth, H. D. C.; Stachowiak, J. C., The Display of Single-Domain Antibodies on the Surfaces of Connectosomes Enables Gap Junction-Mediated Drug Delivery to Specific Cell Populations. *Biochemistry* **2018,** *57* (1), 81-90.

192.    Hoerl, B. J.; Scott, R. E., Plasma membrane vesiculation: a cellular response to injury. *Virchows Arch B Cell Pathol* **1978,** *27* (4), 335-45.

193.    Nishimura, K.; Hosoi, T.; Sunami, T.; Toyota, T.; Fujinami, M.; Oguma, K.; Matsuura, T.; Suzuki, H.; Yomo, T., Population Analysis of Structural Properties of Giant Liposomes by Flow Cytometry. *Langmuir* **2009,** *25* (18), 10439-10443.

194.    Jalmar, O.; François-Moutal, L.; García-Sáez, A.-J.; Perry, M.; Granjon, T.; Gonzalvez, F.; Gottlieb, E.; Ayala-Sanmartin, J.; Klösgen, B.; Schwille, P.; Petit, P. X., Caspase-8 Binding to Cardiolipin in Giant Unilamellar Vesicles Provides a Functional Docking Platform for Bid. *PLOS ONE* **2013,** *8* (2), e55250.

195.    Jaskiewicz, K.; Makowski, M.; Kappl, M.; Landfester, K.; Kroeger, A., Mechanical Properties of Poly(dimethylsiloxane)-block-poly(2-methyloxazoline) Polymersomes Probed by Atomic Force Microscopy. *Langmuir* **2012,** *28* (34), 12629-12636.

196.    Avsar, S. Y.; Kapinos, L. E.; Schoenenberger, C.-A.; Schertler, G. F. X.; Mühle, J.; Meger, B.; Lim, R. Y. H.; Ostermaier, M. K.; Lesca, E.; Palivan, C. G., Immobilization of arrestin-3 on different biosensor platforms for evaluating GPCR binding. *Physical Chemistry Chemical Physics* **2020,** *22* (41), 24086-24096.

197.    Anajafi, T.; Mallik, S., Polymersome-based drug-delivery strategies for cancer therapeutics. *Ther. Deliv.* **2015,** *6* (4), 521-534.

198.    Xu, L.; Ren, N.; Pang, J.; Deng, H.; Zhu, X.; Sun, M.; Yan, D., Fluorescent and "breathable" $CO_2$ responsive vesicles inspired from green fluorescent protein. *Polymer Chemistry* **2017,** *8* (40), 6283-6288.

199.    Edlinger, C.; Einfalt, T.; Spulber, M.; Car, A.; Meier, W.; Palivan, C. G., Biomimetic Strategy To Reversibly Trigger Functionality of Catalytic Nanocompartments by the Insertion of pH-Responsive Biovalves. *Nano Lett.* **2017,** *17* (9), 5790-5798.

200.    Kristiansen, K. A.; Potthast, A.; Christensen, B. E., Periodate oxidation of polysaccharides for modification of chemical and physical properties. *Carbohydrate Research* **2010,** *345* (10), 1264-1271.

201.    Perlin, A. S., Glycol-Cleavage Oxidation. In *Advances in Carbohydrate Chemistry and Biochemistry*, Horton, D., Ed. Academic Press: 2006; Vol. 60, pp 183-250.

202.    Yamashita, E.; Zhalnina, M. V.; Zakharov, S. D.; Sharma, O.; Cramer, W. A., Crystal structures of the OmpF porin: function in a colicin translocon. *The EMBO Journal* **2008,** *27* (15), 2171-2180.

203.    Lee, S.; Housden, N. G.; Ionescu, S. A.; Zimmer, M. H.; Kaminska, R.; Kleanthous, C.; Bayley, H., Transmembrane Epitope Delivery by Passive Protein Threading through the Pores of the OmpF Porin Trimer. *Journal of the American Chemical Society* **2020,** *142* (28), 12157-12166.

204.    Wang, X.; Teng, D.; Guan, Q.; Mao, R.; Hao, Y.; Wang, X.; Yao, J.; Wang, J., Escherichia coli outer membrane protein F (OmpF): an immunogenic protein induces cross-reactive antibodies against Escherichia coli and Shigella. *AMB Express* **2017,** *7* (1), 155.

205.    Gartner, T. E.; Jayaraman, A., Modeling and Simulations of Polymers: A Roadmap. *Macromolecules* **2019,** *52* (3), 755-786.

206.    Shroder, D. Y.; Lippert, L. G.; Goldman, Y. E., Single molecule optical measurements of orientation and rotations of biological macromolecules. *Methods Appl Fluoresc* **2016,** *4* (4), 042004.

207.    Tyagi, S.; Lemke, E. A., Chapter 9 - Genetically Encoded Click Chemistry for Single-Molecule FRET of Proteins. In *Methods in Cell Biology*, Conn, P. M., Ed. Academic Press: 2013; Vol. 113, pp 169-187.

208.    Sudalai, A.; Khenkin, A.; Neumann, R., Sodium periodate mediated oxidative transformations in organic synthesis. *Organic & Biomolecular Chemistry* **2015,** *13* (15), 4374-4394.

209.    Wu, D.; Rigo, S.; Di Leone, S.; Belluati, A.; Constable, E. C.; Housecroft, C. E.; Palivan, C. G., Brushing the surface: cascade reactions between immobilized nanoreactors. *Nanoscale* **2020,** *12* (3), 1551-1562.

210.    Nardin, C.;  Hirt, T.;  Leukel, J.; Meier, W., Polymerized ABA Triblock Copolymer Vesicles. *Langmuir* **2000,** *16* (3), 1035-1041.

211.    Poschenrieder, S. T.;  Schiebel, S. K.; Castiglione, K., Stability of polymersomes with focus on their use as nanoreactors. *Eng Life Sci* **2018,** *18* (2), 101-113.

212.    Draghici, C.;  Mikhalevich, V.;  Gunkel-Grabole, G.;  Kowal, J.;  Meier, W.; Palivan, C. G., Biomimetic Planar Polymer Membranes Decorated with Enzymes as Functional Surfaces. *Langmuir* **2018,** *34* (30), 9015-9024.

213.    Breslmayr, E.;  Hanžek, M.;  Hanrahan, A.;  Leitner, C.;  Kittl, R.;  Šantek, B.;  Oostenbrink, C.; Ludwig, R., A fast and sensitive activity assay for lytic polysaccharide monooxygenase. *Biotechnology for Biofuels* **2018,** *11* (1), 79.

214.    Hogue, M. J., THE EFFECT OF HYPOTONIC AND HYPERTONIC SOLUTIONS ON FIBROBLASTS OF THE EMBRYONIC CHICK HEART IN VITRO. *The Journal of Experimental Medicine* **1919,** *30* (6), 617.

215.    Zollinger, H. U., Cytologic studies with the phase Microscope; the formation of blisters on cells in suspension, photocytosis, with observations on the nature of the cellular membrane. *The American journal of pathology* **1948,** *24* (3), 545-567.

216.    Johnson, S. A.;  Stinson, B. M.;  Go, M. S.;  Carmona, L. M.;  Reminick, J. I.;  Fang, X.; Baumgart, T., Temperature-dependent phase behavior and protein partitioning in giant plasma membrane vesicles. *Biochimica et Biophysica Acta (BBA) - Biomembranes* **2010,** *1798* (7), 1427-1435.

217.    Holowka, D.; Baird, B., Structural studies on the membrane-bound immunoglobulin E-receptor complex. 1. Characterization of large plasma membrane vesicles from rat basophilic leukemia cells and insertion of amphipathic fluorescent probes. *Biochemistry* **1983,** *22* (14), 3466-3474.

218.    Worch, R.;  Petrášek, Z.;  Schwille, P.; Weidemann, T., Diffusion of Single-Pass Transmembrane Receptors: From the Plasma Membrane into Giant Liposomes. *The Journal of Membrane Biology* **2017,** *250* (4), 393-406.

219.    Pae, J.;  Liivamägi, L.;  Lubenets, D.;  Arukuusk, P.;  Langel, Ü.; Pooga, M., Glycosaminoglycans are required for translocation of amphipathic cell-penetrating peptides across membranes. *Biochimica et Biophysica Acta (BBA) - Biomembranes* **2016,** *1858* (8), 1860-1867.

220.    Chiang, P.-C.;  Tanady, K.;  Huang, L.-T.; Chao, L., Rupturing Giant Plasma Membrane Vesicles to Form Micron-sized Supported Cell Plasma Membranes with Native Transmembrane Proteins. *Scientific Reports* **2017,** *7* (1), 15139.

221.    Richards, M. J.;  Hsia, C.-Y.;  Singh, R. R.;  Haider, H.;  Kumpf, J.;  Kawate, T.;  Daniel, S., Membrane Protein Mobility and Orientation Preserved in Supported Bilayers Created Directly from Cell Plasma Membrane Blebs. *Langmuir* **2016,** *32* (12), 2963-2974.

222.    Zemljič Jokhadar, Š.;  Klančnik, U.;  Grundner, M.;  Švelc Kebe, T.;  Vrhovec Hartman, S.;  Liović, M.; Derganc, J., GPMVs in variable physiological conditions: could they be used for therapy delivery? *BMC Biophys* **2018,** *11*, 1-1.

223.    Théry, C.;  Zitvogel, L.; Amigorena, S., Exosomes: composition, biogenesis and function. *Nature Reviews Immunology* **2002,** *2* (8), 569-579.

224.    dos Santos, T.;  Varela, J.;  Lynch, I.;  Salvati, A.; Dawson, K. A., Quantitative Assessment of the Comparative Nanoparticle-Uptake Efficiency of a Range of Cell Lines. *Small* **2011,** *7* (23), 3341-3349.

225.    Doherty, G. J.; McMahon, H. T., Mechanisms of Endocytosis. *Annual Review of Biochemistry* **2009,** *78* (1), 857-902.

226.    Behzadi, S.;  Serpooshan, V.;  Tao, W.;  Hamaly, M. A.;  Alkawareek, M. Y.;  Dreaden, E. C.;  Brown, D.;  Alkilany, A. M.;  Farokhzad, O. C.; Mahmoudi, M., Cellular uptake of nanoparticles: journey inside the cell. *Chemical Society Reviews* **2017,** *46* (14), 4218-4244.

227.    Lea, T., Caco-2 Cell Line. In *The Impact of Food Bioactives on Health: in vitro and ex vivo models*, Verhoeckx, K.; Cotter, P.; López-Expósito, I.; Kleiveland, C.; Lea, T.; Mackie, A.; Requena, T.; Swiatecka, D.; Wichers, H., Eds. Springer International Publishing: Cham, 2015; pp 103-111.

228.    Sezgin, E.; Kaiser, H.-J.; Baumgart, T.; Schwille, P.; Simons, K.; Levental, I., Elucidating membrane structure and protein behavior using giant plasma membrane vesicles. *Nature Protocols* **2012,** *7*, 1042.

229.    Landgraf, L.; Müller, I.; Ernst, P.; Schäfer, M.; Rosman, C.; Schick, I.; Köhler, O.; Oehring, H.; Breus, V. V.; Basché, T.; Sönnichsen, C.; Tremel, W.; Hilger, I., Comparative evaluation of the impact on endothelial cells induced by different nanoparticle structures and functionalization. *Beilstein Journal of Nanotechnology* **2015,** *6*, 300-312.

230.    Bexiga, M. G.; Varela, J. A.; Wang, F.; Fenaroli, F.; Salvati, A.; Lynch, I.; Simpson, J. C.; Dawson, K. A., Cationic nanoparticles induce caspase 3-, 7- and 9-mediated cytotoxicity in a human astrocytoma cell line. *Nanotoxicology* **2011,** *5* (4), 557-567.

231.    Lesniak, A.; Campbell, A.; Monopoli, M. P.; Lynch, I.; Salvati, A.; Dawson, K. A., Serum heat inactivation affects protein corona composition and nanoparticle uptake. *Biomaterials* **2010,** *31* (36), 9511-9518.

232.    Zhu, M.; Nie, G.; Meng, H.; Xia, T.; Nel, A.; Zhao, Y., Physicochemical Properties Determine Nanomaterial Cellular Uptake, Transport, and Fate. *Accounts of Chemical Research* **2013,** *46* (3), 622-631.

233.    Sharifi, S.; Behzadi, S.; Laurent, S.; Laird Forrest, M.; Stroeve, P.; Mahmoudi, M., Toxicity of nanomaterials. *Chemical Society Reviews* **2012,** *41* (6), 2323-2343.

234.    Li, Y.; Gu, N., Thermodynamics of Charged Nanoparticle Adsorption on Charge-Neutral Membranes: A Simulation Study. *The Journal of Physical Chemistry B* **2010,** *114* (8), 2749-2754.

235.    Geisler, N., Chemical crosslinking with disuccinimidyl tartrate defines the relative positions of the two antiparallel coiled coils of the desmin protofilament unit. *FEBS Lett* **1993,** *323* (1-2), 63-7.

236.    Scales, C. W.; Convertine, A. J.; McCormick, C. L., Fluorescent Labeling of RAFT-Generated Poly(N-isopropylacrylamide) via a Facile Maleimide−Thiol Coupling Reaction. *Biomacromolecules* **2006,** *7* (5), 1389-1392.

237.    Lin, C.-C.; Anseth, K. S., Controlling Affinity Binding with Peptide-Functionalized Poly(ethylene glycol) Hydrogels. *Advanced Functional Materials* **2009,** *19* (14), 2325-2331.

238.    Perry, C. R.; Matcham, S. E.; Wood, D. A.; Thurston, C. F., The structure of laccase protein and its synthesis by the commercial mushroom Agaricus bisporus. *J. Gen. Microbiol.* **1993,** *139* (1), 171-8.

## PERSONAL DATA

Address: Unterer Mühlenweg 15
      79859 Schluchsee
      Germany
Phone: +49 (0) 151 1661 0526
Email: luisa.zartner@gmail.com
Nationality: German
Date of birth: 14.11.1991

## PROGRAMS

o SCS Swiss Women in Chemistry - Mentorship from industry
o Feminno - Career Program for Innovative Women in Life Science

## EXTRACURRICULAR WORKSHOPS

o Licenses & Patents
o Pitch Training
o Productive Meetings
o Innovation Workshop
o Funding your Projects
o Negotiation Skills

## SOFT SKILLS

o Fast, solution-oriented knowledge transfer
o Well-organized, detail-oriented, independent methods
o Meet the deadlines
o Team-minded
o Clear communication
o Flexibility

# Curriculum Vitae - Luisa Zartner

## PRACTICAL EXPERIENCE

07.2017 – 06.2021
**PhD student** – University of Basel, Switzerland
- **Projects:**
  **A.** Design and synthesis of stimuli-sensitive compounds for protein modification and labelling; development of catalytic nanocompartments based on encapsulated enzymes and functional membrane proteins reconstituted in the polymeric membrane for periodate detection
  **B.** Screening diverse nanoparticles and optimizing the uptake into cells; detailed investigation of the conditions for an efficient transfer of nanoparticles into cell blebs called Giant Plasma Membrane Vesicles (GPMVs)
- **Writing:** Scientific publications, reviews and reports
- **Research:** Literature research, aseptic sample preparation in the lab, statistical data analysis
- **Teaching:** Supervision of students during physical chemistry internships

08.2016 - 01.2017
**Master thesis** - Roche Diagnostics GmbH, Penzberg, Germany
- Synthesis of modified chromophores and evaluation of their spectroscopic properties and advantages in selective detection of cysteine in aqueous solutions

08 - 09.2015
**Internship** - Eagle Burgmann GmbH & Co. KG, Wolfratshausen, Germany
- Testing and optimizing workflows for processes in patent management
- Database maintenance, cataloguing correspondence
- Translations from German into English

## EDUCATION

04.2015 - 03.2017

**Master in Chemistry (1.52)** - LMU Munich, Germany
- **Thesis:** "*Synthesis and UV/Vis Assays of Cysteine Sensors - Direct and Highly Selective Detection of L-Cysteine with Dyes Carrying Acryloyl Esters*" (1.3)
- **Main subjects:** Organic chemistry, inorganic chemistry
- **Minor subject:** Patent legislation for chemists

10.2011 – 01.2015

**Bachelor in Chemistry (2.1)** - LMU Munich, Germany


## TECHNICAL KNOWLEDGE

- Expression and extraction of proteins
- Chemical modification of membrane proteins
- Organic synthesis, bioconjugation
- Self-assembly of polymers and membrane proteins into functional nanostructures
- Aseptic cell culturing
- Analytical techniques: CLSM, FCS, NMR, LCMS, SDS-PAGE, light scattering: SLS/DLS, column chromatography, TEM, IR and UV/Vis spectroscopy
- Search engine SciFinder
- Image evaluation program ImageJ
- Office software: MS Office (Powerpoint, Word, Excel), Open Office Libre, EndNote, ChemBioDraw, MestReNova
- Further device-specific data analysis softwares


## PUBLICATIONS

**L. Zartner**, V. Maffeis, C.-A., Schoenenberger, I. A. Dinu, C. G. Palivan, *Membrane protein channels equipped with a cleavable linker for inducing catalysis inside nanocompartments*, Journal of Materials Chemistry B 2021

**L. Zartner**, M. Garni, I. Craciun, T. Einfalt, C. G. Palivan, *How Can Giant Plasma Membrane Vesicles Serve as a Cellular Model for Controlled Transfer of Nanoparticles?*, Biomacromolecules 2021

**L. Zartner**, M. S. Muthwill, I. A. Dinu, C.-A. Schoenenberger, C. G. Palivan, *The rise of bio-inspired polymer compartments responding to pathology-related signals*, Journal of Materials Chemistry B 2020

M.E. El Idrissi, C.E. Meyer, **L. Zartner**, & W. Meier, *Nanosensors based on polymer vesicles and planar membranes: a short review*, Journal Nanobiotechnology 2018